INTERROGATING AND TARGETING ESSENTIAL SIGNALING PATHWAYS IN UVEAL MELANOMA

by

Tyler D. Hitchman

A Dissertation

Presented to the Faculty of the Louis V. Gerstner, Jr.

Graduate School of Biomedical Sciences,

Memorial Sloan Kettering Cancer Center

in Partial Fulfillment of the Requirements for the Degree of

Doctor of Philosophy

New York, NY

March 2021

_____ _____

Yu Chen MD/PhD Date

Dissertation Mentor

Copyright © 2021 Tyler Daniel Hitchman

ABSTRACT

Uveal melanoma is the most common intraocular malignancy, which arises from the pigmented layer of melanocytes within the uveal tract of the eye. Metastatic disease develops in ~50% of patients, leading to dismal survival rates of less than six months. UVMs harbor mutually exclusive activating mutations in a G-protein coupled receptor signaling pathway. Approximately 90% of UVMs bear mutations in the G-protein alpha q subunits *GNAQ* and *GNA11*. The remaining known mutations are found in the GPCR *CYSLTR2*.

These mutations aberrantly activate canonical PLCβ signaling, cleavage of PIP_2 into DAG and IP_3 both of which lead to PKC activation. Work from our lab has shown that *RASGRP3*, a Ras-GEF, is highly expressed in UVMs and is an important node connecting to the RAS/ERK pathway. PKC has been shown to activate RASGRP3, which then works to increase the affinity of RAS for its active GTP bound state.

Additionally, hyperactivated Gαq binds the Rho/Rac GTP exchange factor (GEF) Trio and ARF6. Trio-regulated Rho GTPase signaling leads to Hippo-independent YAP activation whereas ARF6 is thought to enhance Gαq signaling to canonical targets as well as activate β-catenin signaling. These recent studies have revealed the underlying genetic landscape of uveal melanoma but have not resulted in any therapeutic options clinically.

We developed an isogenic melanocytic cellular system and systematically examined the hotspot mutations in Gαq (e.g., G48V, R183Q, Q209L) and CYSLTR2 (e.g. L129Q) in

human uveal melanoma. Biochemical and cell viability assays validated YM-254890 as a potent inhibitor of cell signaling and growth. Human uveal melanoma cells and mouse models recapitulated this finding, indicating that YM is also effective in vivo. RNA-Seq and synergy analysis revealed that the combination of YM and MEK inhibition leads to further decreases in MAPK pathway gene expression and cell viability, respectively. Furthermore, our cellular and mouse models show that combination leads to long term signaling inhibition and significant decreases in tumor burden.

The outcome of this research has indicated that inhibition of Gαq by YM-254890 is effective against *in vitro* and *in vivo* models of uveal melanoma. Furthermore, cell viability and tumor burden were significantly lowered when YM-254890 was combined with MEK inhibitors. Our work shows that Gαq inhibition is a potential therapeutic avenue that deserves further investigation and that co-targeting Gαq and MEK could further increase therapeutic potential clinically.

BIOGRAPHICAL SKETCH

Tyler Daniel Hitchman, first of his name, was born March 11, 1994 to parents Kelly and Donald Hitchman. He was raised in northern New York with his two brothers Kale Hitchman and Joshua Loughren, along with his Schnoodle Diesel. He attended Potsdam High School where he first discovered his interest in biology from teacher James Allott. He attended Clarkson University and graduated with “great distinction” in Fall of 2015 with a Bachelor of Science Degree in biomolecular sciences. During his undergraduate time, he worked in the laboratories of Dr. Craig Woodworth studying vulnerabilities of cells from different regions of the cervix and Dr. Artem Melman synthesizing a drug delivery compound. Tyler joined the Louis V. Gerstner, Jr. Graduate School of Biomedical Sciences at Memorial Sloan Kettering Cancer Center for his doctoral studies in July 2016. In the summer of 2017, he joined the laboratory of Dr. Yu Chen in the Human Oncology and Pathogenesis Program and began working on his dissertation studying uveal melanoma.

ACKNOWLEDGEMENTS

I would like to thank my mentor Dr. Yu Chen for his never-ending support and the opportunity to work in his lab. His dedication and commitment to the lab, my work, and my training is a testament to his outstanding mentorship. I would also like to thank Dr. Ping Chi, who mentored me as one of her own students and always advocated for us to push the boundaries of our work. The Chi/Chen lab is a supportive community of scientists and friends that have helped elevate this work. I have been privileged to collaborate with Dr. Thomas Sakmar, Dr. Omar Abdel-Wahab, Dr. Scott Woodman, and Dr. Alexander Shoushtari and their teams. I would like to recognize Dr. Craig Woodworth who gave me the first opportunity to do research at Clarkson University and advised me through the application process of graduate school. I would also like to recognize James Allott who was my high school biology teacher that inspired me to pursue a degree in biology. This work was made possible by funding through my graduate school, internal MSK grants, and the NIH/NCI (1F31CA236030). I would also like to thank the staff of the graduate offices who have been an amazing support network for students adjusting to graduate life and moving onward to new careers.

This journey has come with trying times, but I am so privileged to have a great group of friends and a loving family who have supported me. I will miss the many game nights, beer runs, and complaining about lab with friends but these are memories I will cherish. My biggest support has come from my family, one of my greatest pleasures during my Ph.D. was going home to visit my family. I always looked forward to seeing my parents,

brothers, nieces, nephew and doggos (RIP Diesel). My mom, the women who raised my two brothers and I by herself, always stressed the importance of education and hard work. Without her none of this would have been possible. I love you all. Thanks.

TABLE OF CONTENTS

LIST OF TABLES

LIST OF FIGURES

LIST OF ABBREVIATIONS

UVM	Uveal Melanoma
CM	Cutaneous Melanoma
LMN	Leptomeningeal Melanocytic Neoplasms
Gαq	G-protein-alpha q subunit
$G_{q/11}$	GNAQ/GNA11
GPCR	G-protein coupled receptor
PLCβ	Phospholipase C Beta
PIP_2	Phosphatidylinositol 4,5-bisphosphate
IP_3	Inositol trisphosphate
DAG	Diacylglycerol
Ca^{2+}	Calcium
PKC	Protein Kinase C
TPA	12-O-Tetradecanoylphorbol-13-acetate
GTP	Guanosine triphosphate
GDP	Guanosine diphosphate
GEF	Guanine exchange factor
MAPK	Mitogen-activated protein kinase
YM	YM-254890
MEKi	MEK inhibitor
TCGA	The Cancer Genome Atlas
GSEA	Gene Set Enrichment Analysis

CHAPTER 1: INTRODUCTION

Introduction to Uveal Melanoma

Uveal melanoma (UVM) arises from a layer of pigmented melanocytes of the eye, or uveal tract. The uveal tract is composed of the choroid, ciliary body, and iris **(Figure 1.1)**. The majority of UVM develops in the choroid, the largest part of the uveal tract, with a small portion of cases developing in the ciliary body and in rarer cases the iris. UVM is the most common intraocular malignancy with approximately 3,000 new cases per year in the United States. These cases represent about 3-5% of all melanomas in the U.S. making it the second most common subtype of melanoma behind cutaneous melanoma (CM) (Chattopadhyay et al. 2016; Robertson et al. 2017). UVM preferentially occurs in Caucasians with a median age of diagnosis of 62 years old with equal distribution between male and females (Singh et al. 2011). Despite advances in treatment of primary disease the five-year survival rate has remained stagnate at ~80% (Singh et al. 2011). About half of all patients eventually develop metastatic disease, which occurs most often in the liver (K. G. Griewank et al. 2012). Liver metastasis is associated with poor prognosis, patients have a median survival of less than six months and a five year survival rate of ~15% (Jovanovic et al. 2013). Currently, there are no effective therapeutic options to treat metastatic UVM.

Genetic Alterations in Uveal Melanoma

When compared to CM, UVM is a genetically and clinically distinct disease. UVM has one of the lowest mutation rates among cancers and has significantly lower somatic mutations than CM **(Figure 1.2)**. UVM also lacks mutations in a distinct set of MAPK

activating genes normally found in CM, including *BRAF*, *KIT*, *NRAS*, and *NF1*. UVM is characterized by activating mutations in the Gαq signaling pathway and chromosomal aberrations such as monosomy 3 and amplification of chromosome 8.

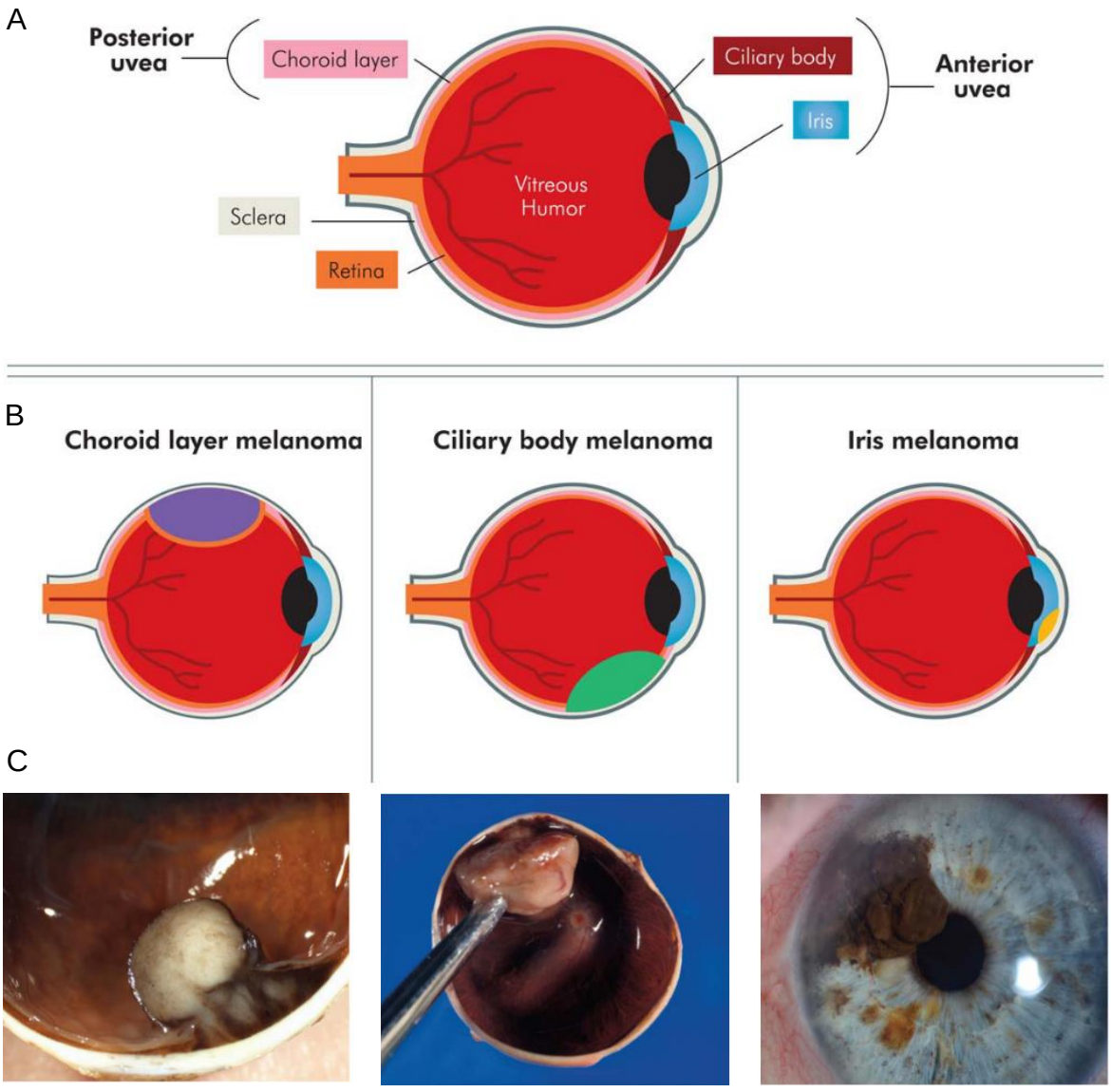

Figure 1.1 Illustration of uveal tract and patient specimens.
(A) Diagram of uveal tract. **(B)** Illustrative and **(C)** patient examples of choroidal, ciliary body and iris melanomas. Figures adapted from (Chattopadhyay et al. 2016).

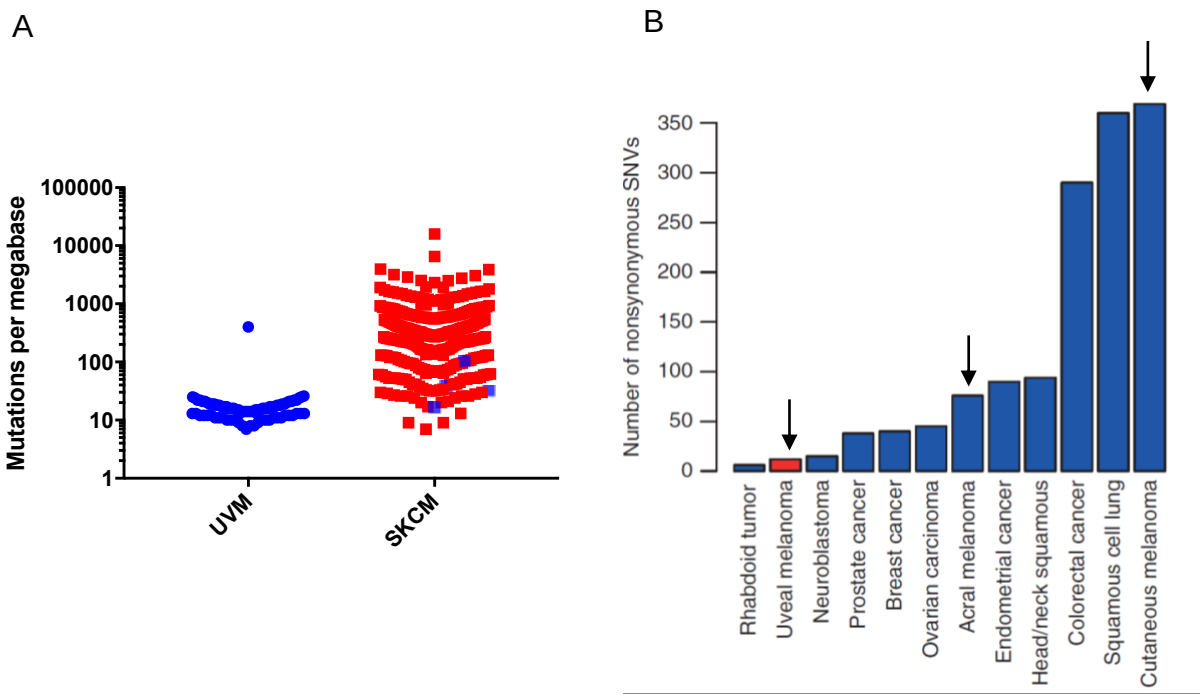

Figure 1.2 Mutational Burden of uveal melanoma.
(A) Mutations per megabase for uveal melanoma and cutaneous melanoma from TCGA dataset. Blue squares in SKCM population represent patients with Gαq mutations **(B)** Comparison of non-synonymous point mutation rates identified from whole genome and exome sequencing studies in various solid tumors, adapted from (Furney et al. 2013).

Driver Mutations within the Gαq signaling pathway

UVM is characterized by a set of mutually exclusive activating mutations within the G-protein alpha q (Gαq) signaling pathway (Alexandrov et al. 2013; Chattopadhyay et al. 2016) **(Figure 1.3)**. Two homologous Gαq subunits, *GNAQ* and *GNA11* ($G_{q/11}$), harbor ~90% of mutations in UVM (Van Raamsdonk et al. 2009, 2010). Less frequent mutations have been found in g-protein coupled receptor (GPCR), cysteinyl leukotriene receptor 2 (*CYSLTR2*). It has also been postulated that mutations in phospholipase C β4 (*PLCB4*) may account for some of the other $G_{q/11}$ wildtype patients. These mutant proteins activate canonical PLCβ signaling; cleavage of phosphatidylinositol 4,5-bisphosphate (PIP_2) into diacylglycerol (DAG) and inositol triphosphate (IP_3) both of which lead to protein kinase

C (PKC) activation. The various activating mutations along this pathway indicate the importance of Gαq signaling to UVM tumorigenesis.

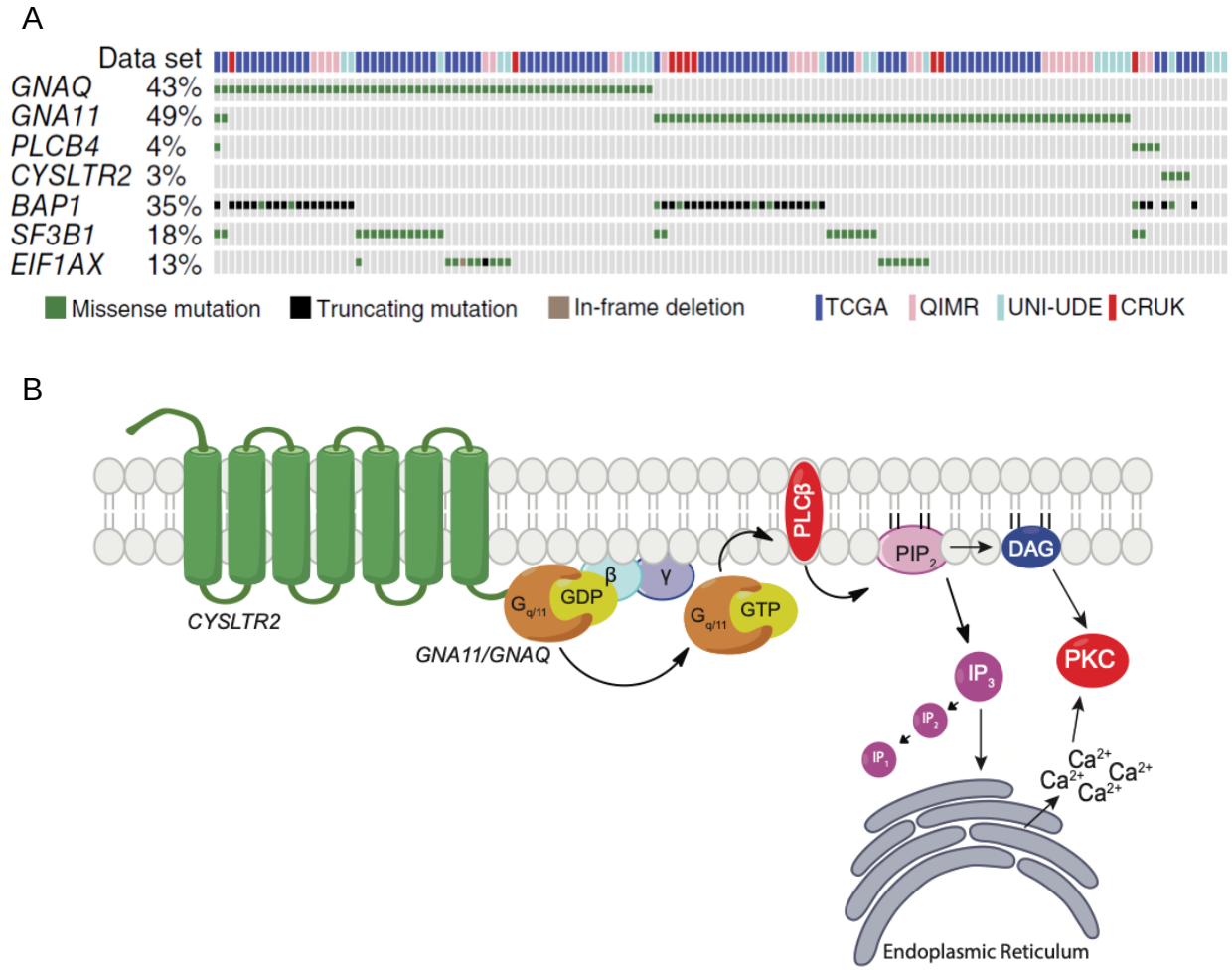

Figure 1.3 Mutational landscape of uveal melanoma.
(A) OncoPrint of activating mutations and prognostic co-mutations in uveal melanomas from four data sets: TCGA (n = 80), UNI-UDE (n = 22), CRUK (n = 9), and QIMR (n = 25). **(B)** Gαq signaling pathway schematic hyperactivated in uveal melanoma. GPCR (CYSLTR2) activation of the Gαq subunit promotes the exchange of GDP for GTP and binding to PLCβ4 to activate cleavage of PIP2 to produce DAG and inositol triphosphate IP_3, both of which activate various PKC isoforms. Adapted from (Moore et al. 2016).

GNAQ and GNA11

GNAQ and GNA11 are paralogous guanine nucleotide-binding proteins that make up the α-subunit of the heterotrimeric G protein complex. Under normal conditions this complex is bound to GPCRs in an inactive GDP bound state. Upon receptor activation, the receptor undergoes a 3D conformational change and catalyzes the exchange of GDP to GTP for Gαq. Gαq then dissociates from the βγ subunits to activate canonical downstream signaling.

GNAQ was first implicated as a driver mutation in uveal melanoma when investigators sequenced a wide spectrum of benign and malignant melanocytic neoplasms (Van Raamsdonk et al. 2009). *GNAQ* was mutated in 46% of cases, all of which occurred at a single residue, Gln209. Additionally, this same *GNAQ* mutation was found in 83% of blue nevi and 50% of "malignant blue nevi". This work was quickly followed by another melanocytic neoplasm sequencing study that also identified *GNAQ* Q209 mutations in uveal melanoma and blue nevi (Van Raamsdonk et al. 2010). However, this study also identified a second mutational hotspot at residue Arg183 and identified the same two mutations in *GNA11*. Interestingly, *GNAQ* mutations were much more prevalent in blue nevi (45% vs. 7%) whereas *GNA11* mutations were more than double *GNAQ* in uveal melanoma metastasis (57% vs. 22%). Arg183 mutations in *GNAQ/11* were only found in 2% of blue nevi and 6% of uveal melanomas. These mutations have since been identified in other melanocytic neoplasms including a small portion of mucosal melanomas, leptomeningeal melanocytic neoplasms (LMN), Sturge Weber syndrome, and Port-Wine stains (Sheng et al. 2016; Küsters-Vandevelde et al. 2015; Shirley et al. 2013). This

pattern further highlights the significance of aberrant Gαq signaling in melanocytic diseases.

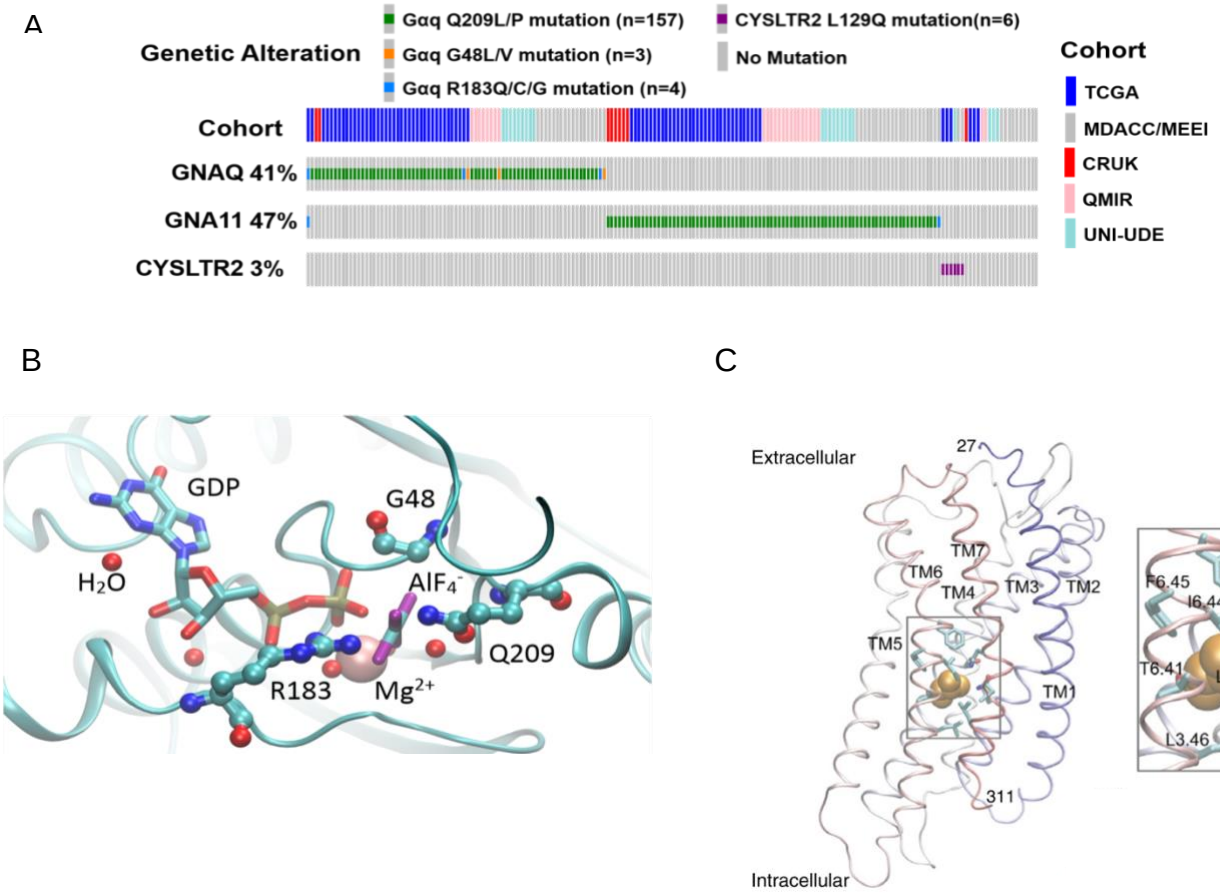

Figure 1.4 Hotspot mutations in GNAQ, GNA11, and CYSLTR2.
(A) Oncoprint of Gαq pathway mutations in 188 UVM patients from five published cohorts including TCGA, Cancer Research UK (CRUK), QIMR Berghofer Medical Research Institute, University of Duisburg-Essen (UNI-UDE) and MD Anderson Cancer Center/Massachusetts Eye and Ear Infirmary (MDACC/MEEI). **(B)** 3D structure of active GNAQ highlighting Gly48 of the P-loop, Arg183 of Switch 1, and Gln209 of Switch 2 (ball-and-stick). The magnesium ion is shown as a pink sphere and water molecules as small red spheres. GDP and AlF4- are both shown as sticks. **(C)** Structural homology model of CysLT2R based on the structure for PAR1. Transmembrane segments are labeled. Leu129 (3.43) is shown in orange space fill. Boxed segment (right) shows residues that interact with position 3.43. (C) Adapted from (Moore et al. 2016)

Uveal melanoma sequencing data has become more prevalent in recent years **(Figure 1.4A)**. About 90% of all patients harbor activating mutations in *GNAQ/11*, where 95% of those mutations occur at Gln209. Arg183 and previously unidentified Gly48 represent the remaining small percent of mutations in *GNAQ/11*. Mutations in *GNAQ/11* at Gln209 and Arg183 have been previously described as constitutively active due to their ability to perturb GTP hydrolysis of GNAQ/11 (Wu et al. 1992; Chidiac and Ross 1999; O'Hayre et al. 2013). The Gln209 mutations in *GNAQ/11* have shown the ability to transform melanocytes both *in vitro* and *in vivo,* as well as induce uveal melanoma tumorigenesis in GEMMs (Van Raamsdonk et al. 2009, 2010; Huang, Urtatiz, and Van Raamsdonk 2015; Moore et al. 2018). The crystal structure of GNAQ shows that Gln209, Arg183, and Gly48 are all in proximity to the GTP binding pocket, indicating that mutations at any of these residues would result in perturbed GTP hydrolysis **(Figure 1.4B)**. More detailed experimentation of mutations at Arg183 and Gly48 will be discussed in chapter 2.

CYSLTR2

CYSLTR2 is a G-protein coupled receptor (GPCR) that activates GNAQ/11 upon ligand binding. Our lab identified and characterized a mutation in *CYSLTR2* that drives UVM and is mutually exclusive from *GNAQ/11* mutations (Moore et al. 2016). The L129Q mutation in CYSLTR2 occurs at the 3.43 position (Ballesteros–Weinstein numbering), a highly conserved region that stabilizes the inactive receptor and has been previously shown to confer constitutive activity upon alteration **(Figure 1.4C)**. The mutant showed increased basal levels of calcium and this was not further increased by addition of receptor agonist. Melanocytes dependent on this mutation grew significantly faster and

were able to continue proliferating in the absence of media supplemented with TPA compared to WT CYSLTR2. This mutation also promoted melanocyte specific gene expression and maintained the cells pigmentation in the absence of TPA. Most strikingly, these CYSLTR2^{L129Q} dependent melanocytes were able to drive tumor formation and growth when allografted into SCID mice. Since identifying CYSLTR2^{L129Q} as a driver mutation in UVM, many other studies have identified the same mutation in blue nevi and meningeal melanocytic tumors (Möller et al. 2017; van de Nes et al. 2017; Küsters-Vandevelde et al. 2018). These studies demonstrate the mutant L129Q's ability to hyperactivate the Gαq pathway and drive UVM, further emphasizing the importance this pathway plays in UVM and other melanocytic neoplasms.

PLCβ4

PLCβ4 is the direct downstream effector of GNAQ/11 that results in PKC activation via DAG and calcium production. Mutation within its catalytic core at Asp630 has been suggested to convey constitutive activation in UVM and LMNs (Johansson et al. 2016; van de Nes et al. 2017). However, these studies were based on a small number of patient sequencing data and there are still no functional studies of this mutation. In both studies, mutations at Asp630 in PLCβ4 are accompanied by BAP1 mutations, the most severe prognostic factor in UVM. In my experiments with melan-a cells, I have been able to make them dependent on all UVM driving mutations found in *GNAQ/11* and *CYSLTR2*. These driving mutations transform the cells, making them TPA independent. However, using the same methodology I haven't not been able to make them dependent upon mutations at PLCβ4^{D630}. Taken together, this limited sequencing data and the inability of this mutation to transform melan-a cells, indicates that this mutation is not sufficient enough to drive

UVM by itself, but may need other cooperative genetic alterations to promote tumorigenesis.

Prognostic Co-mutations

Besides driver mutations in *GNAQ/11* and *CYSLTR2*, there is a set of recurring co-mutations and other genetic alterations that act as prognostic indicators for UVM. A recent study, identified four distinct subsets in UVM that correlate with metastatic risk (Robertson et al. 2017). The two poor prognosis groups (highest metastatic risk) had loss of *BAP1* and monosomy 3. The other two subsets with disomy 3 had mutations in SF3B1 and EIF1AX were associated with intermediate and good prognosis, respectively. Like the driver mutations, these prognostic mutations have also been found in other melanocytic neoplasms and have similar prognostic indications (Küsters-Vandevelde et al. 2016; Klaus G. Griewank et al. 2017).

BAP1

BRCA1-associated protein 1, or *BAP1*, is a deubiquitinase that regulates the E3 ligase activity of the BARD1/BRAC1 complex (Nishikawa et al. 2009). *BAP1* was first identified as a poor prognosis factor in UVM by a study that analyzed sequencing data in search for metastasis related mutations (Harbour et al. 2010). Inactivating mutations in BAP1 were identified in greater than 80% of metastatic tumors sampled. Furthermore, *BAP1* is located on chromosome 3 which loss of one copy has been previously discussed to be an indicator of poor prognosis. Due to monosomy 3, only one copy of *BAP1* must be perturbed in order to promote metastasis. Previous sequencing projects have indicated *BAP1* alterations in ~20-30% of samples **(Figure 1.3A)**. However, a recent study showed

that *BAP1* alterations are more common at around 45%, by using a more robust sequencing and bioinformatic pipeline (Field et al. 2018). Although *BAP1*-loss associates with more metastatic disease, the exact mechanism remains unclear.

SF3B1 & EIF1AX

Both *SF3B1* and *EIF1AX* were first identified as recurrent mutations in UVM through a exome sequencing study (Martin et al. 2013). Both mutations were preferentially found in patients with disomy 3, where EIF1AX and SF3B1 mutations were at 48% and 29%, respectively. Since mutations in these genes are associated with a normal chromosomal 3 count, patients with these mutations are in an intermediate (SF3B1) or good prognosis (EIF1AX) cohort. These co-mutations rarely co-occur with one another or with *BAP1*-loss.

Subunit 1 of splicing factor 3b (SF3B1) is a component of the spliceosome, a complex that splices introns from pre-mRNA. In UVM, mutations in *SF3B1* were found mostly at Arg625 and found to cause alternative splicing in mutant bearing samples (Furney et al. 2013). Interestingly, mutations at Lys700 of *SF3B1* have been reported in breast, hematological, and pancreatic cancers. This different mutation site could indicate that UVM requires a unique mutation in *SF3B1* for alternative splicing to occur. Recent work shows that mutant *SF3B1* causes disruption of the non-canonical BAF complex by alternative splicing of *BRD9* (Inoue et al. 2019). Correcting this mis-splicing of *BRD9* suppressed tumor growth in UVM cells, indicating a new potential therapeutic avenue for *SF3B1* mutant UVMs.

Eukaryotic translation initiation factor 1a (EIF1AX) is a component of the 43S preinitiation complex that works to recruit the 40S ribosomal subunit to the 5' cap of mRNA to initiate translation (Lomakin and Steitz 2013). UVMs with *EIF1AX* mutations rarely metastasize and are in the best prognosis subset. *EIF1AX* mutations are found in the N terminus of the protein but the exact mechanism these mutations play in UVM remains unclear.

Downstream Signaling Pathways Essential for Uveal Melanoma

Since the discovery of mutations in *GNAQ/11* more than 10 years ago a great deal of work has been put into understanding the downstream signaling components that drive UVM. As discussed above, canonical Gαq signaling was known to signal through PLCB and activate various PKC isoforms. Hyperactive Gαq has been shown to lead to increased PLCB activity and calcium levels, as expected (Moore et al. 2016, 2018). However, recent work has revealed important signaling pathways unique to hyperactivated Gαq that drives UVM and other melanocytic neoplasms. This work has provided opportunities to study the effects of specifically targeting these pathways to find an effective therapeutic strategy for UVM.

MAPK

Early on, many believed that the MAPK pathway must be important in UVM because of its prevalence in CM and UVM cell lines showed sensitivity to MEK inhibitors (Van Raamsdonk et al. 2010). In fact, the involvement of MAPK signaling in UVM was being studied before the discovery of *GNAQ/11* (Zuidervaart et al. 2005). *GNAQ/11*

overexpression studies have shown increased activation of MAPK signaling without the mutations in KIT, NF1, NRAS, or BRAF that characterize CM.

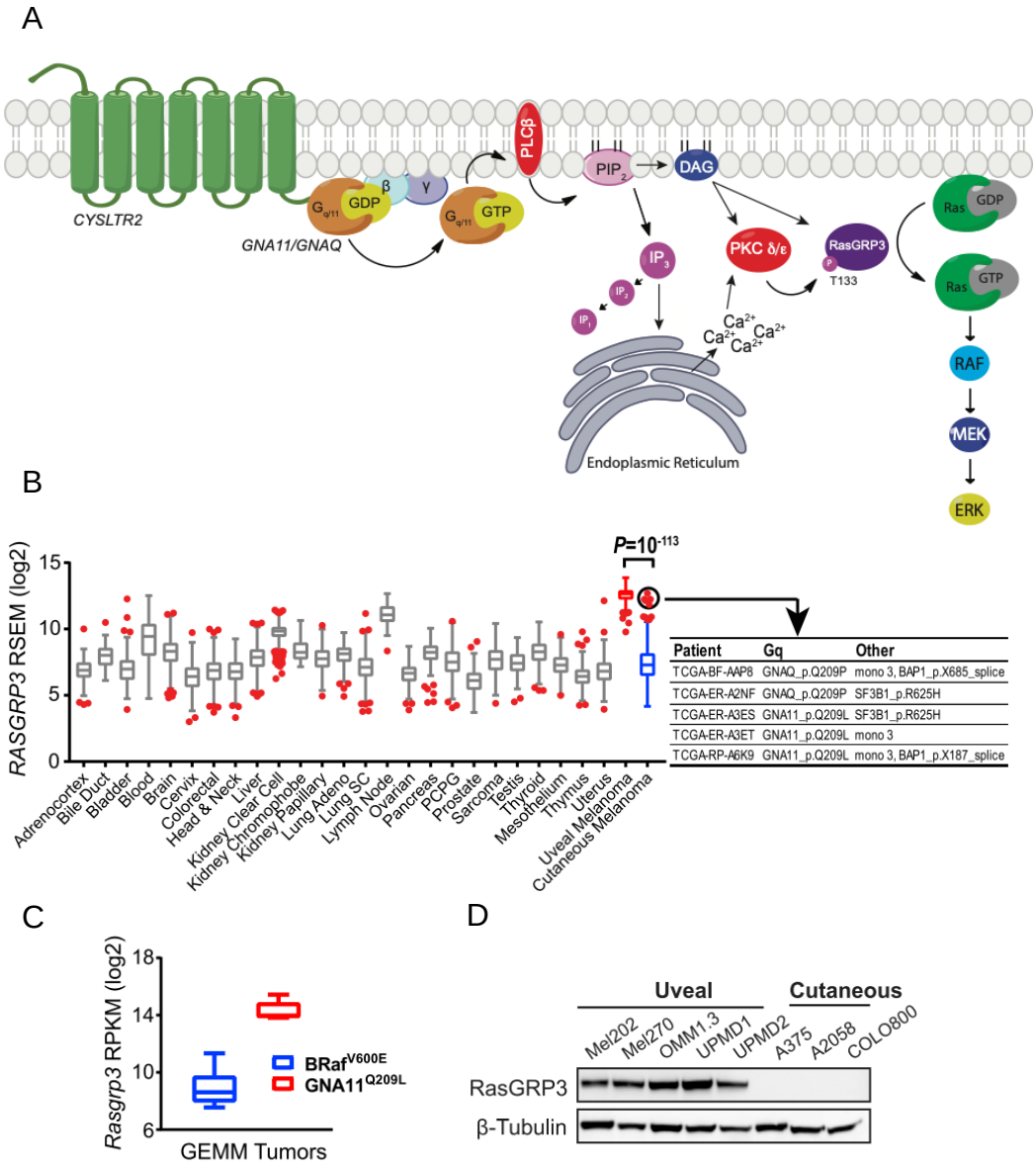

Figure 1.5 RASGRP3 is an essential signaling node that bridges PKC to MAPK signaling in uveal melanoma.
(A) Gαq signaling pathway schematic highlighting activation of RAS-ERK signaling pathway via RASGRP3 activation. **(B)** RASGRP3 expression from pan-cancer TCGA shown as Tukey box-and-whisker plots. Outliers are shown as red dots. UM is highlighted in red. SKCM is highlighted in blue. Outliers with GNAQ, GNA11, BAP1, and SF3B1 mutations are circled and detailed. **(C)** RasGRP3 expression shown as Tukey box- and-whisker plots from GEMM tumors. **(D)** Immunoblot of RASGRP3 in human UM and CM. (B-D) adapted from (Moore et al. 2018).

Two recent works have detailed the importance that RAS guanyl-releasing protein 3 (RASGRP3) plays in the transduction of Gαq signaling to the RAS-ERK signaling cascade. The first, used a series of biochemical assays and transcriptomics to identify and show that PKC isoforms δ and ε phosphorylate RASGRP3 at threonine 133 (Xu Chen et al. 2017), which then activates RAS and stimulates downstream signaling **(Figure 1.5A)**. Furthermore, this work showed that knockdown of this protein in UVM cells decreased tumor burden in xenograft experiments, highlighting the potential for targeting this protein as a therapeutic strategy.

Work from our lab has corroborated these findings using a genetically engineered mouse model to reinforce RASGRP3 as an essential signaling node in UVM (Moore et al. 2018). Our lab generated a melanocyte-specific *GNA11* mutant mouse model with *BAP1* loss: *Tyr-CreER*^{T2};*GNA11*^{Q209L};*Bap1*$^{lox/lox}$, to model the mutations associated with the worst prognosis in patients. Using cross-species comparison between *GNA11*^{Q209L}*Bap1*^{KO} and *BRAF*^{V600E}*Bap1*^{KO} mice and corresponding human melanomas with the same hotspot mutations in *GNA11* and *BRAF*, we found that the GEMM signatures correlated with human transcriptomes of the same driver mutation. We identified *RASGRP3* as an unique and highly expressed gene in GNAQ/11 driven melanomas **(Figure 1.5B, 1.5C, and 1.5D)**. We also showed that RASGRP3 is important for UVM cell growth and RAS activation. These studies have implicated the importance of MAPK signaling in UVM. Yet, core differences in transcriptional signatures between *GNAQ/11*- and *BRAF*- driven tumors suggest activation of important discrepant pathways. Therapies targeting this pathway in

UVM have not yet proven effective, possibly due to alternative growth pathways downstream of GNAQ/11 or relief of negative feedback.

HIPPO-independent activation of YAP

Perturbation of the tumor suppressor Hippo pathway has been studied in a variety of cancers, in which many show elevated nuclear localization of YAP/TAZ. In UVM, a pair of studies published corroborating reports that mutant Gαq signaling leads to YAP activation in UVM (Yu et al. 2014; Feng et al. 2014).

The first report showed that overexpression of oncogenic Gαq in HEK293 cells leads to increased levels of unphosphorylated or activated YAP (Yu et al. 2014). They documented the expression and localization of YAP in several UVM cell lines, noting that nuclear localization of YAP was prevalent in Gαq mutant cell lines and absent in BRAF mutant cell lines. Furthermore, they showed that knockdown of GNAQ in UVM cells lead to increased phosphorylated YAP at serine 127, indicating that active nuclear YAP is dependent on aberrant Gαq signaling. When they knocked down YAP or treated with Verteporfin, a YAP inhibitor, they saw significant reduction in tumor burden. One major caveat for this work is that in the orthotopic xenograft experiment the cells are mixed with verteporfin nanoparticles prior to injection and then followed up with regular injections of the drug. This methodology allows for the drug to localize and take effect prior to tumor engraftment which does not recapitulate any treatment modality for cancer patients.

The second study also implicated YAP activation through oncogenic Gαq signaling but focused more heavily on the signaling pathway connecting Gαq to YAP. They identified that YAP activation in UVM was dependent on Trio and Trio-dependent Rho-GTPases, RhoA and Rac1 (Feng et al. 2014) **(Figure 1.6)**. They showed that Mutant Gαq activates these three proteins and signals through actin remodeling to activate YAP in a HIPPO-independent manner. Perturbing these upstream components led to decreased YAP nuclear localization and cell proliferation. Knockdown of YAP and treatment of Verteporfin led to decreases in tumor burden in xenograft mouse models, further highlighting the YAP pathway's importance to UVM tumorigenesis.

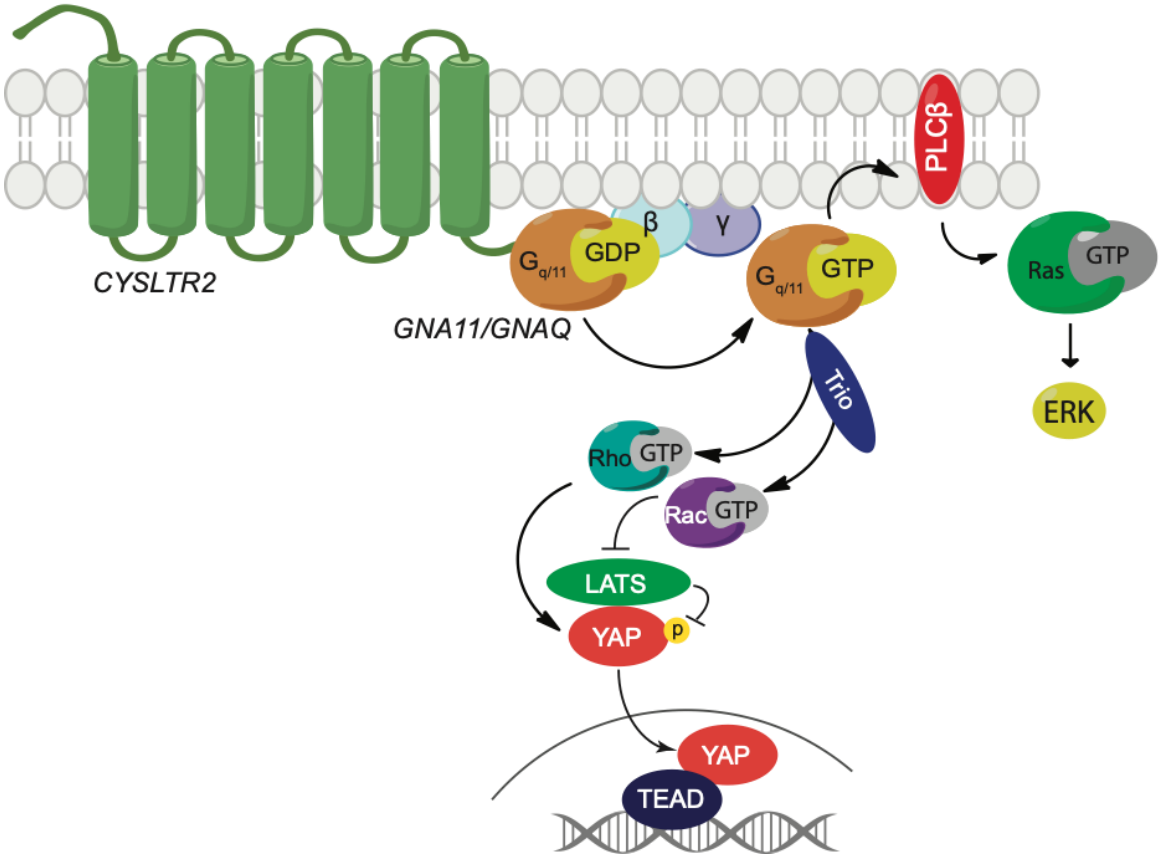

Figure 1.6 Hippo-independent Activation of YAP in Uveal Melanoma.
Schematic of YAP activation via TRIO-RHO/RAC signaling. Mutant $G_{q/11}$ binds to TRIO and leads to the activation of RHO and RAC which activate downstream pathways to inhibit LATS and prevent inhibition of YAP via phosphorylation of S127.

These works have led to interest in targeting YAP in UVM, however historically this has been challenging. YAP is an important transcription factor expressed in many cell types making it difficult to target. Long term targeting of YAP has been shown to be toxic to patients with other ocular malignancies (Arnold et al. 2004; Azab et al. 2004). Currently, there are no YAP inhibitors being used clinically making this pathway particularly difficult to target in UVM (Moroishi, Hansen, and Guan 2015).

FAK

Focal adhesion kinase (FAK), encoded by the *PTK2* gene, is a protein involved in cell adhesion and motility. Following the work on the involvement of HIPPO-independent YAP signaling in UVM, the group published a paper that implicated FAK as a key modulator in this non-canonical YAP signaling pathway. Using a four-step bioinformatics pipeline, they were able to screen for genes overexpressed in UVM, were associated with worse survival, that are essential for UVM tumors, and currently druggable. The result of this screen lead to 7 genes, one of which was *PTK2*. This group showed that the FAK inhibitor was selective for UVM over CM cells and that FAK activation was dependent on TRIO and RhoA, placing it in the non-canonical YAP pathway. Furthermore, they showed that FAK regulated YAP localization through interaction with MOB1 **(Figure 1.7)**. They used sgRNA to knockout *PTK2* and a FAK inhibitor to show that FAK inhibition leads to decreased tumor burden in xenograft experiments. Interestingly, before being implicated in UVM, FAK was shown to play a key role in invasiveness and metastasis of breast cancer (Shen et al. 2018). This study showed that YAP transcriptionally upregulated THBS1, a protein that activates FAK via phosphorylation. They found that inhibiting FAK

lead to decreases in invasiveness and focal adhesion in breast cancer but indicated that FAK was downstream of YAP. This calls into question whether YAP signaling also regulates FAK in UVM, creating a potential positive feedback loop for further study.

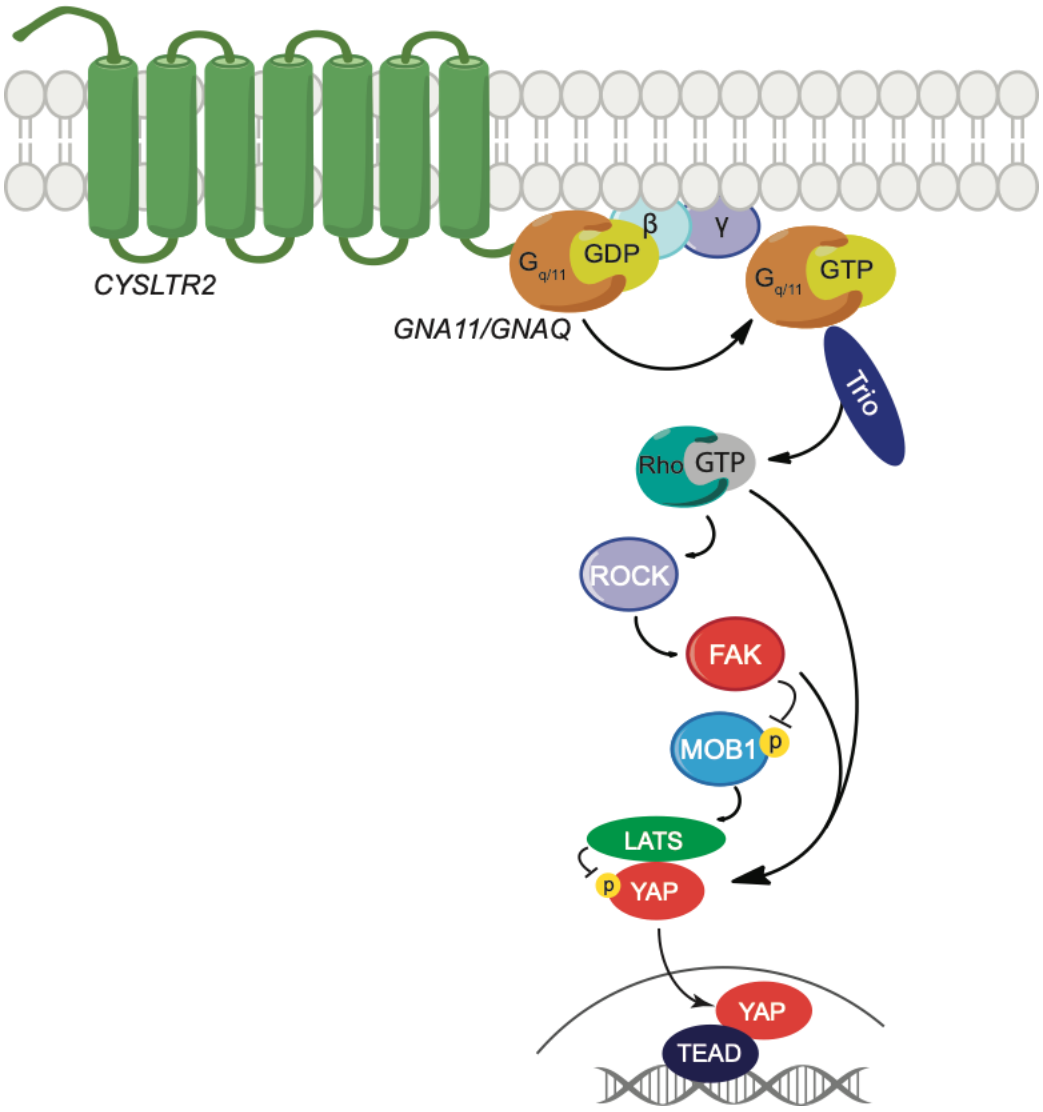

Figure 1.7 Regulation of YAP activity by FAK in uveal melanoma.
Schematic of FAK activation downstream of TRIO-RHO-ROCK signaling. FAK leads to inhibition of MOB1 via phosphorylation, which prevents complex formation with LATS that would normally lead to YAP inactivation. FAK was also shown to play a role in direct activation of YAP via phosphorylation of Y357.

ARF6

ADP-ribosylation factor 6 (ARF6), was implicated as a signaling enhancer of oncogenic Gαq in UVM (Yoo et al. 2016). This work showed that ARF6 is activated by oncogenic Gαq signaling and plays an important role in UVM cell proliferation. Specifically, Gαq binds GEP100 which then activates ARF6, leading to the trafficking of Gαq to cytoplasmic vesicles where signaling is maximal **(Figure 1.8)**. They confirmed that this signaling activates PLCB-PKC-ERK, TRIO-Rho/Rac-YAP, and β-catenin signaling. Knocking down or therapeutically targeting ARF6 resulted in decreased tumor burden in UVM orthotopic xenografts.

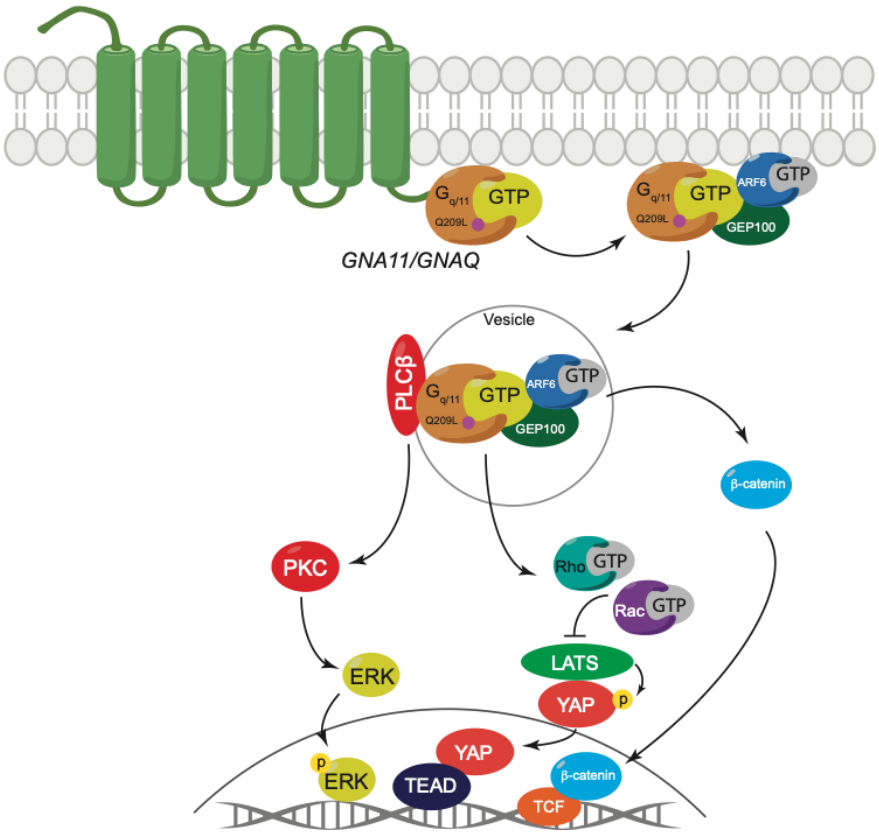

Figure 1. 8 Role of ARF6 in uveal melanoma signaling.
Schematic of ARF6 mediated mutant $G_{q/11}$ vesical signaling. ARF6 binds to a mutant $G_{q/11}$-GEP100 complex and recruits cytoplasmic vesicles that maximize signaling to canonical targets, like PKC and YAP, as well as β-catenin signaling.

These studies, discussed above, have highlighted important pathways downstream of Gαq and established that inhibition of these pathways hinders UVM proliferation and tumorigenesis. However, there have been no clinical applications that have resulted from these works, indicating the need for novel therapeutic strategies.

Therapeutic Strategies for Uveal Melanoma

Localized Therapies for Primary Disease

If UVM is caught in the primary stage of the disease, there are a couple of local therapeutic options available to patients. Before treatment of local disease there should be a thorough examination to determine if any metastasis has already occurred. Current therapeutic options include laser therapy, radiation therapy, and surgery (Chattopadhyay et al. 2016). Although methodologies for local therapy have not changed in many years, small advancements have allowed physicians to prioritize preserving the patient's eyesight while treating the disease.

Laser therapy, or transpupillary thermotherapy, involves the use of infrared lasers to radiate the tumors. This therapy is best suited for small tumors located away from the optic nerve. Although it is well tolerated by patients, this has limited therapeutic potential because of local relapse rates as high as 20% (Journée- De Korver, Oosterhuis, and Keunen 1996; Chattopadhyay et al. 2016). However, this therapy is commonly used as an ancillary to radiation therapy. Radiation therapy is the most common sight preserving method for local disease. It was shown to have no change on mortality when compared to enucleation of the eye. The technique used is known as ocular brachytherapy, or

plaque radiotherapy. This involves the use of radioactive seeds placed onto a thin piece of gold, called a plaque, which is then sewn onto the eye where the tumor is located. Over a period of several days the seeds release radiation to kill the cancer before being removed **(Figure 1.9)**. The final approach and most vision impairing is surgery or enucleation of the eye. For local tumors of large size, microsurgeries are used to remove the tumors and attempt to preserve vision, however this is not always possible and in some cases full enucleation is required (Chattopadhyay et al. 2016). Primary disease treatment is quite invasive but usually can preserve eyesight of the patient. Nevertheless, novel treatments and early detection are key to preserve vision and prevent tumor metastasis.

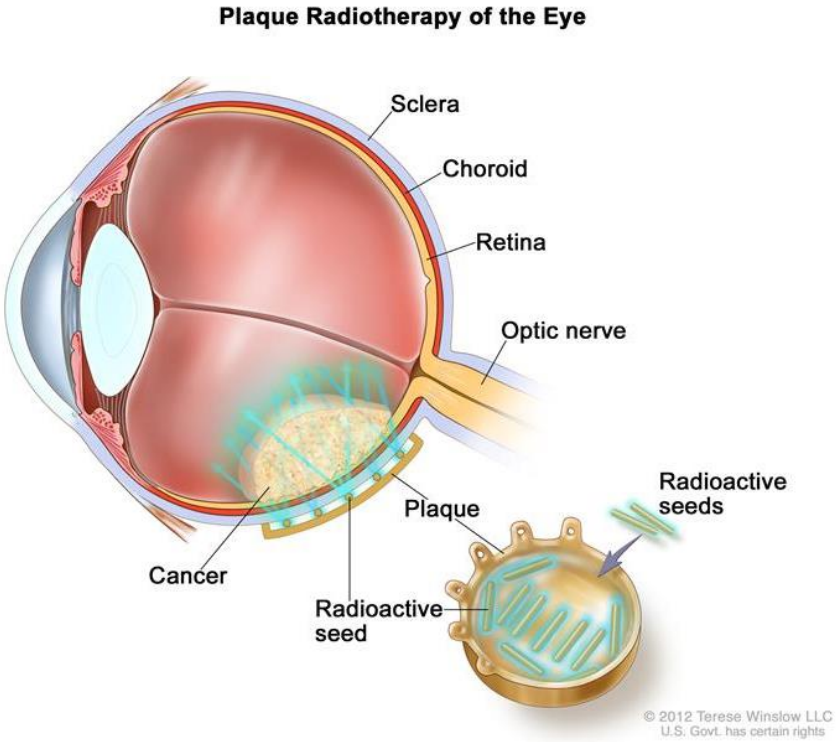

Figure 1. 9 Plaque radiotherapy for treatment of primary uveal melanoma. Radioactive seeds are placed onto a thin piece of medal, or plaque, which is then sewn onto the outside wall of the eye opposite the tumor. The radiation from the seeds kills the cancer and the plaque is then removed after a couple days of treatment. Photo from: https://www.cancer.gov/types/eye/patient/intraocular-melanoma-treatment-pdq#_38

Clinical Trials for Metastatic Disease

Treatments for primary UVM are effective for small tumors caught early, however, it has been suggested that micrometastasis can occur early in tumor progression (Chattopadhyay et al. 2016). UVM metastasis, especially to the liver, is the main cause of disease related death and targeting metastatic disease has proven difficult. Currently, there are no effective therapies for patients with advanced metastatic disease. Chemotherapy response rates have been less than 1% and immunotherapy has not shown increases in progression free survival (PFS) or overall survival rates (Chua et al. 2017; Luke et al. 2015; Rossi et al. 2019). As discussed above, many studies have highlighted potential targets downstream of oncogenic Gαq but have not resulted in any treatments for patients.

Preclinical studies illustrating the effectiveness of targeting RASGRP3, FAK, and ARF6 still require more preclinical study in UVM and must undergo the gauntlet of clinical trials. To put it bluntly, many past clinical trials for UVM have not been backed by rigorous preclinical studies targeting the disease, but have instead been based on treatments with good efficacy for CM (Chattopadhyay et al. 2016) **(Table 1.1)**. Many UVM patients have been placed in these trials due to the lack of available treatment options. One clinical trial, based on promising preclinical studies of UVM (X. Chen et al. 2014), focused on cotargeting downstream effectors, PKC and MEK1/2, however these studies also did not yield increased PFS (Carvajal et al. 2018) **(Figure 1.10)**. To more effectively target UVM, we need therapeutic options that are more specific to mutant Gαq signaling, targeting all important downstream effectors instead of subsets. The lack

of efficacious therapies for UVM illustrates the need for more preclinical work to identify novel druggable targets and development of drugs for previously discovered targets in UVM.

Table 1.1 Completed studies of metastatic uveal melanoma in the United States. Table from (Chattopadhyay et al. 2016).

National Clinical Trials No.	Treatment	Trial Phase	No. of Patients	Status	Primary Endpoint
NCT00506142	Marqibo (liposomal vincristine)	2	52	Completed, results pending	Overall survival
NCT00738361	Abraxane (nanoparticle albumin-bound paclitaxel)	2	25	Completed, results pending	Objective response rate
NCT01200238	Ganetespib (HSP90 inhibitor)	2	30	Completed, results pending	Progression-free survival and expression of MET
NCT01413191	Cixutumumab (anti-IGF-1R antibody)	2	18	Completed, results pending	Objective response rate
NCT01801358	AEB071 (protein kinase C inhibitor) + MEK162 (MEK inhibitor)	1b/2	38	Completed, results pending	DLT and progression-free survival
NCT01974752	Selumetinib (MEK inhibitor) + dacarbazine vs placebo + dacarbazine (SUMIT)	3	128	Completed	Progression-free survival; no difference between arms
NCT01252251	Everolimus (mTOR inhibitor) + pasireotide (somatostatin analog)	2	25	Terminated for poor accrual	Clinical benefit rate (CR + PR + SD) at 16 wk: 26%

Abbreviations: CR, complete remission; DLT, dose-limiting toxicities; HSP90, heat-shock protein 90; IGF-1R, insulin-like growth factor 1 receptor; MEK, mitogen-activated protein kinase kinase; MET, MET proto-oncogene, receptor tyrosine kinase; PR, partial remission; SD, stable disease.

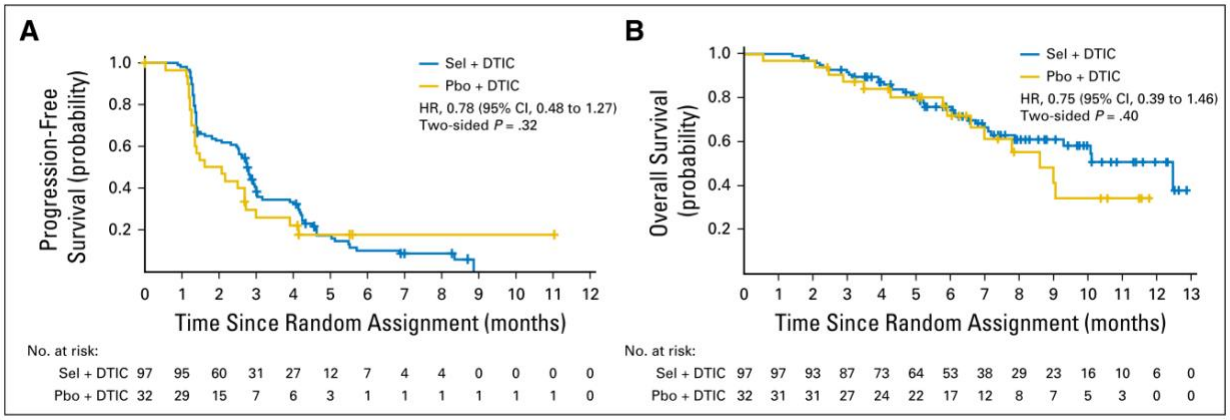

Figure 1. 10 Combination of selumetinib and dacarbazine in metastatic uveal melanoma.
(A) Progression free survival and **(B)** overall survival of clinical trial NTC01974752 comparing selumetinib combined with dacarbazine to dacarbazine alone. DTIC, dacarbazine; HR, hazard ratio; Pbo, placebo; Sel, selumetinib. Figure from (Carvajal et al. 2018).

Directly Targeting Gαq in Uveal Melanoma

YM-254890

YM-254890 (YM) is a naturally occurring cyclic depsipeptide, having both amide and ester linkages, which contains several uncommon amino acids **(Figure 1.11)**. YM was isolated from the culture broth of *Chromobacterium* sp. QS3666, a strain originally identified in soil samples from Japan (Taniguchi, Nagai, et al. 2003; Takasaki et al. 2004). YM was first studied for its ability to inhibit platelet aggregation by perturbing GNAQ/11-mediated Ca^{2+} mobilization (Taniguchi, Nagai, et al. 2003; Takasaki et al. 2004). Further studies investigated YM's inhibitory effect on vasodilation using rat aortas and it's antithrombic effect using femoral arteries from cynomolgus monkeys (Uemura, Kawasaki, et al. 2006; Uemura, Takamatsu, et al. 2006).

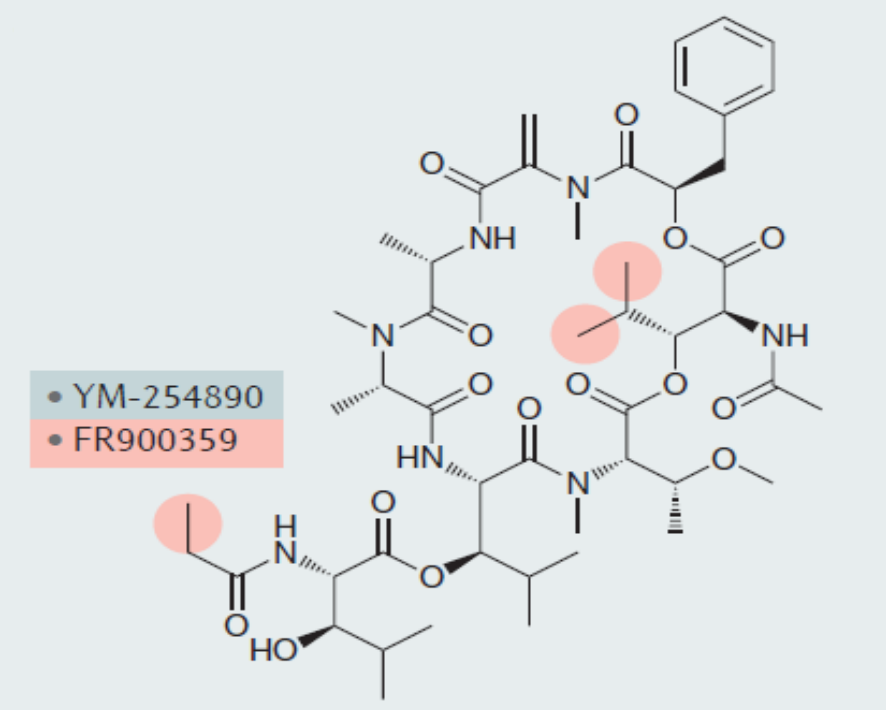

Figure 1. 11 Structure of YM-254890 and FR900359.
The structure of YM-254890 is black only and FR900359 includes the modifications highlighted in red. Figure from (Campbell and Smrcka 2018).

Later biochemical and structural analyses determined that YM's mechanism of action is to inhibit nucleotide exchange, perturbing GDP to GTP exchange of Gαq proteins by preventing GDP dissociation **(Figure 1.12)**. YM binds to the hydrophobic cleft between two inter-domain linkers, stabilizing the inactive GDP-bound form by hindering the flexibility of the linkers (Nishimura et al. 2010). Early overexpression studies, indicated that YM was unable to inhibit the activity of Q209L mutant Gαq and only mildly inhibit R183C mutant Gαq (Takasaki et al. 2004). These mutations were thought to be constitutively active due to their perturbed hydrolysis rates of GTP and therefore YM would have little effect on these mutants. However, many studies have shown that YM and its analogs are potent inhibitors of mutant Gαq in the context of UVM **(Figure 1.13)**. These will be discussed further in the next section on FR900359 and is a main topic in chapter 2.

Since the discovery of YM, many studies have characterized other Gαq inhibitors and synthesized new YM analogs (Taniguchi et al. 2004; Schrage et al. 2015; Xiong et al. 2016; Kamato et al. 2017; Zhang et al. 2017). Hopefully, this leads to identification of novel analogs that are more potent, easier and cheaper to synthesize, and potentially specific to mutant forms of the protein.

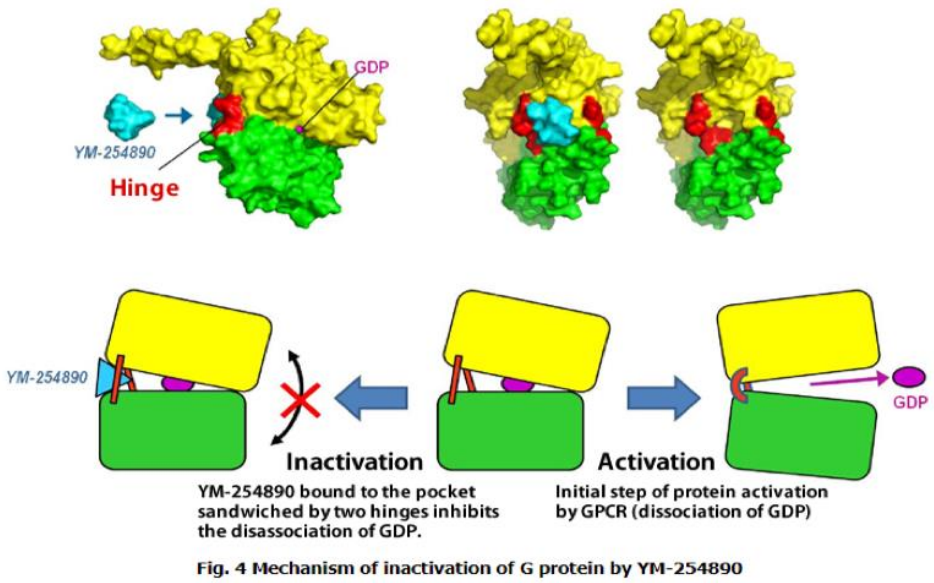

Figure 1. 12 Mechanism of action for YM-254890.
YM-254890 (cyan) binds the inactive form of Gαq proteins (green and yellow) through a hydrophobic pocket located between two linker domains (red). This binding hinders the flexibility of the linker domains and prevents the release of GDP to bind GTP, thus locking it into an inactive conformation. Figure from http://www.spring8.or.jp/en/news_publications/press_release/2010/100713/

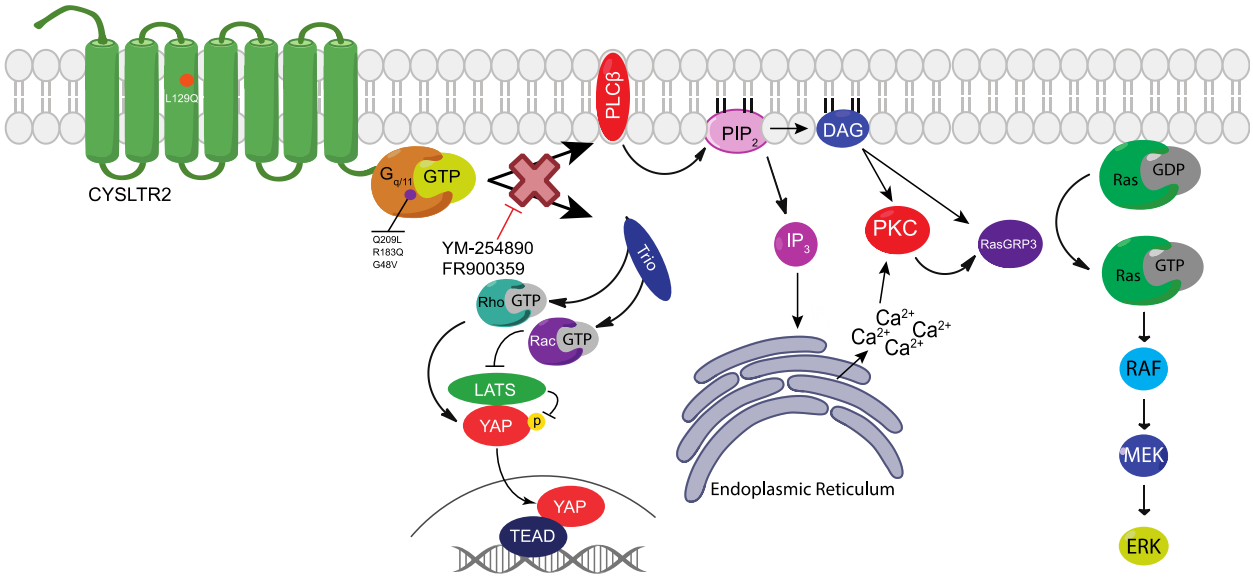

Figure 1. 13 Inhibition of oncogenic signaling in uveal melanoma by YM-254890 and FR. Schematic highlighting the four oncogenic mutations found in GNAQ/11 and CYSLTR2 and where YM-254890/FR900359 targets this pathway. Gαq inhibition leads to decreases in ERK and YAP singling pathways.

FR900359

The most notable and well-studied YM analog is FR900359 (FR) **(Figure 1.11)**. FR was originally isolated from the plant *Ardisia cretana* and studied for its ability to inhibit platelet aggregation and decrease blood pressure (Fujioka et al. 1988). More recent studies have detailed FR's ability to inhibit Gαq and shown that a symbiotic bacterium found in the nodules of the leaf is responsible for the compounds production (Schrage et al. 2015; Crüsemann et al. 2018).

Three recent reports have shown that FR effectively inhibits downstream signaling of oncogenic Gαq in several human UVM cell lines (Onken et al. 2018; Lapadula et al. 2019; Annala et al. 2019). The first of these studies showed that FR traps the $GNAQ^{Q209L}$ mutant in the inactive GDP-bound state, indicating that this mutant does cycle back to the inactive form, challenging the traditional paradigm that mutations at Q209 are trapped in the GTP-bound state due to perturbed hydrolysis (Onken et al. 2018). The next study showed that FR inhibits downstream targets of oncogenic Gαq signaling, p-ERK and YAP, in several cells lines (Lapadula et al. 2019). The most recent study expanded these findings to more UVM cell lines and showed that FR inhibited Mel270 xenograft growth (Annala et al. 2019). Taken together, these recent studies highlight the possibility of inhibiting oncogenic Gαq signaling characteristic of UVM and the importance of pursuing this strategy further. Chapter 2 details our recent work that expands upon these findings.

Challenges Facing Therapeutic Potential

Although the two compounds discussed above show promising therapeutic potential there are still some major pitfalls that must be overcome before targeting Gαq is clinically viable. First, the two compounds are commercially limited and difficult to obtain. At the time of writing, YM is available for purchase from Wako pharmaceuticals at $363 per 1mg, with larger amounts available in 10mg quantities ($1200+). The larger quantities required for *in vivo* experimentation make this drug prohibitively expensive for most labs and requires a wait time of 1-3 months for synthesis at 95% purity. Currently, FR900359 is not readily available from reputable manufacturers as many researchers have isolated it from the plant themselves. For our studies we did reach out to a lab about purchasing FR or collaborating but were turned down. To make matters worse, these natural compounds are extremely difficult to synthesize and have only been reported once (Xiong et al. 2016). Despite the many current issues with acquiring these drugs I am hopeful that they will become widely available and more affordable for all the research community.

The second challenge of targeting Gαq with these compounds has to do with the pharmacology. As mentioned above these compounds are very complex and bulky, which will require thorough investigation into the pharmacokinetic and pharmacodynamic properties in humans before clinical application. In our pilot *in vivo* mouse studies, we found that the half-life of YM-254890 after bolus injection was quite short in the bloodstream (data not shown). However, in the liver the half-life was longer, albeit at lower concentrations when compared to the bloodstream. One option for addressing these potential issues is to use targeting mechanisms (nanoparticles etc.) to

deliver the drug more efficiently to the liver or combined the drug with liver directed therapies like liver embolization.

The last major challenge of targeting Gαq is the potency of these compounds. While both molecules effectively inhibit oncogenic Gαq, they are not specific to the oncogenic form and inhibit the wild type protein more potently. This on-target effect raises potential toxicity issues because Gαq is ubiquitously expressed in cells and plays important rolls in many biological processes in the body. The limited therapeutic window will be a difficult challenge to overcome for these molecules however many studies including ours in Chapter 2 have shown that it is indeed possible to target oncogenic Gαq and combination with other therapeutics may prove beneficial.

Thesis Aims

AIM 1: *Generate isogenic cellular system to test Gαq inhibition on different activating mutations found in UVM.*

In the UVM field there are only a couple UVM cell lines publicly available to researchers and generation of new cell lines has proven difficult as there is no standard protocol for generating UVM cell lines from patient samples. The cell lines available all harbor mutations at Q209 in *GNAQ/GNA11* making it impossible to study the rarer mutations in a melanocyte context. To this end, I have generated melanocytes dependent on different mutations in the Gαq signaling pathway to study pathway inhibition and therapeutic efficacy. This includes cell lines driven by rare mutations that are not readily available or

existent in patient derived cell lines. Using YM, a highly specific Gαq inhibitor, I will ask how Gαq inhibition effects different activating mutations in UVM using this syngeneic system. This aim is discussed in further detail throughout Chapter 2 and specifically relates to Figures 2.1 and 2.2.

AIM 2: *Determine the preclinical efficacy of YM-254890 in vivo and potential synegistic combination treaments.*

Expanding on *in vitro* work from **AIM 1** we also wanted to determine if YM has clinical potential and the appropraite dosing schedule for further experimentation. Using the melanocytes I have generated along with UVM cell lines we tested YM's efficacy in mice and it's ability to inhibit tumor growth and signaling in a variety of xenograft experiments. Furthermore, I have shown that combination treatment of YM and MEKi acts synergistically to enhance theraputic efficacy *in vivo*. This aim is discussed in further detail throughout Chapter 2 and has been briefly mentioned in the above section on the "Challenges Facing Theraputic Potential."

AIM 3: *Elucidate other important pathways downstream of Gαq.*

Taking advantage of the ability to inhibit active Gαq I will aim to identify other pathways activated downstream of Gαq using proteomic and transcriptomic approaches. This may provide alternative therapeutic strategies to target this recalcitrant disease. This aim is a continuous process that I am still working on and elude to more in Chapter 3.

CHAPTER 2. COMBINED INHIBITION OF Gαq AND MEK ENHANCES THERAPEUTIC EFFICACY IN UVEAL MELANOMA*

Translational Relevance

All uveal melanoma and a fraction of other melanoma subtypes are driven by activation of the $G\alpha_q$ pathway. There are no clinically efficacious systemic therapies for these melanomas. Recent work has shown promising preclinical activity of natural compounds that directly inhibit $G\alpha_q$, but their clinical use is potentially limited by narrow therapeutic window from inhibition of normal $G\alpha_q$. Here, we describe synergistic efficacy of the $G\alpha_q$ inhibitor YM-254890 and clinically used MEK inhibitors in engineered models driven by distinct mutations in $G\alpha_q$ and in *CYSLTR2* as well as in multiple human uveal melanoma cell lines. Our work suggests that the combination leads to sustained inhibition of the MAPK pathway and synergistic growth inhibition. Combination treatment *in vivo* led to increased MAPK pathway inhibition and tumor shrinkage. Together, this work nominates combination of $G\alpha_q$ and MEK inhibition as a strategy for targeting $G\alpha_q$ driven melanoma clinically.

Abstract

Purpose

All uveal melanoma and a fraction of other melanoma subtypes are driven by activation of the $G\alpha_q$ pathway. Targeting these melanomas has proven difficult despite advances in the molecular understanding of key driver signaling pathways in the disease pathogenesis. Inhibitors of $G\alpha_q$ have shown promising preclinical results, but their

*Hitchman, Tyler D., Gabriella Bayshtok, Emilie Ceraudo, Amanda R. Moore, Cindy Lee, Ruobing Jia, Naitao Wang et al. "Combined Inhibition of Gαq and MEK Enhances Therapeutic Efficacy in Uveal Melanoma." *Clinical Cancer Research* (2020).

therapeutic activity in distinct $G\alpha_q$ mutational contexts and *in vivo* have remained elusive.

Experimental Design

We used an isogenic melanocytic cellular system to systematically examine hotspot mutations in *GNAQ* (*e.g.*, G48V, R183Q, Q209L) and *CYSLTR2* (L129Q) found in human uveal melanoma. This cellular system and human uveal melanoma cell lines were used *in vitro* and *in vivo* xenograft studies to assess the efficacy of $G\alpha_q$ inhibition as a single agent and in combination with MEK inhibition.

Results

We demonstrate that the $G\alpha_q$ inhibitor YM-254890 inhibited downstream signaling and *in vitro* growth in all mutants. *In vivo*, YM-254890 slowed tumor growth but did not cause regression in human uveal melanoma xenografts. Through comprehensive transcriptome analysis, we observed that YM-254890 caused inhibition of the MAPK signaling with evidence of rebound by 24 hours and combination treatment of YM-254890 and a MEK inhibitor led to sustained MAPK inhibition. We further demonstrate that the combination caused synergistic growth inhibition *in vitro* and tumor shrinkage *in vivo*.

Conclusions

These data suggest that the combination of $G\alpha_q$ and MEK inhibition provides a promising therapeutic strategy and improved therapeutic window of broadly targeting $G\alpha_q$ in uveal melanoma.

Introduction

Uveal Melanoma (UVM) is the most common intraocular malignancy with approximately 3,000 new cases per year in the U.S. (Chattopadhyay et al. 2016; Chua et al. 2017). Metastatic UVM has a median survival of less than six months and a five-year survival rate of ~15% (Jovanovic et al. 2013). Unlike cutaneous melanoma, where there has been significant progress in targeted therapy and immunotherapy, there remains no effective systemic therapeutic option for advanced UVM.

UVM is characterized by aberrant activation of the heterotrimeric G-protein alpha-q ($G\alpha_q$) pathway, which canonically activates phospholipase Cβ (PLCB) and downstream effectors, including inositol 1,4,5-triphosphate (IP_3), diacylglycerol (DAG), and protein kinase C (PKC) (Goldsmith and Dhanasekaran 2007). Approximately 90% of UVMs harbor activating mutations in two homologous α subunits of $G\alpha_q$ *GNAQ* and *GNA11;* the remaining cases harbor activating mutations in the upstream G protein-coupled receptor (GPCR) cysteinyl leukotriene receptor 2 (*CYSLTR2*) (Moore et al. 2016; Van Raamsdonk et al. 2010, 2009) and downstream target PLCB4 (Johansson et al. 2016). These mutations are not exclusive to UVM, as they have been identified in a majority of blue nevi, leptomeningeal melanocytic neoplasms (LMNs), hepatic small vessel neoplasms, Sturge-Weber syndrome, and in a small subset of cutaneous and mucosal melanomas (Van Raamsdonk et al. 2009; Möller et al. 2017; Küsters-Vandevelde et al. 2010; Shirley et al. 2013; Sheng et al. 2016; Küsters-Vandevelde et al. 2015; Gill et al. 2016; Joseph et al. 2018). The identification of similar genetic aberrations among these diseases

demonstrates the significance of this pathway and the need for effective therapeutic options against it.

The MAPK pathway is an important downstream signaling output of $G\alpha_q$; prior studies highlighted the high levels of MAPK activity in the absence of canonical drivers found in cutaneous melanoma (Zuidervaart et al. 2005; Van Raamsdonk et al. 2009, 2010). Despite this, single agent MEK inhibitors (MEKi) have failed to provide clinical benefit (Chattopadhyay et al. 2016; Carvajal et al. 2018; Ambrosini et al. 2012). Recent mechanistic studies identified the RAS guanine exchange factor, RasGRP3, as an essential intermediary between $G\alpha_q$ and RAS/MAPK signaling (Moore et al. 2018; Xu Chen et al. 2017). Inhibition of RasGRP3 reduced ERK signaling and cell growth further implicating the dependence of MAPK signaling in UVM (Moore et al. 2018). Promising preclinical studies have pointed to the combination of a pan-PKC inhibitor with MEKi as a potential therapeutic approach. However, clinical applications of these compounds have been hampered by toxicity from pan-PKC inhibition and therefore the lack of therapeutic window (Chattopadhyay et al. 2016; Carvajal et al. 2018; Luke et al. 2015; X. Chen et al. 2014; Ambrosini et al. 2012). Direct inhibition of mutant $G\alpha_q$ signaling could potentially circumvent such toxicity and provide an effective therapeutic window and conceivably durable response. The recent development of allele-specific RAS inhibitors revealed mutations in *KRAS*, another small GTPase can continue to cycle between the GTP-GDP states, albeit at reduced rates compared to wild-type (Moore et al. 2020). In fact, $KRAS^{G12C}$-specific inhibitors, similar to YM, target the GDP-bound state and are efficacious in inhibiting $KRAS^{G12C}$-driven cancers (Lito et al. 2016; Patricelli et al. 2016;

Janes et al. 2018). These studies have shown that direct targeting of a mutant GTPase is not only possible, but highly efficacious in $KRAS^{G12C}$-driven cancers.

YM-254890 (YM) is a naturally-occurring cyclic depsipeptide that inhibits platelet aggregation by perturbing $G\alpha_q$-mediated Ca^{2+} mobilization (Takasaki et al. 2004; Taniguchi, Suzumura, et al. 2003). YM is an allosteric inhibitor that binds to the hydrophobic cleft between two inter-domain linkers of $G\alpha_q$, stabilizing the inactive GDP-bound form by hindering the flexibility of the linkers (Nishimura et al. 2010). YM inhibition of $G\alpha_q$ prevents canonical nucleotide exchange; without binding GTP, the protein is unable to activate downstream signaling partners. Studies have shown YM can act as a therapeutic agent for inhibition of platelet aggregation and hypocalcemia (Uemura, Kawasaki, et al. 2006; Roszko et al. 2017; Uemura, Takamatsu, et al. 2006). However, initial studies using overexpression systems indicated YM was unable to inhibit mutant $G\alpha_q^{Q209L}$ (Takasaki et al. 2004). The lack of inhibition was hypothesized to be due to the reduced GTPase activity of the $G\alpha_q^{Q209L}$ mutant preferentially locking the mutant protein in the GTP-bound state, similar to the paralogous $G\alpha_s^{Q227L}$ mutant (Graziano and Gilman 1989). Three recent studies have highlighted the use of FR900359 (FR), an analog of YM, to directly target Q209-mutant $G\alpha_q$. These studies demonstrated FR's ability to inhibit signaling and growth in Q209 mutant UVM cell lines, and efficacy against one human xenograft model (Onken et al. 2018; Lapadula et al. 2019; Annala et al. 2019). These reports illustrate direct inhibition of Q209 mutant $G\alpha_q$ as a potential therapeutic avenue for UVM. However, both YM and FR are potent inhibitors of physiologically active wild-type $G\alpha_q$ signaling (Takasaki et al. 2004; Taniguchi, Suzumura, et al. 2003; Nishimura et al. 2010; Schrage et al. 2015), which raises concerns of therapeutic window of YM and

FR in targeting mutant $G\alpha_q$ in UVM. Thus, discovery of novel synergistic combinations that can potentiate therapeutic efficacy and broaden the therapeutic window of YM or FR is imperative. Furthermore, there remains a need for a comprehensive understanding of direct $G\alpha_q$ inhibition across the mutational landscape of UVM.

Here, we identified a novel *GNAQ* mutational hotspot, G48, and showed exogenous expression of *GNAQ*^{G48V}, similar to the canonical *GNAQ* mutants, transformed melanocytes. We demonstrated YM effectively inhibited cellular growth and downstream $G\alpha_q$ signaling in four UVM mutants, *GNAQ* (G48V, R183Q, Q209L) and *CYSLTR2* (L129Q). We further confirmed the efficacy of YM in a series of *in vivo* experiments with human UVM cell lines harboring $G\alpha_q^{Q209}$ mutations. Furthermore, transcriptomic and synergistic analysis revealed that together, YM and MEKi led to enhanced and sustained inhibition of MAPK signaling to significantly decrease tumor growth. These results suggest direct $G\alpha_q$ inhibition provides an effective therapeutic strategy in UVM and synergizes with MEKi to further increase therapeutic potential.

Methods

Study approval

MSK-IMPACT testing for UVM patients was ordered by the treating physician who signed informed consent to research protocol (ClinicalTrials.gov, NCT01775072). All animal studies were performed in accordance to MSKCC IACUC 11-12-029.

Drugs and Chemicals

YM-254890 was purchased from Wako Pure Chemical Industries (CAT# 257-00631). MEK162 (binimetinib) was purchased from Array BioPharma Inc. Trametinib was purchased from Selleck Chemicals (Catalog No. S2673).

Mutational Analysis

For the MSKCC uveal melanoma cohort, all patients provided informed consent for tissue procurement and mutational testing, and the study was approved by the institutional review board (ClinicalTrials.gov, NCT01775072). Patients had a confirmed diagnosis of uveal melanoma. A total of 124 specimens from 116 patients were analyzed including 47 specimens from primary UVM and 77 from metastasis (56 liver, 6 lymph node, 5 lung, 10 other). In the 7 patients with multiple samples, the $G\alpha_q$ mutational status were identical. Tumor samples were sequenced using MSK-IMPACTv3, v5, or v6 that captures 341, 410, and 468 genes respectively. The MSK-IMPACT panel includes GNAQ and GNA11 in all versions and CYSLTR2 was added to v6.

For integrative analysis of published cohorts, Level 2 whole-exome mutational data were downloaded from the NIH TCGA server. Processed whole-exome sequencing data from the UNI-UDE (n = 22) and MDACC/MEEI (n = 52) uveal melanoma cohorts and processed whole-genome sequencing data from the CRUK (n = 12) and QIMR (n = 28) cohorts were extracted from the supplementary tables of relevant publications (20-24). For downstream analysis, we merged the data for 3 duplicate samples present in both the CRUK and TCGA databases and removed 3 samples from the QIMR database that lacked any somatic mutations, leaving 188 samples. The OncoPrint was generated using MSKCC cBioPortal.

Exogenous Gene Expression

For transient transfection experiments in HEK-293T, we used a synthetic gene for codon optimized *CYSLTR2* (5) and WT cDNA for *GNAQ* (cDNA.org). We performed site-directed mutagenesis to generate mutants Q209L, R183Q and G48V using QuickChange (Agilent Technologies) site-directed mutagenesis. HEK-293T cells were transiently transfected with the plasmids encoding for GNAQ WT and mutants subcloned into pcDNA3.1(+) using Lipofectamine according to the manufacturer's instructions. Briefly, 7,000 HEK-293T cells were transfected in low-volume 384-well plates with 11 ng of total DNA/well for 24 hours.

For stable expression in melan-a cells, we employed human cDNAs for *CYSLTR2* and *GNAQ* obtained from Origene, mutagenized using QuickChange and cloned into the retroviral vector MSCV-Puro (Addgene plasmid #68469) (Akama-Garren et al. 2016). $NRAS^{Q61K}$ (Addgene plasmid #49404) and MEKDD (Addgene plasmid #15268) (Boehm et al. 2007) constructs for rescue experiments were purchased from addgene. Retroviral production was performed through transfection of retroviral expression vector with the pCl-Ampho packaging vector with X-tremeGENE 9 (Sigma-Aldrich). QuikChange primers were used to introduce the various mutant constructs. All constructs were confirmed by sequencing. Site directed mutagenesis primers are listed in **Supplementary Table S1.**

Cell Culture

Mutation dependent melan-a cells were generated by transducing cells with cDNAs in MSCV-PURO (retrovirus) and then selecting cells with puromycin (1µg/ml) for two days.

TPA (Sigma-Aldrich) was then withdrawn from cultures. Cells with activating mutations ($CysLT_2R^{L129Q}$, $GNAQ^{G48V/R183Q/Q209L}$, $KRAS^{G12V}$, $BRAF^{V600E}$, and $NRAS^{Q61K}$) continued to proliferate over several passages (>2 weeks). Vector and WT controls were unable to maintain proliferation or pigmentation after a few passages without TPA. All cells were cultured in media containing 10% FBS, L-glutamine (2nM), penicillin (100U/ml), streptomycin (100 µg/ml). Melan-a cells provided by D. Bennett, St. George's Hospital, University of London were cultured in RPMI supplemented with 200nM TPA unless otherwise noted (Bennett, Cooper, and Hart 1987). HEK-293T (from ATCC) and A375 cells were cultured in DMEM and UVM cells were cultured in RPMI. All cells tested negative for mycoplasma. Human UVM cell lines Mel202, OMM1.3, and OMM1 were described previously (Moore et al. 2018) and MP41 was purchased from ATCC (CRL-3297).

Cell Growth Assays and Dose Response Curves

Cell growth and dose response curves for YM were assayed using CellTiter-Glo 2.0 (Promega) and readout on a Glomax Luminometer (Promega). For growth assays, melan-a cells were seeded in the absence of TPA, 1,000 cells/well in a 96-well plate and then counted on days 1, 3, and 6. Growth assays were baselined to day 1 readings. For dose response curves melan-a and human UVM cells were seeded 1,000-3,500 cells/well in a 96-well plate and treated 24 hours later with YM for 5 days. Data was baselined to vehicle. Growth assays and dose response curves were analyzed and IC_{50} values calculated using GraphPad Prism 7.0 software. Data shown is representative of at least three independent experiments with at least three technical replicates.

Crystal Violet Growth Assay

Cells were seeded in 12- or 6-well plates, media and drug were replenished every two days. Cells were washed twice with ice cold 1X PBS, fixed with ice cold 100% methanol, and stained with 0.5% crystal violet (sigma) solution in 25% ethanol. Plates were imaged with a GELCOUNT (Oxford Optronix).

Drug Synergy Analysis

Synergy assays were performed in 96 well plates (1,000-3,000 cells/well) for 5 days with Trametinib and YM, readout by CellTiter-Glo 2.0. Viability was baselined to vehicle (100%), input into Combenefit software to obtain HSA synergy and viability plots (Di Veroli et al. 2016). Data shown is representative of at least three independent experiments with three technical replicates.

Mouse experiments

For melan-a allograft studies, 2.0×10^6 cells were resuspended in 100µL of 1:1 mix of RPMI media and Matrigel (BD Biosciences) and subcutaneously injected into 6-8-week-old C57BL/6J mice (Jackson Laboratory). For Mel202 xenograft studies, 3.0×10^6 cells were injected into 6-8-week-old CB17-SCID mice (Taconic). Tumor sizes were measured twice a week with calipers starting from three weeks post graft and were calculated using the following formula: tumor volume = (D2 × d2× h2)/6, whereby D, d and h refers to long diameter, short diameter and height of the tumor, respectively. Treatment began at a tumor size of ~100mm^3. Mice were treated with YM-254890 (daily intraperitoneal

injection), binimetinib (twice daily oral gavage), a combination of both drugs, or a matched vehicle (0.5% DMSO in 1X PBS and 1% Carboxymethyl cellulose + 0.5% Tween 80 in ddH_2O, or both, respectively). Mice were treated for five days and then given two days for recovery for the length of the experiment. Mice were euthanized in response but not limited to the following: tumor ulceration, tumors located too close to the trunk of the mice to impede movement and blood flow, and tumor burden. For all experiments, mice were grafted double flank, except Figure 2.6A (single flank).

Luciferase Imaging

OMM1.3 cells were transduced with pBMN (CMV-copGFP-Luc2-Puro) for luciferase expression (Addgene plasmid # 80389) (Jin et al. 2016). OMM1.3 xenografts were setup the same as Mel202 grafts described above. Treatment was started 3 days after grafting, following the methods described above. Mice were injected with 15mg/ml D-luciferin potassium salt (GoldBio) in 1X PBS and imaged 15 minutes later using Xenogen IVIS Spectrum. The raw photon flux was calculated using Living Image 4.4 Software and baselined to day 1 readings.

Western Blotting Analysis

Cell lysates were harvested after indicated treatments as previously described (Moore et al. 2018, 2016). For western blots of OMM1.3 tumors, mice were treated once (q.d.) with vehicle, YM, binimetinib, or combo and then scarified four hours later. For western blots of Mel202 tumors, mice were treated with vehicle, YM (q.d.), binimetinib (b.i.d), or combo for a week and then scarified four hours after the last treatment. Tumor lysates were

generated as previously described (Moore et al. 2018). Primary antibodies were incubated at a 1:1,000 dilution, unless noted otherwise. Western blot antibodies are listed in **Supplementary Table S2**.

Immunohistochemistry

All tissues were fixed at 4°C overnight in 4% paraformaldehyde. Tissue processing, embedding, sectioning, and H&E staining were performed by Histoserv. Staining was done as previously described (Moore et al. 2018). IHC antibodies and dilutions are listed in **Supplementary Table S3.**

RNA Isolation and qRT-PCR

RNA was extracted from cells using Trizol (Invitrogen) following the manufacturers standard Trizol extraction protocol. 2 µg of RNA from each sample was reverse transcribed to cDNA using the High Capacity cDNA Reverse Transcription Kit (Applied Biosystems). Power SYBR Green PCR Master Mix (Applied Biosystems) was then used for PCR on a QuantStudio 6 Flex System (Applied Biosystems). Expression was normalized to ribosomal protein RPL27. Relative expression of mRNA was plotted as $2^{-\Delta\Delta Ct}$ and each experiment was performed in triplicate and repeated in at least three independent experiments. qRT-PCR primers are listed in **Supplementary Table S4.**

Bioinformatics Analysis

TCGA uveal melanoma (UVM) and skin cutaneous melanoma (SKCM) mutational and RNA-seq data were download from cBioPortal (www.cbioportal.org) using the

PanCancer Atlas Version. The six SKCM samples with GNAQ or GNA11 Q209L mutations are TCGA-RP-A6K9-06, TCGA-RP-A690-06, TCGA-ER-A3ET-06, TCGA-ER-A3ES-06, TCGA-ER-A2NF-06, TCGA-ER-A2NF-01. All RNA-seq was performed by MSKCC genomics core facility using poly-A capture. The libraries were sequenced on an Illumina HiSeq-2500 platform with 50 bp paired-end to obtain a minimum yield of 40 million reads per sample. The sequence data for all melan-a cells were mapped to the mouse reference genome (GRCm38), whereas, Mel202 and OMM1.3 were mapped to the human reference genome (GRCh38) using STAR v2.330 (Dobin et al. 2013). Gene counts were quantified using STAR to Ensembl gene annotations GRCm38.91 and GRCh38.90 for mouse and human samples, respectively. Counts were r-log transformed using DESeq2 (Love, Huber, and Anders 2014). Hierarchical clustering and heatmaps of wild-type melan-a cells grown in TPA and $GNAQ^{Q209L}$ and $KRAS^{G12V}$ transduced melan-a cells grown without TPA was performed on r-log transformed genes with STDEV>1.5 using Partek Genomics Suite. K-means clustering and heatmaps of drug treated melan-a and human uveal melanoma cells were performed on r-log transformed, Z-scored (mean = 0, stdev = 1), and then partition clustered (k-means) were performed using Partek Genomics Suite. Sum Z-scores were calculated by adding transformed gene expression data from the specified gene signatures. Gene sets are listed in **Supplementary Table S5**. Cluster and gene set (Hallmark) enrichment analysis were obtained from https://www.gsea-msigdb.org/gsea/index.jsp and are shown in **Supplementary Table S6-S11**. Raw and processed data are deposited in Gene Expression Omnibus (GEO) Accession #: GSE152705 and GSE160112.

IP_1 Accumulation Assay

IP_1 concentrations in transfected HEK-293T cells, stably transduced melan-a cells, and uveal melanoma cells were measured using a competitive homogenous time resolved fluorescence (HTRF) assay (CisBio). Briefly, 7,000 transiently transfected HEK-293T cells, 5,000 melan-a cells and 5,000 uveal melanoma cells were seeded in low-volume 384-well plates in 7 µL media for 24 hours prior to YM treatment. Cells were then treated with various concentrations of YM at 37°C for 3 or 24 hours. 1 hour and 45 minutes prior lysis, cells were supplemented with 1X Stimulation Buffer provided by the manufacturer (HEPES 10 mM, CaCl2 1 mM, MgCl2 0.5 mM, KCl 4.2 mM, NaCl 146 mM, glucose 5.5 mM, LiCl 50 mM, pH 7.4) with 0.2% BSA and 50 mM of LiCl (to prevent IP_1 degradation). Following incubation, cells were lysed by addition of 3 µL/well of d2-labeled IP_1 analogue as the fluorescence acceptor and the Terbium cryptate-labeled anti-IP1 mAb as the fluorescence donor, diluted in the kit-supplied lysis buffer. The plates were incubated overnight at RT and time-resolved fluorescence signals were read using the BioTek Synergy NEO plate reader (BioTek Instruments, Winooski, VT) at 620 nm and 665 nm. Results were calculated as a 665nm/620nm signal ratio, and IP_1 concentrations were interpolated from a standard curve prepared using the supplied IP_1 calibrator. Results are shown as IP_1 (nM). Dose response curves and bar graphs were analyzed using GraphPad Prism 7.0 software.

Statistical analysis

All statistical comparisons were done with Graphpad Prism 7.0 software and used a two-tailed Student's t-test for comparison between groups. Data is shown as the mean ± SEM

(unless otherwise noted) from triplicate samples from at least three independent experiments. P less than 0.05 was used to designate significance. Significant differences between groups are indicated by $P > .05$; ns, $P < 0.05$; *, $P < 0.005$; **, $P < 0.0005$; ***, $P < 0.0001$, ****.

Results

$G\alpha_q$ mutations occur at three hotspot residues that are known to perturb GTP hydrolysis

We examined the $G\alpha_q$ pathway mutations from a series of 116 consecutive patients with UVM seen at Memorial Sloan Kettering Cancer Center (MSKCC) and who had undergone clinical sequencing on the MSK-IMPACT platform (Zehir et al. 2017). Similar to previously reported cohorts, 107 of 116 patients harbored mutually exclusive activating mutations in either *GNAQ* or *GNA11* and two patients had a *CYSLTR2*^{L129Q} mutation (**Figure 2.1A**) (Moore et al. 2016). For *GNAQ*, in addition to previously known recurrent mutations at amino acids Q209 and R183, one sample harbored a novel G48L mutation. To further evaluate the *GNAQ*^{G48} mutation, we next integrated 188 uveal melanoma patients from 5 published whole-exome or whole-genome uveal melanoma cohorts (Robertson et al. 2017; Furney et al. 2013; Johansson et al. 2016; Martin et al. 2013; Johnson et al. 2017). We identified two patients with *GNAQ*^{G48L} and one patient with a *GNAQ*^{G48V} mutation, indicating G48 as a third mutational hotspot in *GNAQ* (**Figure 2.1B**). The codon G48 resides in the phosphate binding loop (P-loop) of $G\alpha_q$ and is paralogous to codon G12 in RAS GTPases, which is frequently mutated in various cancers (Moore et al. 2020). Furthermore, the paralogous G47V mutation in *GNAS*

exhibits constitutive activity (Graziano and Gilman 1989). Structural studies of active $G\alpha_q$ illustrate G48 of the P-loop, R183 of switch I, and Q209 of switch II are in spatial proximity adjacent to the nucleotide-binding pocket (**Figure 2.1C**) (Taylor, Bommarito, and Tesmer 2016), indicating mutations in G48, like Q209 and R183 would hinder GTPase activity.

Generation of isogenic melanocytes dependent on mutations found in UVM

To determine the role of distinct UVM driver mutations in a genetically defined context, we stably expressed human cDNAs encoding *CYSLTR2*^{L129Q}, *GNAQ*^{G48V}, *GNAQ*^{R183Q}, *GNAQ*^{Q209L}, WT controls, as well as *BRAF*^{V600E}, *KRAS*^{G12V}, and *NRAS*^{Q61K} in melan-a cells **(Supplementary Figure S1A and S1B)** (Bennett, Cooper, and Hart 1987). BRAF^{V600E}, KRAS^{G12V}, and NRAS^{Q61K} hyperactivate the RAS-RAF-MEK-ERK kinase (MAPK) signaling pathway, distinct from the GPCR-$G\alpha_q$-PLCβ signaling axis. Melan-a cells are immortalized mouse melanocytes that require media supplemented with 12-O-tetradecanoyl-phorbol-13-acetate (TPA), a DAG analog, for continued proliferation and are characterized by pigmentation and melanocytic morphology (Bennett, Cooper, and Hart 1987; Moore et al. 2016). After TPA withdrawal, melan-a cells expressing empty vector, *CYSLTR2*^{WT} or *GNAQ*^{WT} lost pigmentation and eventually growth arrested **(Figure 2.1D and 2.1E; Supplementary Figure S1C)**. However, cells expressing activating mutations of *GNAQ* and *CYSLTR2* exhibited TPA-independent growth and enhanced melanocytic features (e.g. dark pigmentation, enlarged melanosomes). Interestingly, expression of *BRAF*^{V600E}, *KRAS*^{G12V}, and *NRAS*^{Q61K} that hyperactivate MAPK signaling also conveyed TPA-independence but failed to maintain pigmentation **(Figure 2.1D and 2.1E; Supplementary Figure S1C and S1D)**.

We next examined the ability of $G\alpha_q$ to stimulate PLCβ and generate IP_3, by measuring accumulation of the IP_3 degradation product IP_1. Melan-a cells expressing *CYSLTR2*^{L129Q} and all three *GNAQ* mutations exhibited enhanced IP_1 accumulation, whereas the *CYSLTR2*^{WT}-, *GNAQ*^{WT}-, *BRAF*^{V600E}-, *KRAS*^{G12V}-, and *NRAS*^{Q61K}-expressing cells did not, indicating that this cellular system faithfully recapitulates the distinct signaling pathways driven by $CysLT_2R$ and $G\alpha_q$ oncoproteins (**Figure 2.1F; Supplementary Figure S1E**). Western blot analysis of melan-a cells following TPA-withdrawal showed that UVM associated $CysLT_2R$ and $G\alpha_q$ oncoproteins maintained expression of melanocyte markers MITF, c-KIT, TRP2/DCT, and RASGRP3 (UVM specific), whereas wild-type CYSLTR2^{WT}, GNAQ^{WT}, KRAS^{G12V}, and NRAS^{Q61K} did not (**Figure 2.1G; Supplementary Figure S1F**). In TCGA datasets, we found these genes (MITF, KIT, DCT, and RASGRP3) were expressed higher in uveal melanoma (UVM) and $G\alpha_q$ -mutated skin cutaneous melanoma (SKCM) compared to RAS/RAF mutated SKCM (**Supplementary Figure S1G**), suggesting that the engineered melan-a cells capture important oncogene-specific biology of human melanomas (Moore et al. 2016, 2018).

To determine the transcriptome response to expression of activated $G\alpha_q$ and RAS/RAF pathway in melan-a cells, we performed RNA-seq in wild-type melan-a cells grown in TPA, melan-a expressing *GNAQ*^{Q209L} and melan-a expressing *KRAS*^{G12V} cells after TPA-withdrawal. Unsupervised hierarchical clustering showed wild-type cells in TPA were more similar with *GNAQ*^{Q209L} cells than *KRAS*^{G12V} cells, consistent with direct $G\alpha_q$ signaling to phospholipase C-beta to generate DAG and IP3 (**Supplementary Figure S1H**). To determine pathways activated in these melan-a lines, we performed enrichment analysis of gene ontology (GO), Hallmark, and KEGG gene sets as well as custom gene

sets defined by genes differentially expressed between human $G\alpha_q$ vs BRAF/NRAS/KRAS mutated melanoma from TCGA uveal and cutaneous melanoma datasets (Robertson et al. 2017; Akbani et al. 2015) and by genes differentially expressed in genetically engineered mouse melanoma in $Bap1^{KO}$;$Gna11^{Q209L}$ vs $Bap1^{KO}$;$BRAF^{V600E}$ mice (Moore et al. 2018). We found that *GNAQ*^{Q209L} melan-a cells had increased expression of genes in human $G\alpha_q$ mutated melanomas and mouse $Bap1^{KO}$;$Gna11^{Q209L}$ tumors while *KRAS*^{G12V} melan-a cells had increased expression of genes in human RAS/RAF mutated tumors and mouse $Bap1^{KO}$;$Braf^{V600E}$ tumors (**Supplementary Figure S1I**). In addition gene sets including calcium mediated signaling and melanogenesis were strongly enriched in $GNAQ^{Q209L}$ cells, whereas MAPK signaling was enriched in $KRAS^{G12V}$ cells (**Supplementary Figure S1I**). (Moore et al. 2018). These data indicate $G\alpha_q$ activation generates a distinct oncogenic phenotype that maintains melanocyte lineage specification, and is consistent with previous observations in genetically engineered murine models of UVM (Moore et al. 2018; Huang, Urtatiz, and Van Raamsdonk 2015). This system of engineered mutant oncoprotein-transformed melanocytes allows for context-relevant systematic evaluation of $G\alpha_q$-pathway activating mutations that are not available in human cancer cell lines or patient-derived xenograft (PDX) UVM models.

YM-254890 inhibits mutation dependent melan-a cells *in vitro* and *in vivo*

We next determined the ability of YM to inhibit the activity of distinct UVM mutations. Since YM is thought to stabilize the GDP-bound state of $G\alpha_q^{WT}$, we hypothesized $CysLT_2R^{L129Q}$ would be particularly sensitive to YM. First, we tested the ability of YM to

inhibit $G\alpha_q$ signaling in a panel of HEK-293T cells transfected with oncoprotein cDNA constructs and assayed the dose response of IP_1 accumulation 24-hours following treatment of YM. In this system, $CysLT_2R^{L129Q}$ and $G\alpha_q^{G48V}$ appeared to be most sensitive to YM with subnanomolar potency (**Supplementary Figure S2A**). $G\alpha_q^{R183Q}$ was ~20-fold less sensitive to YM compared to $CysLT_2R^{L129Q}$ and $G\alpha_q^{G48V}$, whereas $G\alpha_q^{Q209L}$ was the least sensitive to YM and its signaling was incompletely inhibited within 24-hour YM treatment, consistent with previous reports (**Supplementary Figure S2A**) (Takasaki et al. 2004).

Transient transfection experiments in HEK-293T cells result in non-physiologic overexpression of oncoproteins and can lead to misleading observations. In the more physiologic context of $G\alpha_q$ pathway mutant-transformed melan-a cells, when we assayed IP_1 after 3 hours of treatment, rapid reduction of IP_1 was observed with UVM oncoproteins except $G\alpha_q^{Q209L}$, which achieved only half-maximal inhibition **(Figure 2.2A)**. Interestingly, 24-hour treatment with YM completely inhibited IP_1 accumulation across all UVM activating mutants, including $G\alpha_q^{Q209L}$. $CysLT_2R^{L129Q}$ and $G\alpha_q^{G48V}$ were most sensitive to YM, whereas $G\alpha_q^{R183Q}$ and $G\alpha_q^{Q209L}$ mutants were approximately 10-fold less sensitive **(Figure 2.2A)**. These data suggest activating $G\alpha_q$ mutants, while prominently GTP-bound, undergo GTP hydrolysis, albeit presumably at decreased levels compared to wild-type, allowing for YM to bind in the $G\alpha_q$ GDP-state, reminiscent of covalent $KRAS^{G12C}$ inhibitors (Nishimura et al. 2010; Lito et al. 2016; Patricelli et al. 2016; Janes et al. 2018).

We next assayed the effect of YM on downstream $G\alpha_q$ signaling, including RASGRP3 phosphorylation by PKC, MAPK signaling by CRAF, MEK, and ERK phosphorylation and cyclin D1 expression that integrates signaling to promote cell cycle

progression. YM inhibited these downstream signaling targets, with slower kinetics in $G\alpha_q^{R183Q}$ and $G\alpha_q^{Q209L}$ expressing cells compared to $CysLT_2R^{L129Q}$ and $G\alpha_q^{G48V}$ expressing cells (**Figure 2.2B**), consistent with the IP_1 biochemical assay. Since TPA is a DAG analog and acts downstream of $G\alpha_q$, supplementing it in the media restored downstream signaling targets 24 hours after YM treatment (**Figure 2.2B**). YM was ineffective in inhibiting MAPK signaling in $BRAF^{V600E}$, $KRAS^{G12V}$, and $NRAS^{Q61K}$-expressing cells (**Supplementary Figure S2B**), confirming the specificity of YM to $G\alpha_q$ inhibition. Expressing $KRAS^{G12V}$ in $CysLT_2R^{L129Q}$ and $G\alpha_q^{Q209L}$ melan-a cells rescued YM-mediated MAPK inhibition (**Supplementary Figure S2E**). We next examined if YM could effectively inhibit TPA-independent cell growth in the engineered melan-a cells. Consistent with IP_1 accumulation, all UVM activating mutants were highly sensitive to YM. $CysLT_2R^{L129Q}$ and $G\alpha_q^{G48V}$ cells exhibited low-nanomolar sensitivity to YM, and the $G\alpha_q^{R183Q}$- and $G\alpha_q^{Q209L}$-expressing cells were modestly less sensitive, whereas the $BRAF^{V600E}$, $KRAS^{G12V}$, and $NRAS^{Q61K}$ -expressing cells were insensitive (**Figure 2.2C; Supplementary Figure S2C**). TPA supplementation or $KRAS^{G12V}$ expression rescued YM-mediated growth inhibition in $CysLT_2R^{L129Q}$-expressing cells (**Supplementary Figure S2D**).

We performed pilot pharmacokinetic studies suggesting YM has a short serum half-life in mice (data not shown). However, given its potency, YM may engage and inhibit $G\alpha_q$ more durably. We thus performed a pharmacodynamic study examining downstream signaling in $CysLT_2R^{L129Q}$ cells allografted into C57BL/6J mice. After a single dose of YM given at 7.5 mg kg^{-1} intraperitoneally, we observed inhibition of downstream signaling in $CysLT_2R^{L129Q}$ tumors as early as 30 minutes **(Figure 2.2D)**. By 24 hours, a sustained

decreased in ERK phosphorylation and cyclin D was observed despite rebound of CRAF phosphorylation. We observed a paradoxical increase in RASGRP3 phosphorylation levels which may indicate feedback activation in this model.

Given these data, we proceeded to dose YM daily and assessed efficacy. We observed YM significantly inhibited tumor growth of $CysLT_2R^{L129Q}$ or $G\alpha_q^{Q209L}$ allografts **(Figure 2.2E and 2F)**. Importantly, YM treatment did not cause adverse effects such as weight loss **(Supplementary Figure S2F and S2G)**. These data suggest YM is a highly selective inhibitor against $G\alpha_q$ signaling and can effectively inhibit proliferation both *in vitro* and *in vivo*.

YM-254890 inhibits growth of human UVM cells and xenograft models

Given the sensitivity of all three activating hotspot mutations to YM, including the most common *GNAQ*^{Q209L} mutation, in the melan-a system, we proceeded to study the effect of YM on a panel of human UVM cell lines that harbor *GNAQ*$^{Q209L/P}$ or *GNA11*^{Q209L} mutations and A375 (*BRAF*^{V600E}) cutaneous melanoma cell line as control. UVM cells exhibited high basal activity of IP_1 accumulation, which was inhibited upon YM treatment at 24 hours **(Figure 2.3A; Supplementary Figure S3A)**. Analysis of downstream signaling showed RASGRP3, MAPK output, and cyclin D1 proteins were inhibited in UVM cells, but not in A375 cells, upon treatment with YM **(Figure 2.3B; Supplementary Figure S3B)**. Expressing $NRAS^{Q61K}$ or MEK^{DD} in UVM cells completely rescued YM-mediated MAPK inhibition **(Supplementary Figure S3G)**. In OMM1.3 and Mel270 cells, treatment with YM rapidly inhibited the MAPK pathway while suppression of the intermediary target, p-RASGRP3, required prolonged drug exposure. In contrast, YM

treatment in Mel202 cells showed potent inhibition of p-RASGRP3 at early time points, but the MAPK pathway was only mildly inhibited; p-ERK1/2 rebounded by 24 hours. These results indicate UVM cells may have different wiring downstream of $G\alpha_q$. Regardless, YM potently and effectively inhibited cell viability in $G\alpha_q$ mutant UVM cell lines but not A375 cells (**Figure 2.3C; Supplementary Figure S3C and S3D)**. TPA supplementation, $NRAS^{Q61K}$, or MEK^{DD} expression rescued YM-mediated growth inhibition in UVM cells **(Supplementary Figure S3C, S3E, and S3F)**.

We next used a UVM xenograft model to test the efficacy of YM *in vivo*. In mice with xenografts of OMM1.3 cells, YM inhibited tumor formation compared to vehicle and no adverse weight loss was observed **(Figure 2.3D; Supplementary Figure S3H)**. Taken together, these data indicate that $G\alpha_q$ inhibition is effective against human UVM xenografts *in vivo*, in agreement with previously reported data using FR (K. G. Griewank et al. 2012).

$G\alpha_q$ inhibition and MEKi synergistically sustain MAPK inhibition and suppress growth in UVM models

To gain further mechanistic insight, we compared the transcriptional response to YM with that of trametinib treatment for 4- or 24-hours in the $CysLT_2R^{L129Q}$ melan-a cells. Perturbed genes were partitioned into six clusters by *k*-means clustering algorithm **(Figure 2.4A).** Genes downregulated by either YM or trametinib behaved similarly to one another (Clusters 1, 2, 3), whereas upregulated genes were distinct (Clusters 4, 5, 6). We then computed the top five GSEA HALLMARK gene set overlaps with each cluster to better understand the impact of treatment on these clusters (**Supplementary Figure**

S4A). YM, similar to trametinib, effectively inhibited the cell cycle progression (E2F targets) of $CysLT_2R^{L129Q}$ cells at 24-hours (cluster 1; **Figure 2.4B**). However, trametinib more potently suppressed KRAS and inflammatory signaling than YM (cluster 2; **Figure 2.4B; Supplementary Figure S4A)**. To further understand the suppression of KRAS genes, we used a 52-gene set comprised of genes rapidly downregulated by MEK inhibition in melanoma cells (Pratilas et al. 2009), PRATILAS_MAPK signature. This gene signature was downregulated by both YM and trametinib at 4 hours, but by 24 hours, genes rebounded with YM treatment while trametinib further suppressed this gene signature (**Figure 2.4C**). Specifically, this rebound pattern was seen in MAPK signaling output genes *DUSP6* and *SPRY2/4* **(Figure 2.4D)**. This suggests that YM does not durably suppress MAPK signaling at 24 hours, potentially limiting therapeutic effect.

This prompted us to ask whether YM could be used in combination with MEKi to prevent potential MAPK rebound and induction. In our melan-a cellular system, we found significant synergy in an HSA assay between YM and trametinib in cells dependent on *CYSLTR2* or *GNAQ* mutants but not in melan-a cells still dependent on TPA **(Figure 2.4E; Supplementary Figure S4B)**. Long term treatment of YM plus trametinib greatly reduced proliferation of $CysLT_2R^{L129Q}$ cells at 26 days compared to single agent treatments **(Figure 2.4F)**. In melan-a cells with TPA, only trametinib showed long term effects on proliferation. Combination treatment in $CysLT_2R^{L129Q}$ melan-a cells led to rapid MAPK signaling inhibition that was sustained for 72 hours, whereas p-ERK had returned to basal levels in single treatment groups **(Figure 2.4G)**. To further investigate these findings, we used UVM cell lines to assess the effect of YM and MEKi on viability, transcriptomics, and signaling. We performed HSA synergy assays on four UVM cell lines and found significant

synergy between YM and trametinib **(Figure 2.5A; Supplementary Figure S5A)**. Growth assays in these UVM cell lines showed variable sensitivity to either YM or MEKi, but combination of the two drugs lead to fewer colonies than single agents in all UVM cells **(Figure 2.5B)**. However, $BRAF^{V600E}$ mutant A375 cells did not show synergy and only showed sensitivity to MEKi and combination with YM did not lead to a decrease in colonies (**Supplementary Figure S5B and S5C)**.

To better understand the synergistic effect of the combination, we performed RNA-seq in two human UVM cell lines treated with vehicle, single agent YM or trametinib, or a combination of both for 24 hours **(Supplementary Figure S5D and S5E)**. Similar to the melan-a cells, we observed trametinib suppressed the PRATALIS_MAPK gene signature with a greater effect than YM **(Figure 2.5C)**. Combination resulted in more dramatic gene expression changes when compared to single agent or vehicle and also led to greater inhibition of MAPK, cell cycle, and MYC gene sets, with the exception of cell cycle in Mel202 cells (**Figure 2.5C; Supplementary Figure S5D and S5E)**. Specifically, combination led to greater suppression of MAPK signaling output genes *DUSP6* and *SPRY2/4* **(Figure 2.5D)**. This transcriptomic data indicates that YM and trametinib have very similar effects on gene expression, however combination of the drugs further enhances the effects on gene expression.

We next determined the effects of YM, trametinib and combination treatment on signaling. In Mel202 cells, YM treatment alone inhibited RASGRP3, CRAF, and MEK phosphorylation at all time points but downstream ERK and cyclin D inhibition was modest **(Figure 2.5E)**. Trametinib treatment alone inhibited ERK phosphorylation at 24 hours with rebound by 48 hours, and combination treatment sustained robust inhibition at all

timepoints. Similarly, in OMM1.3 and MP41 cells, YM single agent was very effective at inhibiting RASGRP3, CRAF, and MEK phosphorylation but ERK phosphorylation rebounded by 72 hours **(Figure 2.5F and 5G)**. Combination treatment led to sustained inhibition of ERK phosphorylation and cyclin D. Expression of $KRAS^{G12V}$ in OMM1.3 cells was sufficient to rescue YM-mediated p-ERK inhibition, but not trametinib- or combination-mediated p-ERK inhibition **(Supplementary Figure S5F)**. These data suggest that $G\alpha_q$ and MEK inhibition are more effective against UVM cell growth and signaling than single agents, indicating that combination therapy may have an increased clinical benefit.

In vivo combination of YM-254890 and binimetinib inhibits tumor growth and potently suppresses the MAPK pathway

We tested the combination of YM with an FDA-approved MEK inhibitor binimetinib *in vivo*. Using the $G\alpha_q^{Q209L}$ melan-a allograft model, we tested the combination on immunocompetent C57BL/6J mice treated over the course of 20 days. Mice treated with YM or binimetinib alone had a significant inhibition in tumor growth, with about a two-fold increase compared to day one size **(Figure 2.6A)**. However, combination treatment led to significant tumor reduction compared to vehicle or single agents **(Figure 2.6A)**. Similarly, we found that the combination greatly reduced tumor growth in the $CysLT_2R^{L129}$ allograft model. **(Figure 2.6B)**. No treatment group resulted in weight loss **(Supplementary Figure S6A and S6B)**. These experiments show that together, YM and MEKi further reduced tumor burden in allograft models driven by two different activating mutations found in patients.

In the OMM1.3 luciferase xenograft model, single agent treatments did inhibit growth, but combination treatment decreased tumor luminescence by 1000-fold, and we were unable to identify the grafts at the end of treatment **(Figure 2.6C; Supplementary Figure S6C)**. OMM1.3 tumors from mice treated for 4 hours showed that combination potently inhibited both PKC and MAPK signaling **(Figure 2.6D)**. Single agent binimetinib inhibited p-ERK but increased p-MEK, typical of MAPK feedback (Lito et al. 2014), whereas YM treatment potently inhibited RASGRP3 and MAPK signaling despite minimal changes in ERK phosphorylation **(Figure 2.6D)**. Immunohistochemistry of these OMM1.3 tumors showed no change in Ki67 staining, most likely due to the short treatment time, but did show a dramatic decrease in p-S6R staining **(Supplementary Figure S6E).** We also tested this combination in Mel202 xenografts, which exhibit much slower *in vivo* growth. YM and binimetinib both showed a tumor reduction of about 30% whereas combination led to a greater than 75% average tumor reduction **(Figure 2.6E; Supplementary Figure S6D)**. Tumors from Mel202 xenografted mice, treated for one-week, displayed low basal levels of activated RASGRP3, CRAF, and MEK but did have measurable p-ERK levels **(Figure 2.6F)**. YM treatment decreased p-RASGRP3 and downstream ERK signaling, while p-ERK remained unchanged, whereas binimetinib potently inhibited p-ERK and downstream targets but caused rebound in p-RASGRP3, p-CRAF, and p-MEK. Combination treatment suppressed the reactivation of p-MEK and p-CRAF compared to single agent binimetinib and lead to more potent inhibition of p-ERK and p-P90RSK. Immunohistochemistry of these Mel202 tumors show residual Ki67 and p-S6R staining and no significant p-ERK staining in combination treated mice **(Figure 2.6G)**, which corroborates the western blot analysis. These *in vivo* data indicate that

combination treatment in mice is feasible, highly active, and more efficacious than single agent YM or MEKi.

Discussion

Advances in targeted therapy have shown that direct inhibition of mutated oncoproteins, such as EGFR, KIT, KRAS and BRAF can be highly efficacious, due to the high selectivity against the oncoprotein over wild-type. Inhibition of downstream signaling is more challenging and often limited by on-target toxicity and narrow therapeutic window. UVM is molecularly defined by mutational activation of the $G\alpha_q$ pathway and harbor low mutational burden suggesting effective direct $G\alpha_q$ inhibition could have high efficacy. Compared to kinases, rational design of drugs against mutant GTPases, such as $G\alpha_q$ and RAS, have been challenging for a number of reasons: activating mutations in GTPases are enzymatically impaired whereas those in kinases are enzymatically hyperactive; GTPases activate downstream effectors through protein-protein interactions whereas kinases activate effectors through enzymatic modification; the abundance of intracellular GTP also makes it difficult to design high-affinity inhibitors that can directly access and bind to the GTP-binding pocket (McCormick 2018). Therefore, GTPases cannot be targeted through inhibition of enzymatic activity but require allosteric drugs that affect conformation or effector binding. Nature has evolved strategies that target human GTPases, including brefeldin A that inhibits ARF, pertussis toxin inhibits $G\alpha_i$, YM from bacteria and FR from the plant *Ardisia crenata* inhibit $G\alpha_q$. In each case, the inhibitor functions through stabilization of the GDP-bound inactive or transitional states, suggesting that active cycling is critical for inhibitor function.

The varying susceptibility to YM across our panel of $G\alpha_q$ mutants underscores the biochemical differences of these mutants. These novel findings have strong parallels to mutant RAS proteins. Structurally, RAS and $G\alpha_q$ share homologous mutational "hotspots", Q61/Q209 and G12/G48, respectively. Interestingly, codon Q61 mutations in *KRAS* are thought to be more active than those at codon G12, with higher rates of intrinsic nucleotide exchange and a greater reduction of intrinsic hydrolysis (Moore et al. 2020). This is consistent with our observations of increased IP_1 output for $G\alpha_q^{Q209L}$ and could also explain the differences in YM sensitivity we see between $G\alpha_q$ mutants. The GDP-bound state of $G\alpha_q^{Q209L}$ may be short-lived compared to $G\alpha_q^{G48V}$ or wild-type $G\alpha_q$ in $CysLT_2R^{L129Q}$ cells, making it less susceptible to inhibition by YM. While YM effectively inhibits the panel of mutants both *in vitro* and *in vivo*, these biochemical differences require foresight clinically.

As observed in *RAS*-mutant tumors, allele-specific inhibitors show limited efficacy as monotherapies and will require combinations with other inhibitors (Moore et al. 2020). As oncogenic mutations in UVM activate RAS proteins through RasGRP3, we hypothesize resistance mechanisms to direct inhibitors of $G\alpha_q$ could occur through reactivation of the MAPK pathway. In fact, compared to trametinib, we observed YM fail to fully suppress the MAPK gene signature. Therefore, the combination strategy of YM plus MEKi could prevent reactivation and durably suppress MAPK signaling. This strategy may also circumvent some of the disadvantages of targeting wild-type $G\alpha_q$, which allows for lower doses of YM and MEKi and broadens the therapeutic window for maximal clinical benefit.

Our work and recent studies highlight the possibility of directly targeting oncogenic $G\alpha_q$ signaling characteristic of UVM and the importance of pursuing this strategy further (Onken et al. 2018; Lapadula et al. 2019; Annala et al. 2019). One important limitation of this study and others is the lack of testing $G\alpha_q$ inhibition in liver metastasis models of UVM. Although these models are technically difficult and typically require intrasplenic injection of cells it is important to understand $G\alpha_q$ inhibition efficacy in the liver tumor microenvironment. Recently, complete synthesis of YM as well as FR, and novel analogs of each have been reported (Taniguchi et al. 2004; Schrage et al. 2015; Xiong et al. 2016; Kamato et al. 2017; Zhang et al. 2017) and a large toolbox of $G\alpha_q$ inhibitors will likely soon be available.

In summary, we showed cells harboring activating mutations at one of three residues in *GNAQ,* as well as wild-type $G\alpha_q$ driven by *CYSLTR2*^{L129Q} were exquisitely sensitive to YM treatment. Transcriptomic and synergy analysis revealed combination of YM with MEKi provides an efficacious and durable response. Our work demonstrates that combination of YM and MEKi leads to enhanced reduction in tumor growth and signaling in UVM, making it an ideal treatment strategy to pursue clinically.

Authors' Contributions

Conception and design: T.D. Hitchman, Y. Chen, P. Chi, T.P. Sakmar, E. Ceraudo, T. Huber

Development of methodology: T.D. Hitchman, E. Ceraudo, A.R. Moore, Y. Guan, J. Chen, C. Lee, G. Bayshtok, N. Wang, M. Pachai, R. Jia

Acquisition of data (provided animals, acquired and managed patients, provided facilities, etc.): Y. Chen, P. Chi, T.P. Sakmar, A. Shoushtari, J.H. Francis, B.S. Taylor

Analysis and interpretation of data (e.g., statistical analysis, biostatistics, computational analysis): Y. Chen, T.D. Hitchman, M.T. Chang, B.S. Taylor

Writing, review, and/or revision of the manuscript: T.D. Hitchman, Y. Chen, P. Chi, T.P. Sakmar, A.R. Moore, G. Bayshtok

Administrative, technical, or material support (i.e., reporting or organizing data, constructing databases): T.D. Hitchman, Y. Chen

Study supervision: Y. Chen

Acknowledgements

This work was supported by the Ruth L. Kirschstein National Research Service Award (NRSA) Individual Predoctoral Fellowship from the NCI (1F31CA236030-01A1, TDH), MSKCC Support Grant/Core Grant (P30 CA008748) and grants from the NCI (K08CA140946 YC; R01CA193837, YC; P50CA092629, YC; P50CA140146, PC; K08CA151660, PC; DP2 CA174499, PC), US DOD (W81XWH-10-1-0197, PC), Prostate Cancer Foundation (YC), Starr Cancer Consortium (YC, PC), Geoffrey Beene Cancer Research Center (YC, PC), Gerstner Family Foundation (YC), Bressler Scholars Fund (YC), and Cycle for Survival (YC). B.S.T. is supported by R01 CA204749 and R01 CA245069. EC was supported by the Francois Wallace Monahan Fellowship and the Thomas Haines Fellowship. We thank the Robertson Therapeutic Development Fund for partial support.

Figure 2.1

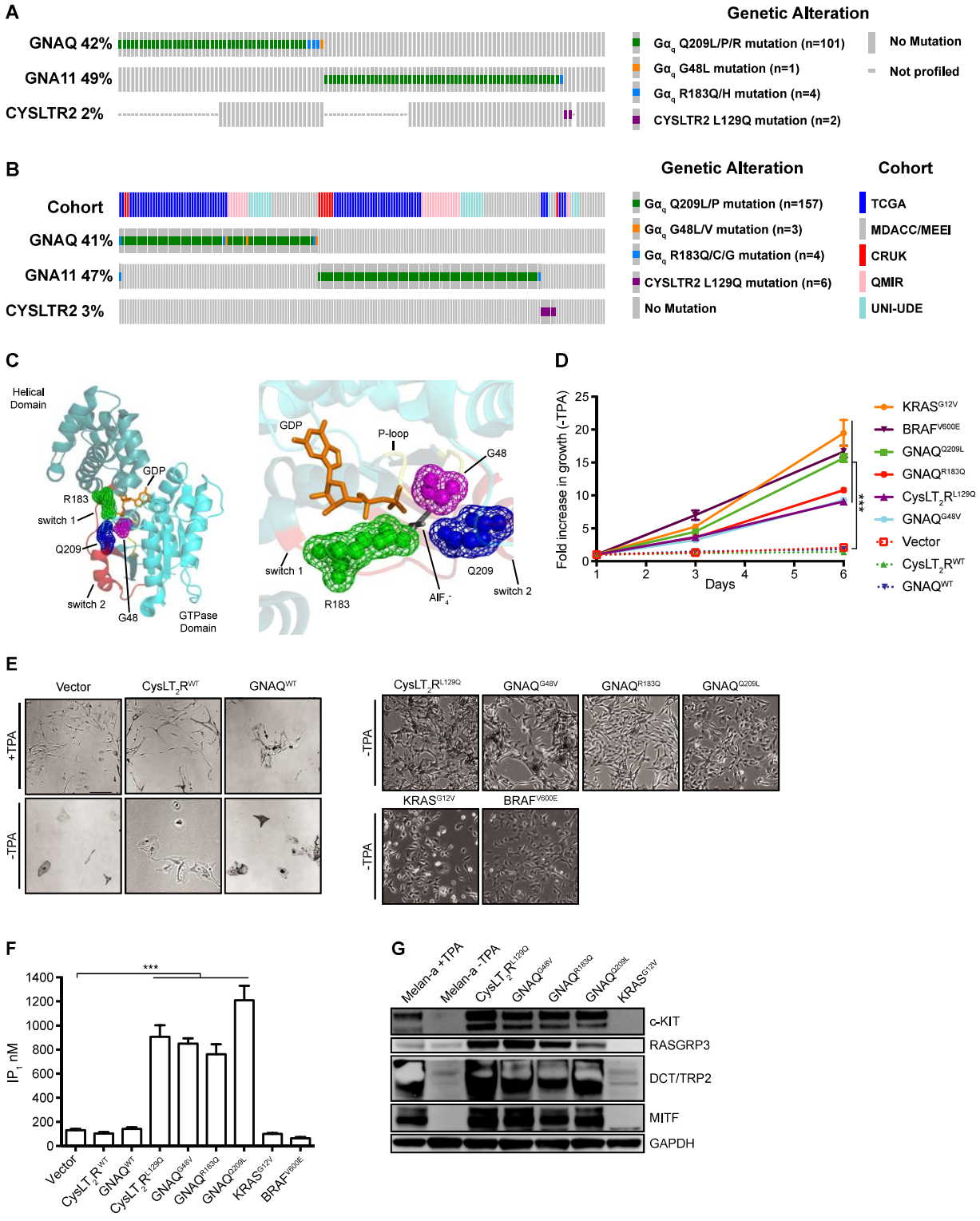
A
GNAQ 42%
GNA11 49%
CYSLTR2 2%
Genetic Alteration
Gαq Q209L/P/R mutation (n=101)
Gαq G48L mutation (n=1)
Gαq R183Q/H mutation (n=4)
CYSLTR2 L129Q mutation (n=2)
No Mutation
Not profiled
B
Cohort
GNAQ 41%
GNA11 47%
CYSLTR2 3%
Genetic Alteration
Gαq Q209L/P mutation (n=157)
Gαq G48L/V mutation (n=3)
Gαq R183Q/C/G mutation (n=4)
CYSLTR2 L129Q mutation (n=6)
No Mutation
Cohort
TCGA
MDACC/MEEI
CRUK
QMIR
UNI-UDE
C
Helical Domain
GDP
R183
switch 1
Q209
switch 2
G48
GTPase Domain
P-loop
switch 1
switch 2
AlF4-
D
Fold increase in growth (-TPA)
Days
KRASG12V
BRAFV600E
GNAQQ209L
GNAQR183Q
CysLT2RL129Q
GNAQG48V
Vector
CysLT2RWT
GNAQWT
***
E
Vector
CysLT2RWT
GNAQWT
CysLT2RL129Q
GNAQG48V
GNAQR183Q
GNAQQ209L
KRASG12V
BRAFV600E
+TPA
-TPA
F
IP1 nM
***
Vector
CysLT2RWT
GNAQWT
CysLT2RL129Q
GNAQG48V
GNAQR183Q
GNAQQ209L
KRASG12V
BRAFV600E
G
Melan-a +TPA
Melan-a -TPA
CysLT2RL129Q
GNAQG48V
GNAQR183Q
GNAQQ209L
KRASG12V
c-KIT
RASGRP3
DCT/TRP2
MITF
GAPDH

Figure 2.1 $G\alpha_q$ mutations occur at three hotspot residues that are known to affect the guanine-nucleotide binding pocket.
(A) Oncoprint of $G\alpha_q$ pathway mutations in 116 UVM patients who have undergone MSK-IMPACT testing. **(B)** Oncoprint of $G\alpha_q$ pathway mutations in 188 UVM patients from five published cohorts including TCGA (Robertson et al. 2017), Cancer Research UK (CRUK) (Furney et al. 2013), QIMR Berghofer Medical Research Institute (Johansson et al. 2016), University of Duisburg-Essen (UNI-UDE) (Martin et al. 2013) and MD Anderson Cancer Center/Massachusetts Eye and Ear Infirmary (MDACC/MEEI) (Johnson et al. 2017). **(C)** 3D cartoon structure of GNAQ (left) highlighting Gly48 (magenta) of the P-loop (yellow), Arg183 (green) of Switch 1 (red), and Gln209 (blue) of Switch 2 (red). GDP (orange) and AlF_4^- (grey) are both shown as sticks and the three residues are shown as mesh spheres. Close up view of GTP binding pocket (right). Structure from Protein Data Bank Entry 5DO9 (Taylor, Bommarito, and Tesmer 2016). **(D)** Growth assay for melan-a cells in the absence of TPA for six days. Growth was assayed by Celltiter-Glo 2.0 at D1, D3, and D6. Fold increase in luminescence is shown relative to D1 cell number. **(E)** Phase contrast images of engineered melan-a cells after TPA withdrawal for 2 weeks (scale bar 100μm). **(F)** Basal level of IP_1 accumulation in melan-a cells. Vector and WT controls are cultured with TPA whereas the remaining samples were cultured without TPA. **(G)** Western blot of melanocyte lineage markers (MITF, TRP2/DCT, c-KIT, and RASGRP3) upon TPA withdrawal for 2 weeks. For all cases (mean ± SEM, n = 3), $P < 0.0005$; ***, vector compared against each condition.

Figure 2.2

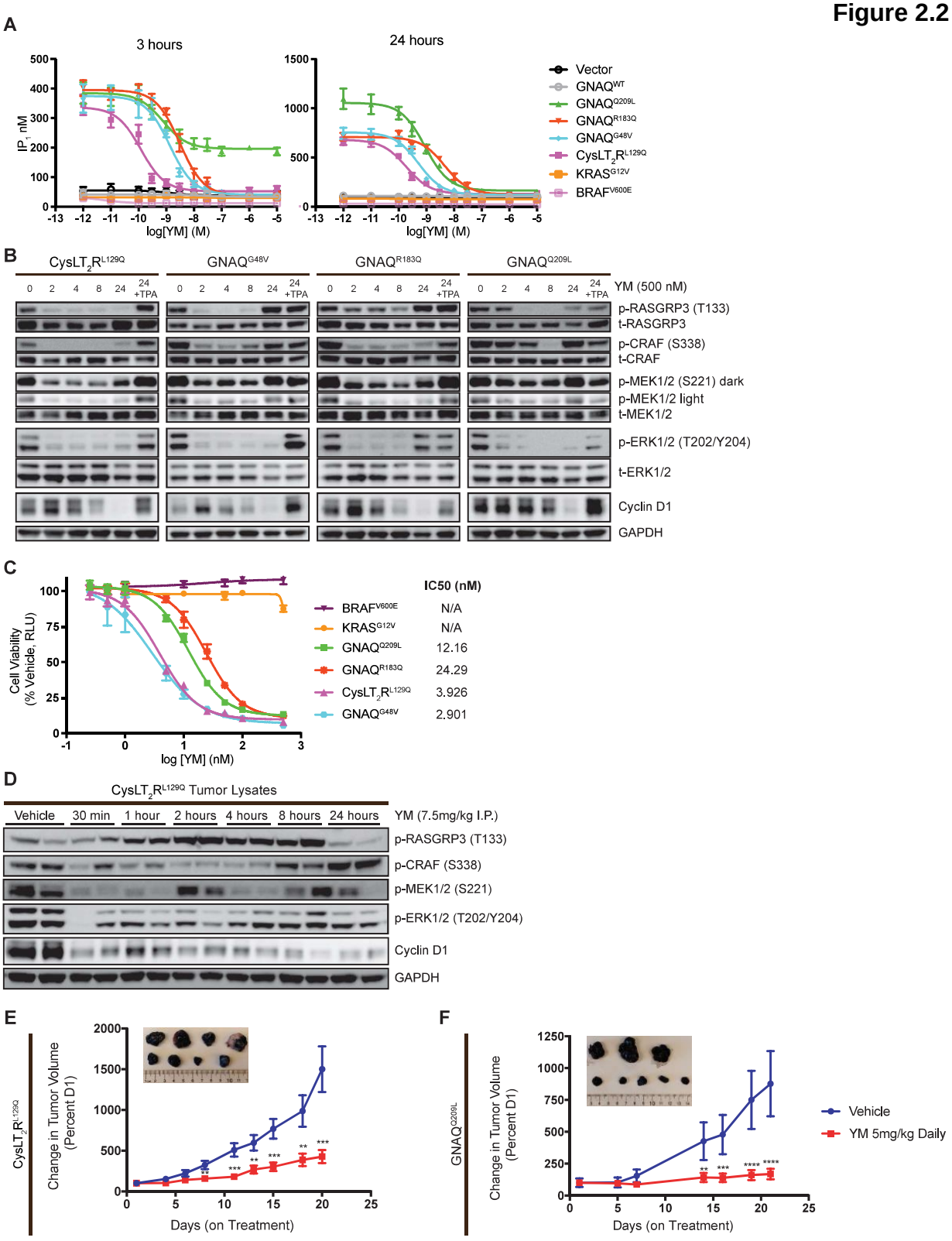
A
3 hours
24 hours
IP1 nM
log[YM] (M)
Vector
GNAQWT
GNAQQ209L
GNAQR183Q
GNAQG48V
CysLT2RL129Q
KRASG12V
BRAFV600E
B
CysLT2RL129Q
GNAQG48V
GNAQR183Q
GNAQQ209L
YM (500 nM)
p-RASGRP3 (T133)
t-RASGRP3
p-CRAF (S338)
t-CRAF
p-MEK1/2 (S221) dark
p-MEK1/2 light
t-MEK1/2
p-ERK1/2 (T202/Y204)
t-ERK1/2
Cyclin D1
GAPDH
C
Cell Viability (% Vehicle, RLU)
log [YM] (nM)
IC50 (nM)
BRAFV600E N/A
KRASG12V N/A
GNAQQ209L 12.16
GNAQR183Q 24.29
CysLT2RL129Q 3.926
GNAQG48V 2.901
D
CysLT2RL129Q Tumor Lysates
Vehicle
30 min
1 hour
2 hours
4 hours
8 hours
24 hours
YM (7.5mg/kg I.P.)
p-RASGRP3 (T133)
p-CRAF (S338)
p-MEK1/2 (S221)
p-ERK1/2 (T202/Y204)
Cyclin D1
GAPDH
E
CysLT2RL129Q
Change in Tumor Volume (Percent D1)
Days (on Treatment)
F
GNAQQ209L
Change in Tumor Volume (Percent D1)
Days (on Treatment)
Vehicle
YM 5mg/kg Daily

Figure 2.2 YM-254890 inhibits mutation dependent melan-a cell tumor growth and signaling.
(A) IP_1 accumulation assays in mutation dependent melan-a cells. Cells were treated with increasing concentrations of YM for 3 hours (left) and 24 hours (right). Data are expressed as IP_1 concentration (nM) (mean ± SEM, n = 3). **(B)** Western blot analysis of MAPK signaling in melan-a cells treated with 500nM YM at 0, 2, 4, 8, and 24 hours; the last sample for each cell line was also treated with TPA for 24 hours showing rescue of the pathway. **(C)** Dose response of melan-a cells treated with YM for 5 days at increasing dose and readout by CellTiter Glo 2.0. Data are expressed as the percentage RLU relative to that observed with vehicle. (mean ± SEM, n = 3). **(D)** Western blot of lysates from $CysLT_2R^{L129Q}$ melan-a tumors harvested at the indicated time after a single dose YM (7.5mg/kg). **(E)** Percent tumor volume of $CysLT_2R^{L129Q}$ and **(F)** $GNAQ^{Q209L}$ melan-a allografts treated with vehicle or YM daily. Pictures of representative tumors are vehicle (top) and YM treated (bottom) at the end of treatment (mean ± SEM, n = 6-10). For all cases $P < 0.005$; **, $P < 0.0005$; ***, $P < 0.0001$; ****.

Figure 2.3

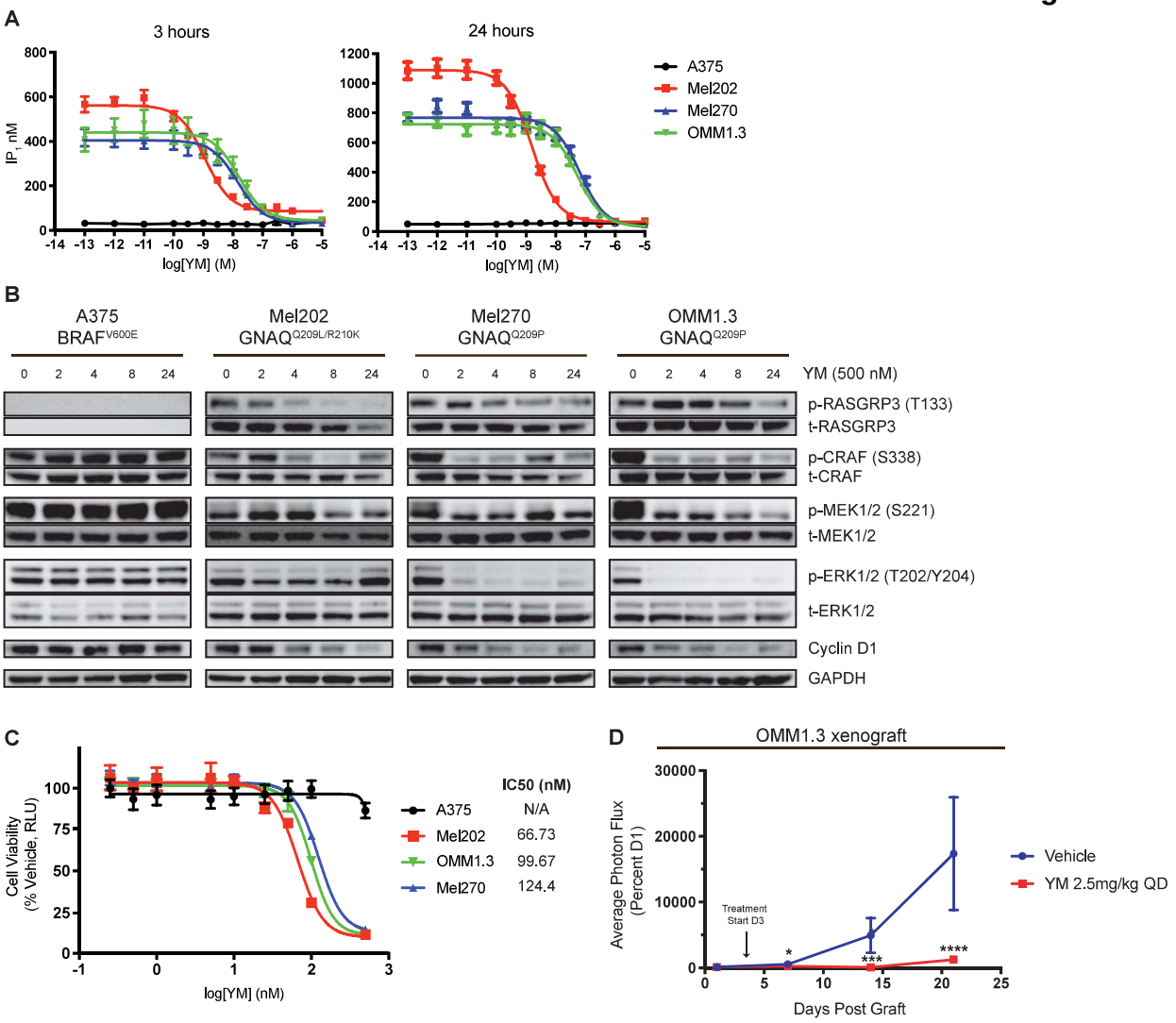

Figure 2.3 YM-254890 inhibits human UVM cell signaling and tumor growth. **(A)** IP_1 accumulation assay in UVM cells and A375 cells (cutaneous $BRAF^{V600E}$). Cells were treated with increasing concentrations of YM for 3 hours (left) and 24 hours (right). Data are expressed as IP_1 concentration (nM) (mean ± SEM, n = 3) **(B)** Western blot analysis of indicated proteins in UVM cells and A375 cells treated with 500nM YM at 0, 2, 4, 8, and 24 hours. **(C)** Dose response of UVM and A375 cells treated with YM for 5 days at increasing dose and readout by CellTiter Glo 2.0. Data are expressed as the percentage RLU relative to that observed with vehicle. (mean ± SEM, n = 3). **(D)** Percent photon flux of OMM1.3 xenografts treated with vehicle or YM (2.5mg/kg) for 21 days (mean ± SEM, n = 10). Cells were transduced with pBMN for luciferase expression. Arrow indicates start of treatment at day 3. $P < 0.05$; *, $P < 0.0005$; ***, $P < 0.0001$, ****.

Figure 2.4

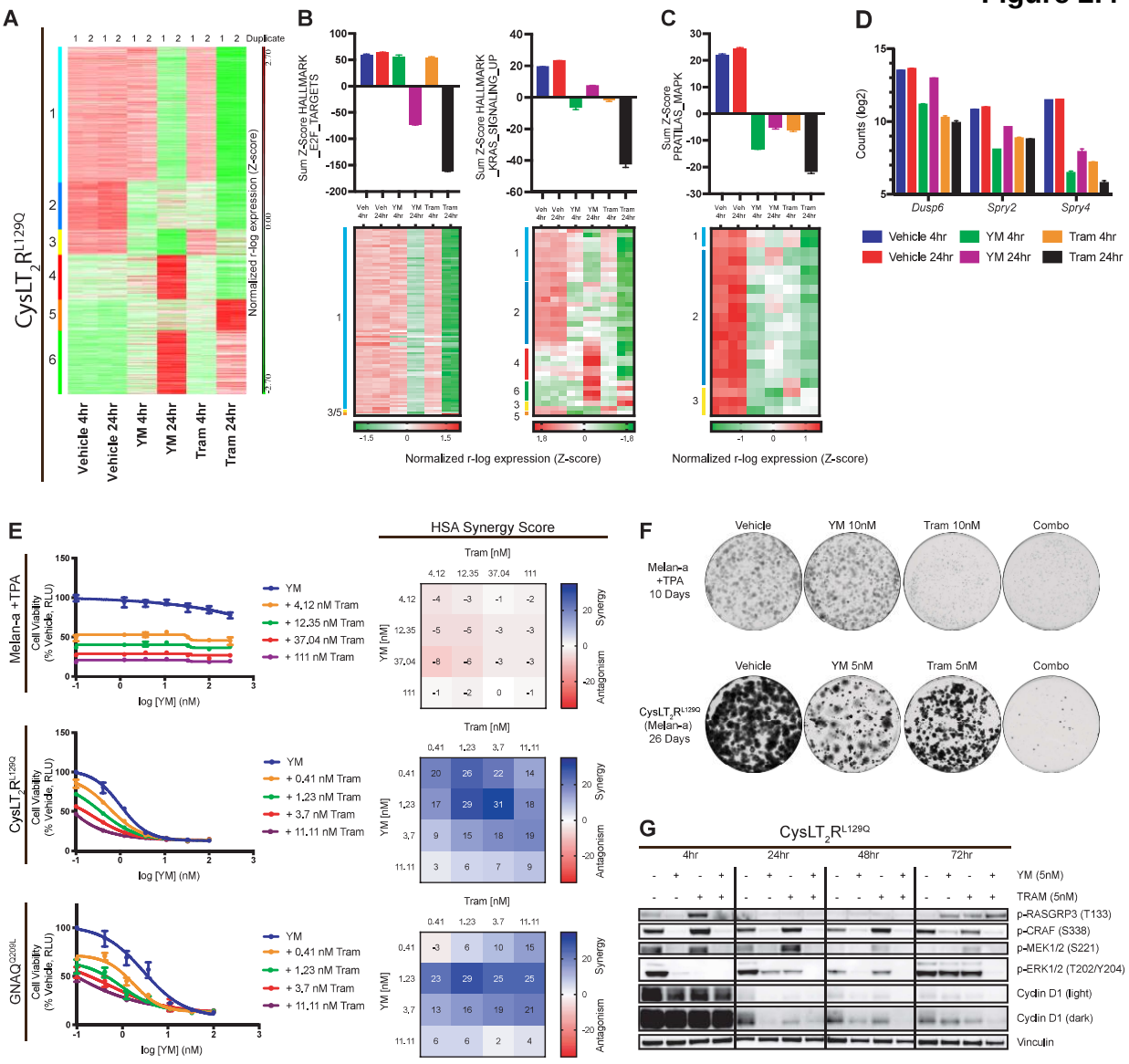
A
CysLT2RL129Q
Duplicate
Normalized r-log expression (Z-score)
Vehicle 4hr
Vehicle 24hr
YM 4hr
YM 24hr
Tram 4hr
Tram 24hr
B
Sum Z-Score HALLMARK_E2F_TARGETS
Sum Z-Score HALLMARK_KRAS_SIGNALING_UP
Normalized r-log expression (Z-score)
C
Sum Z-Score PRATILAS_MAPK
Normalized r-log expression (Z-score)
D
Counts (log2)
Dusp6
Spry2
Spry4
Vehicle 4hr
YM 4hr
Tram 4hr
Vehicle 24hr
YM 24hr
Tram 24hr
E
HSA Synergy Score
Melan-a +TPA
Cell Viability (% Vehicle, RLU)
log [YM] (nM)
YM
+ 4.12 nM Tram
+ 12.35 nM Tram
+ 37.04 nM Tram
+ 111 nM Tram
Tram [nM]
YM [nM]
Synergy
Antagonism
CysLT2RL129Q
+ 0.41 nM Tram
+ 1.23 nM Tram
+ 3.7 nM Tram
+ 11.11 nM Tram
GNAQQ209L
F
Vehicle
YM 10nM
Tram 10nM
Combo
Melan-a +TPA 10 Days
YM 5nM
Tram 5nM
CysLT2RL129Q (Melan-a) 26 Days
G
CysLT2RL129Q
4hr
24hr
48hr
72hr
YM (5nM)
TRAM (5nM)
p-RASGRP3 (T133)
p-CRAF (S338)
p-MEK1/2 (S221)
p-ERK1/2 (T202/Y204)
Cyclin D1 (light)
Cyclin D1 (dark)
Vinculin

Figure 2.4 Transcriptomics implicates synergistic action between $G\alpha_q$ inhibition and MEK inhibition in melan-a cells.
(A) Heatmap of RNA-seq gene expression from $CysLT_2R^{L129Q}$ melan-a cells treated with vehicle, YM (100nM), or trametinib (100nM) for 4 or 24 hours (duplicates shown). Data was r-log transformed, Z-scored, and then k-means clustered. Clusters are labeled 1-6 and color coordinated (left). **(B)** Sum Z-scores of E2F_Targets, KRAS_SIGNALING_UP, and **(C)** Pratilas_MAPK are shown (top) with heatmaps (bottom) showing expression of individual signature genes (mean ± SEM, n = 2). **(D)** RNA-seq based expression (log_2 count) of *Dusp6*, *Spry2*, and *Spry4* (mean ± SEM, n = 2). **(E)** Viability curves for melan-a cell lines treated with increasing doses of YM in combination with four doses of trametinib (left) and corresponding HSA synergy diagrams (right) (mean ± SEM, n = 3). **(F)** Growth assays for parental melan-a cells (+TPA) and $CysLT_2R^{L129Q}$ melan-a cells (-TPA) in the presence of vehicle, YM, trametinib, or Combo for 10 or 26 days, respectively. **(G)** Western blot analysis of indicated proteins in $CysLT_2R^{L129Q}$ melan-a cells. Cells were treated with vehicle, YM, trametinib, or Combo for 4, 24, 48, and 72 hours.

Figure 2.5

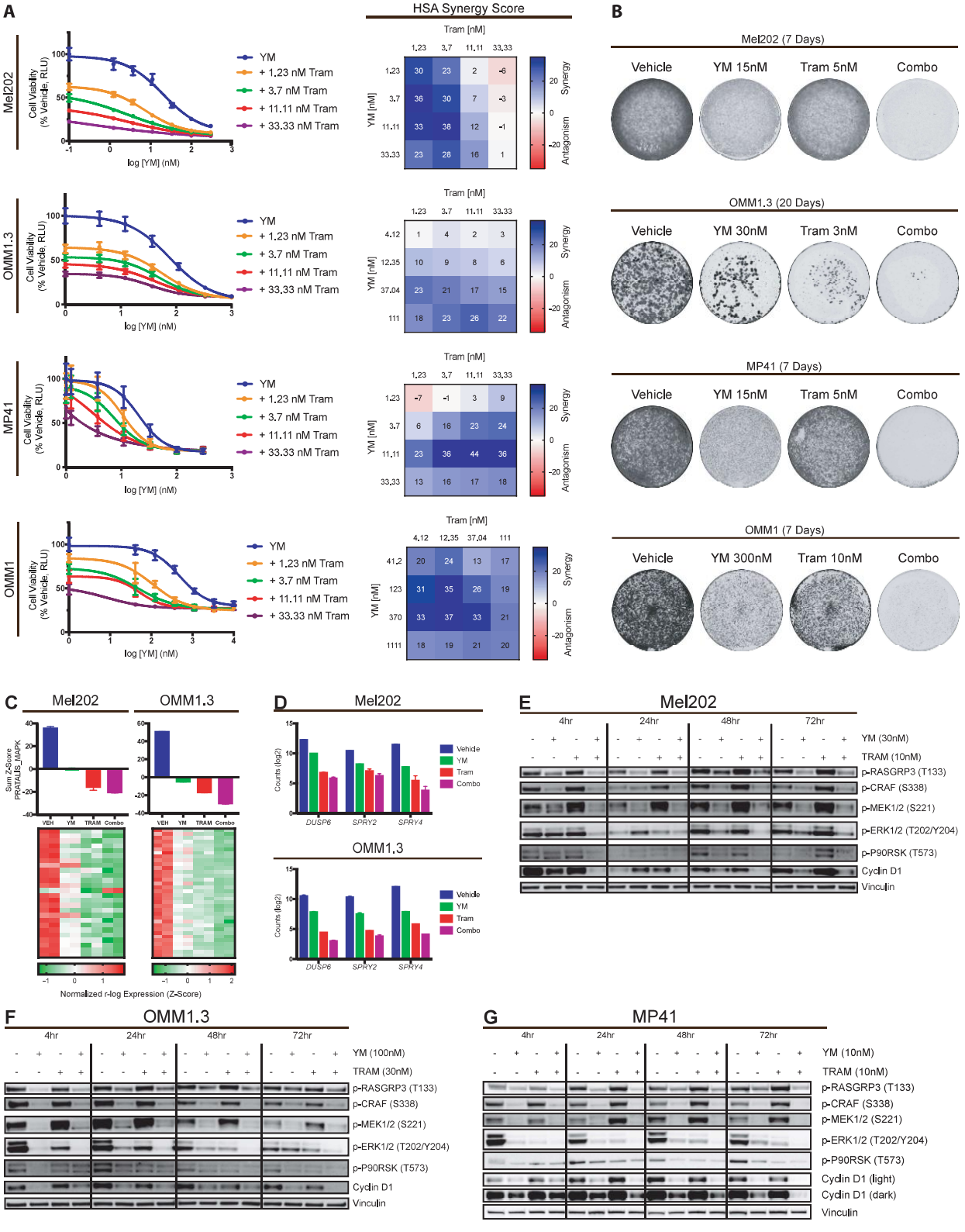
A
Mel202
OMM1.3
MP41
OMM1
Cell Viability (% Vehicle, RLU)
log [YM] (nM)
YM
+ 1.23 nM Tram
+ 3.7 nM Tram
+ 11.11 nM Tram
+ 33.33 nM Tram
HSA Synergy Score
Tram [nM]
YM [nM]
Synergy
Antagonism
B
Mel202 (7 Days)
Vehicle
YM 15nM
Tram 5nM
Combo
OMM1.3 (20 Days)
YM 30nM
Tram 3nM
MP41 (7 Days)
OMM1 (7 Days)
YM 300nM
Tram 10nM
C
Mel202
OMM1.3
Sum Z-Score PRATALIS_MAPK
VEH
YM
TRAM
Combo
Normalized r-log Expression (Z-Score)
D
Mel202
OMM1.3
Counts (log2)
DUSP6
SPRY2
SPRY4
Vehicle
YM
Tram
Combo
E
Mel202
4hr
24hr
48hr
72hr
YM (30nM)
TRAM (10nM)
p-RASGRP3 (T133)
p-CRAF (S338)
p-MEK1/2 (S221)
p-ERK1/2 (T202/Y204)
p-P90RSK (T573)
Cyclin D1
Vinculin
F
OMM1.3
YM (100nM)
TRAM (30nM)
G
MP41
YM (10nM)
TRAM (10nM)
Cyclin D1 (light)
Cyclin D1 (dark)

Figure 2.5 YM-254890 and MEKi lead to sustained MAPK inhibition in UVM cells.
(A) Viability curves for four UVM cell lines treated with increasing doses of YM in combination with four doses of trametinib (left) and corresponding HSA synergy diagrams (right). (mean ± SEM, n = 3). **(B)** Growth assays of Mel202, OMM1.3, MP41, and OMM1 cells treated with vehicle, YM, trametinib, or Combo. **(C)** Mel202 and OMM1.3 sum Z scores of Pratilas_MAPK are shown (top) with heatmaps (bottom) showing expression of individual signature genes (mean ± SEM, n = 2). **(D)** Expression counts (log_2) of *DUSP6*, *SPRY2*, and *SPRY4* from RNA-seq data for Mel202 and OMM1.3 cells (mean ± SEM, n = 2). **(E)** Western blot analysis of indicated proteins in Mel202, **(F)** OMM1.3, and **(G)** MP41 cells. Cells were treated with vehicle, YM, trametinib, or Combo for 4, 24, 48, and 72 hours.

Figure 2.6

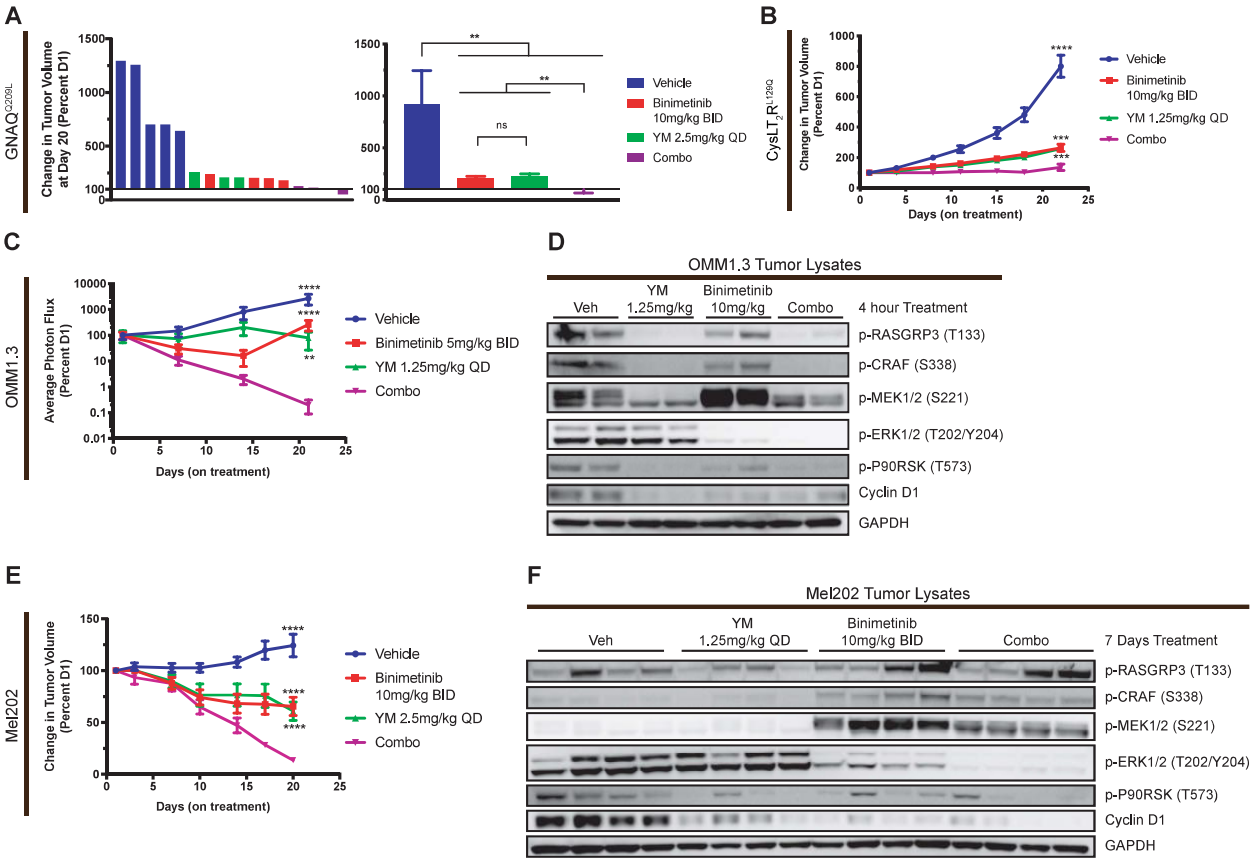
A
GNAQ Q209L
Change in Tumor Volume at Day 20 (Percent D1)
Vehicle
Binimetinib 10mg/kg BID
YM 2.5mg/kg QD
Combo
B
CysLT2R L129Q
Change in Tumor Volume (Percent D1)
Days (on treatment)
C
OMM1.3
Average Photon Flux (Percent D1)
Vehicle
Binimetinib 5mg/kg BID
YM 1.25mg/kg QD
Combo
D
OMM1.3 Tumor Lysates
Veh
YM 1.25mg/kg
Binimetinib 10mg/kg
Combo
4 hour Treatment
p-RASGRP3 (T133)
p-CRAF (S338)
p-MEK1/2 (S221)
p-ERK1/2 (T202/Y204)
p-P90RSK (T573)
Cyclin D1
GAPDH
E
Mel202
Change in Tumor Volume (Percent D1)
Vehicle
Binimetinib 10mg/kg BID
YM 2.5mg/kg QD
Combo
F
Mel202 Tumor Lysates
Veh
YM 1.25mg/kg QD
Binimetinib 10mg/kg BID
Combo
7 Days Treatment
p-RASGRP3 (T133)
p-CRAF (S338)
p-MEK1/2 (S221)
p-ERK1/2 (T202/Y204)
p-P90RSK (T573)
Cyclin D1
GAPDH
G
Mel202 Tumors (1 week treatment)
Ki67
p-ERK
p-S6R
Vehicle
YM
Binimetinib
Combo

Figure 2.6 Combination of YM-254890 and binimetinib in vivo inhibits tumor growth and signaling.

(A) Percent tumor volume of individual tumors (left) and averaged (right) of $GNAQ^{Q209L}$ melan-a allografts treated with vehicle, YM, binimetinib, or Combo for 20 days (mean ± SEM). Origin (Y=100) represents no change in tumor volume. **(B)** Percent tumor volume of $CysLT_2R^{L129Q}$ melan-a allografts treated with vehicle, YM, binimetinib, or Combo for 22 days (mean ± SEM, n = 10). **(C)** Percent photon flux of OMM1.3 xenografts treated with vehicle, YM, binimetinib, or Combo daily for 21 days (mean ± SEM, n = 4-10). Cells were transduced with pBMN for luciferase expression. **(D)** Western blot of OMM1.3 tumors treated for 4 hours with vehicle, YM, binimetinib, and Combo. **(E)** Percent tumor volume of Mel202 xenografts treated with vehicle, YM, binimetinib, or Combo for 20 days (mean ± SEM, n = 4-6). **(F)** Western blot of Mel202 tumors treated for 1 week with vehicle, YM, binimetinib, and Combo. **(G)** Immunohistochemistry of Mel202 tumors from (Figure 6F) for Ki67, p-ERK, and p-S6R. Scale bar, 50μm for insert (left) and 2mm for whole tumor (right). For all cases $P > .05$; ns, $P < 0.005$; **, $P < 0.0005$; ***, $P < 0.0001$, ****.

APPENDIX

Supplementary Tables

Supplementary Figures

Supplementary Figure S1

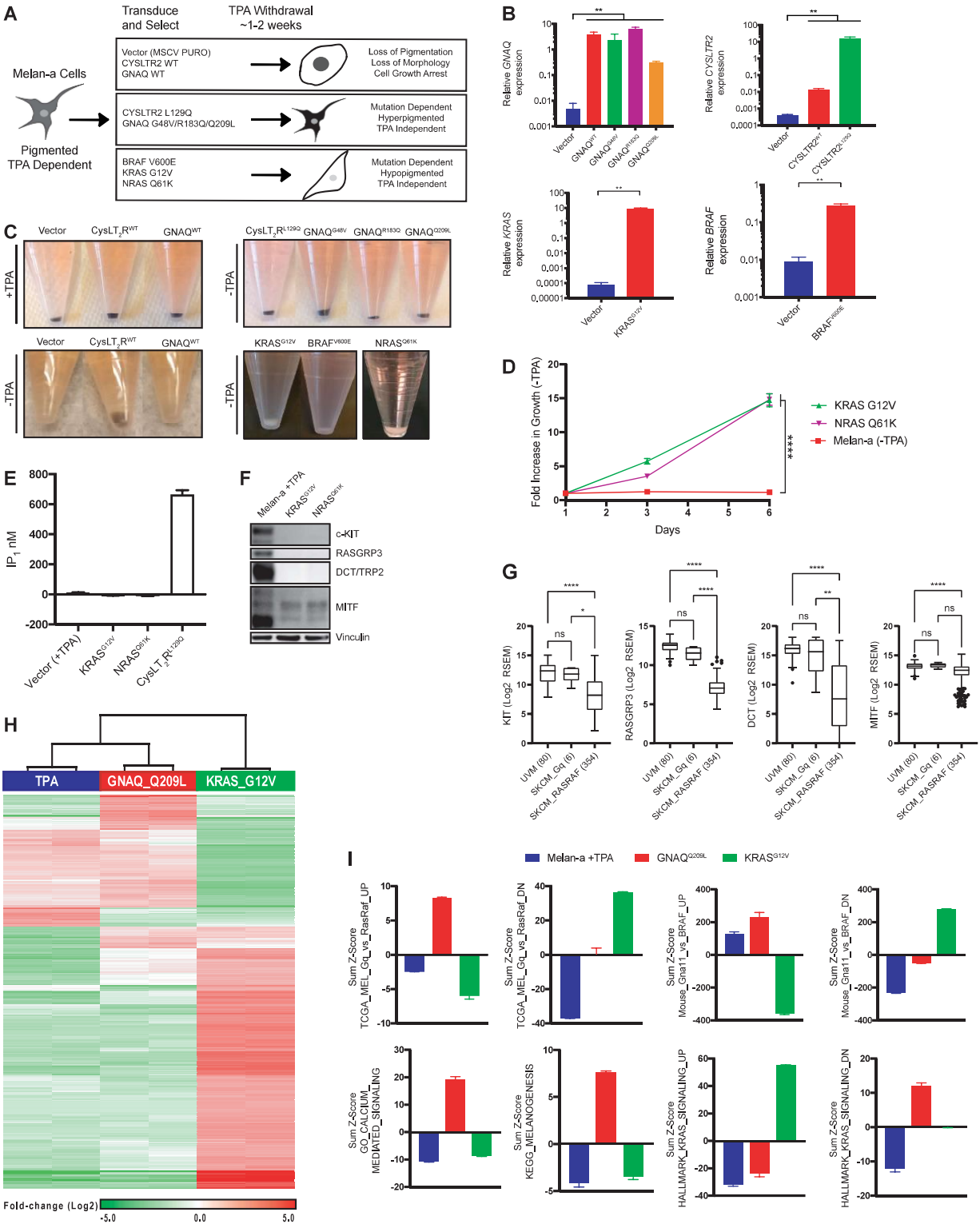

Supplementary Figure S1

(A) Workflow diagram of generating mutation dependent melan-a cells. Cells were transduced with vector control (MSCV PURO), human cDNAs with WT or activating mutations found in UVM patients (CYSLTR2 and GNAQ), or downstream MAPK activating mutations ($KRAS^{G12V}$, $BRAF^{V600E}$, or $NRAS^{Q61K}$). TPA was then withdrawn from the media to drive mutation dependence. **(B)** Expression of *GNAQ*, *CYSLTR2*, *KRAS*, and *BRAF* in melan-a cells transduced with cDNAs. All samples were compared to expression of RPL27 (mean ± SD, n = 3). **(C)** Cells pellets in melan-a cells after TPA withdrawal for 2 weeks to show pigmentation. **(D)** Growth assay for $NRAS^{Q61K}$ melan-a cells compared to parental and $KRAS^{G12V}$ melan-a cells without TPA for six days. Growth was assayed by Celltiter-Glo 2.0 at D1, D3, and D6. Fold increase in luminescence is shown relative to D1 cell number (mean ± SEM, n = 3). **(E)** Basal level of IP_1 accumulation in $NRAS^{Q61K}$ melan-a cells compared to other melan-a cells. **(F)** Western blot of melanocyte lineage markers (MITF, TRP2/DCT, c-KIT, and RASGRP3) upon TPA withdrawal for 2 weeks in $NRAS^{Q61K}$ melan-a cells. **(G)** Tukey box plot of expression of KIT, RASGRP3, DCT, and MITF from TCGA datasets in UVM and $G\alpha_q$-mutated SKCM compared to RAS/RAF mutated SKCM. **(H)** Unsupervised hierarchical clustering of RNA-seq data from melan-a cells (+TPA), $GNAQ^{Q209L}$, and $KRAS^{G12V}$ melan-a cells (-TPA) (duplicates shown). **(I)** Sum Z-scores of 8 gene sets highlighting the differences between groups from (H) (n = 2). Custom genes sets (first row) include genes up or downregulated in UVM and $G\alpha_q$-mutated SKCM versus RAS/RAF mutant SKCM from TCGA (TCGA_MEL_Gq_vs_RasRaf) as well as genes up or downregulated in our $GNA11^{Q209L}$ $Bap1^{-/-}$ versus $BRAF^{V600E}$ $Bap1^{-/-}$ GEMM (Mouse_Gna11_vs_Braf). For all cases $P > .05$; ns, $P < 0.05$; *, $P < 0.005$; **, $P < 0.0005$; ***, $P < 0.0001$, ****.

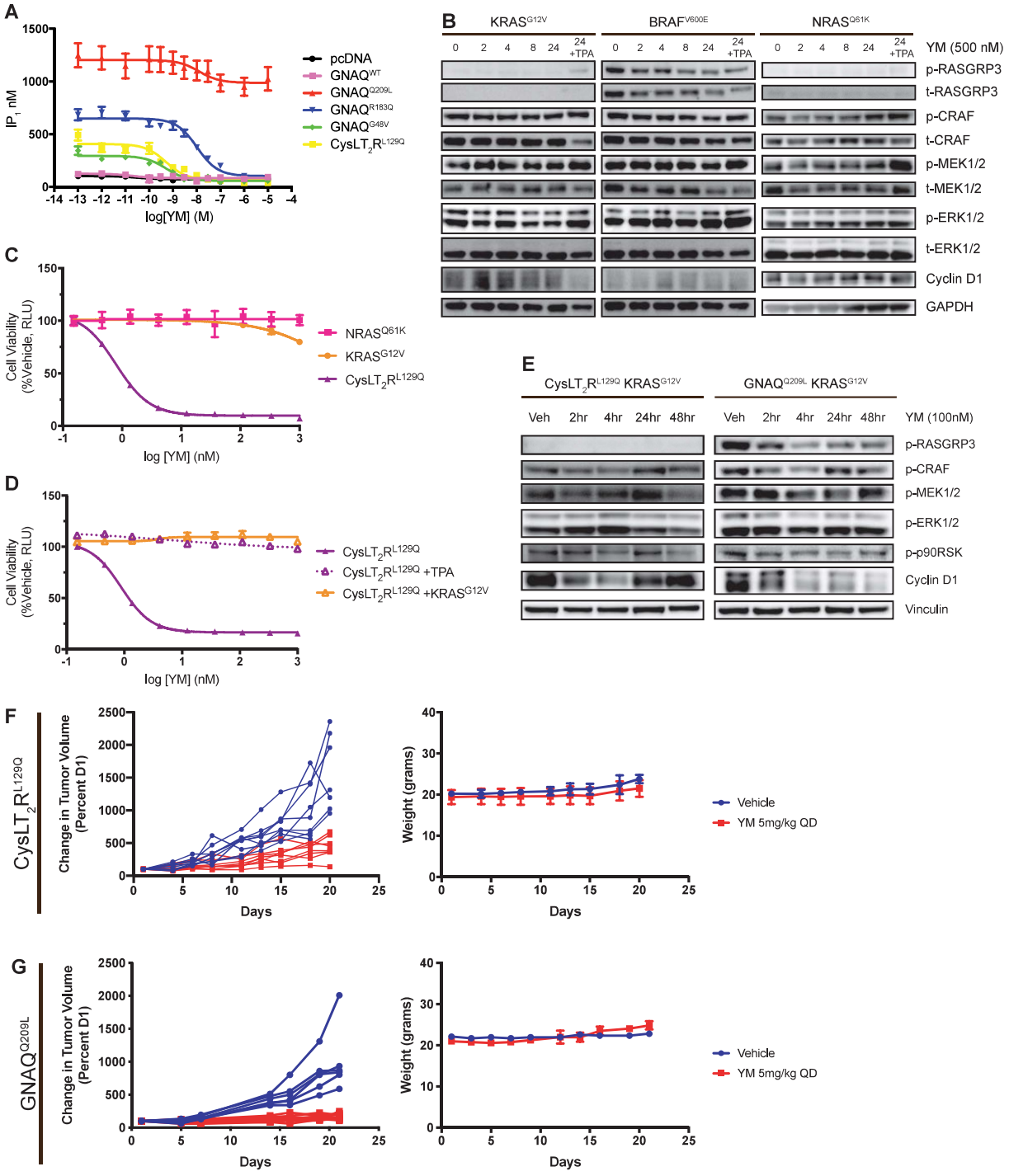

Supplementary Figure S2

(A) IP_1 accumulation in HEK-293T cells transfected with constructs at 11ng/well. Cells were treated with YM at increasing dose for 24 hours. Data are expressed as IP_1 concentration (nM) (mean ± SEM, n = 3). **(B)** Western blot analysis of $KRAS^{G12V}$, $BRAF^{V600E}$, and $NRAS^{Q61K}$ melan-a cells. Samples were treated with 500nM YM for 0, 2, 4, 8, and 24 hours with the last lane being treatment plus TPA add back. **(C)** Viability curves for $NRAS^{Q61K}$ melan-a cells treated with YM for

5 days assayed by Celltiter-glo 2.0 (mean ± SEM, n = 3). **(D)** Viability curves for $CysLT_2R^{L129Q}$ melan-a cells supplemented with TPA or expressing oncogenic *KRAS*^{G12V} treated with YM for 5 days assayed by Celltiter-glo 2.0. Data are expressed as the percentage RLU relative to that observed with vehicle (mean ± SEM, n = 3). **(E)** Western blot analysis of $CysLT_2R^{L129Q}$ and $GNAQ^{Q209L}$ melan-a cells expressing oncogenic *KRAS*^{G12V} treated with 100nM YM for 0, 2, 4, 24, and 48 hours. **(F)** Percent tumor volume of $CysLT_2R^{L129Q}$ and **(G)** $GNAQ^{Q209L}$ melan-a allografts as individual flanks treated with vehicle or YM for 20 or 21 days, respectively. Mouse weight throughout the course of experiment is plotted (right) (mean ± SEM, n = 3-5).

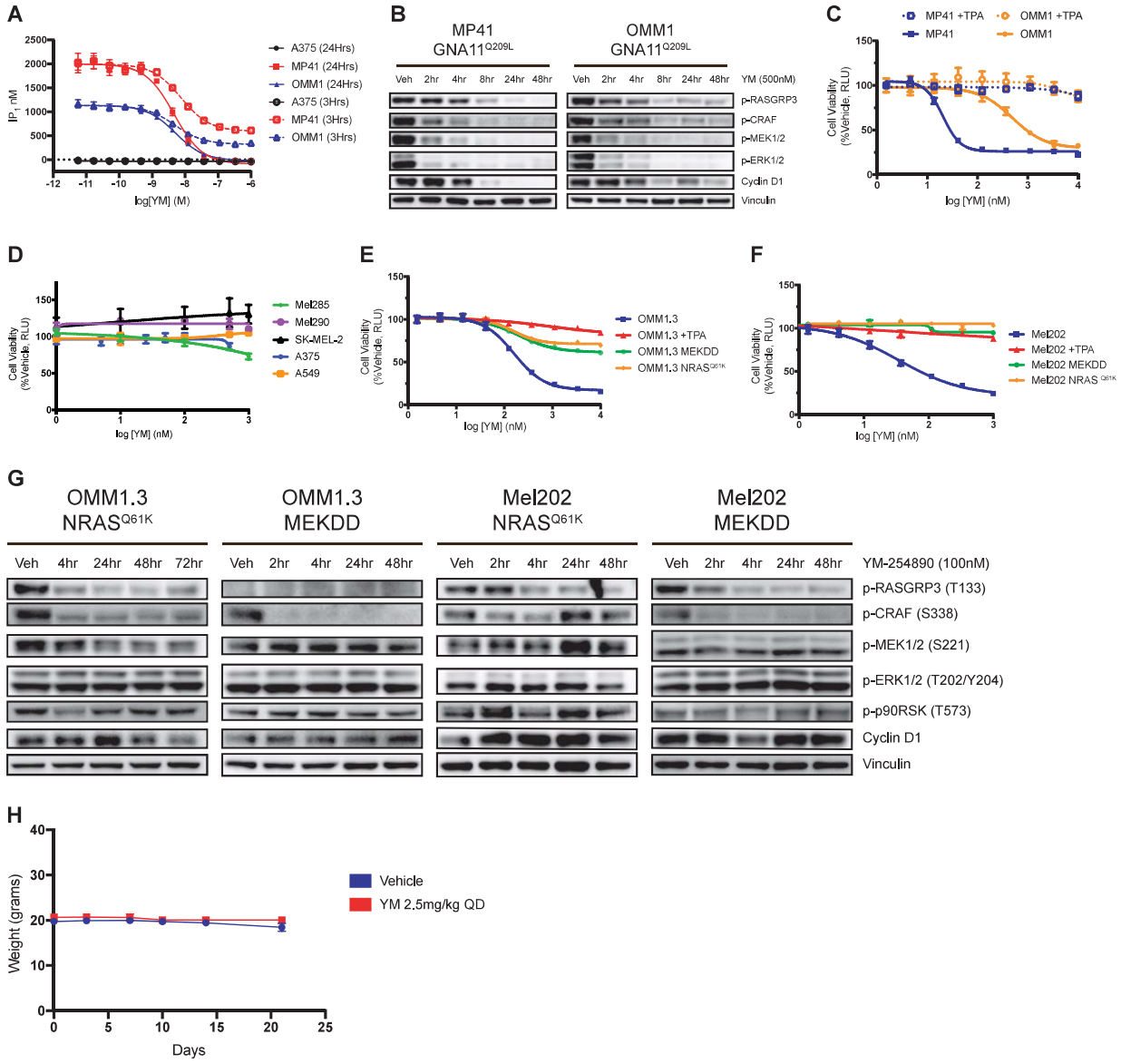

Supplementary Figure S3

(A) IP_1 accumulation assay in MP41 and OMM1 cells (*GNA11*^{Q209L}) compared to A375 cells. Cells were treated with increasing concentrations of YM for 3 hours (dotted lines) and 24 hours (solid lines). Data are expressed as IP_1 concentration (mean ± SEM, n = 3). **(B)** Western blot analysis of indicated proteins in MP41 and OMM1 cells treated with 500nM YM at 0, 2, 4, 24, and 48 hours. **(C)** Viability Curves for MP41 and OMM1 cells treated with YM in the presence or absence of TPA for 5 days. **(D)** Viability curves for non-Gq mutant UVM cell lines Mel285 and Mel290, cutaneous melanomas A375 ($BRAF^{V600E}$ from Figure 4C for reference) and SK-MEL-2 ($NRAS^{Q61R}$), and lung adenocarcinoma cells A549 ($KRAS^{G12S}$) treated with YM for 5 days. **(E)** Viability curves for OMM1.3 and **(F)** Mel202 cells treated with YM for 5 days in the presence or absence of TPA or expressing indicated MAPK activating mutations. All viability curves were assayed by Celltiter-glo 2.0 and expressed as the percentage RLU relative to that observed with vehicle (mean ± SEM, n

= 3). **(G)** Western blot analysis of indicated proteins in OMM1.3 or Mel202 cells expressing NRAS^{Q61K} or MEKDD treated with 100nM YM at 0, 2, 4, 24, and 48 hours. **(H)** Weight for OMM1.3 xenografted mice from Fig. 3D (mean ± SEM, n = 5).

Supplementary Figure S4

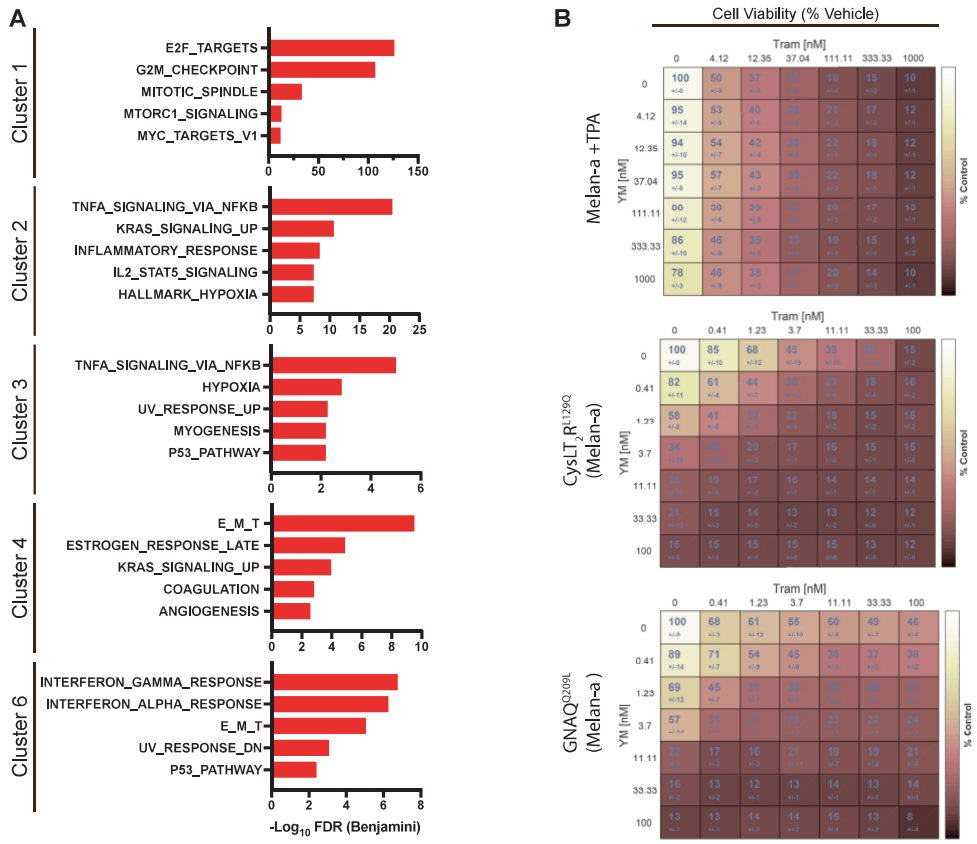

Supplementary Figure S4

(A) Top five HALLMARK gene set enrichments for each cluster of Fig. 4A, cluster 5 yielded no significantly enriched gene sets. Epithelial_Mesenchymal_Transition is abbreviated with E_M_T. **(B)** Cell viability diagrams for melan-a cell synergy analysis (mean ± SEM, n = 3).

Supplementary Figure S5

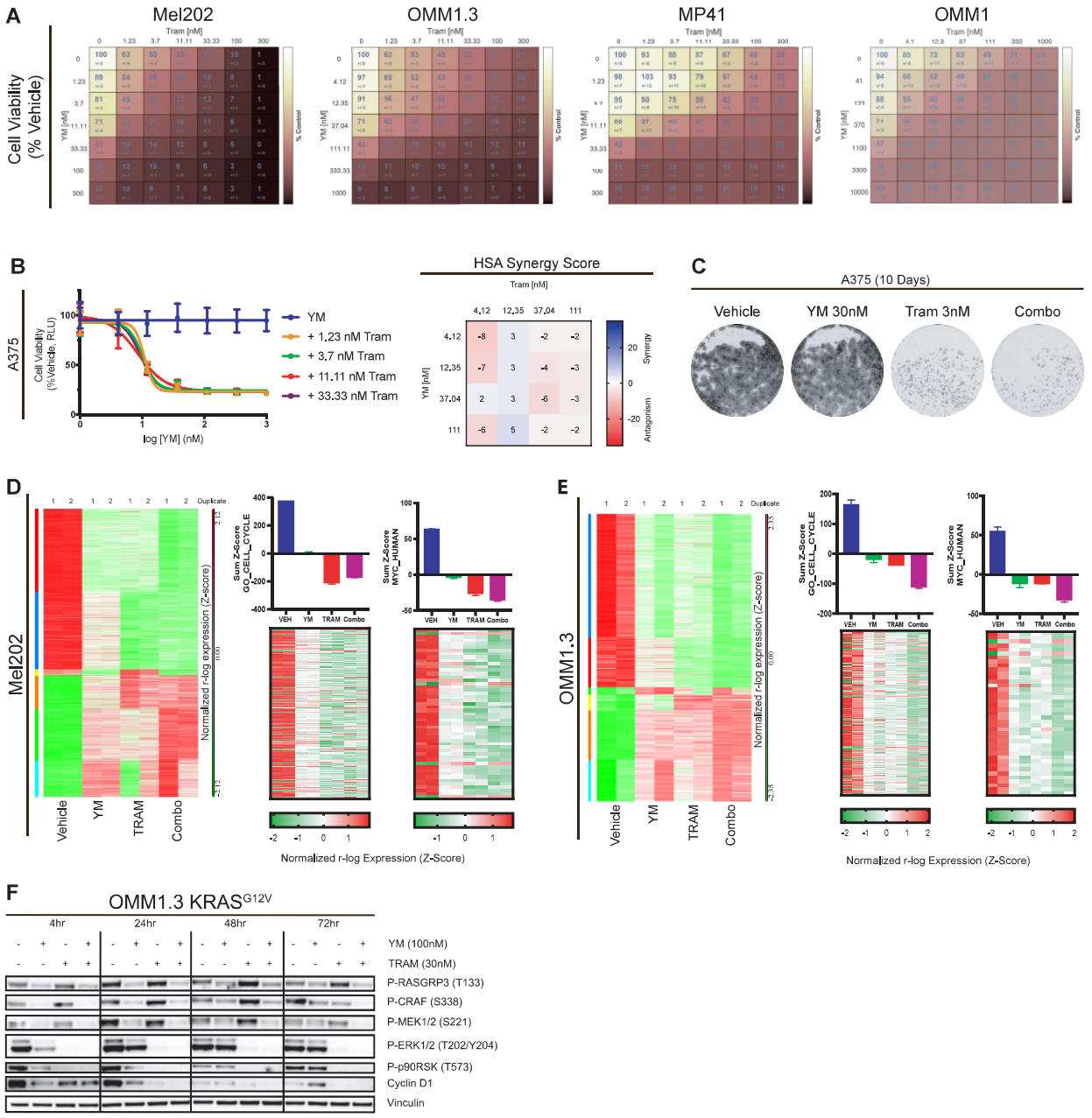

Supplementary Figure S5

(A) Cell viability diagrams for human UVM cell synergy analysis (mean ± SEM, n = 3). **(B)** Viability curves for A375 cells treated with increasing doses of YM in combination with four doses of trametinib (left) and corresponding HSA synergy diagrams (right). (mean ± SEM, n = 3). **(C)** Growth assays for A375 cells in the presence of vehicle, YM, trametinib, or Combo. **(D)** Mel202 cells treated with vehicle, YM (30nM), trametinib (10nM), or Combo for 24 hours, and **(E)** OMM1.3 cells treated with vehicle, YM (100nM), trametinib (30nM), or Combo for 24 hours (left) (duplicates shown). Data was r-log transformed, Z-scored, and then k-means clustered. Sum Z scores (top) shown for cell cycle (middle) and MYC (right) with heatmaps (bottom) showing expression of individual signature genes (mean ± SEM, n = 2). **(F)** Western blot analysis of indicated proteins

for OMM1.3 cells expressing KRAS^{G12V} (~50% population expression). Cells were treated with vehicle, YM, trametinib, or Combo for 4, 24, 48, and 72 hours.

Supplementary Figure S6

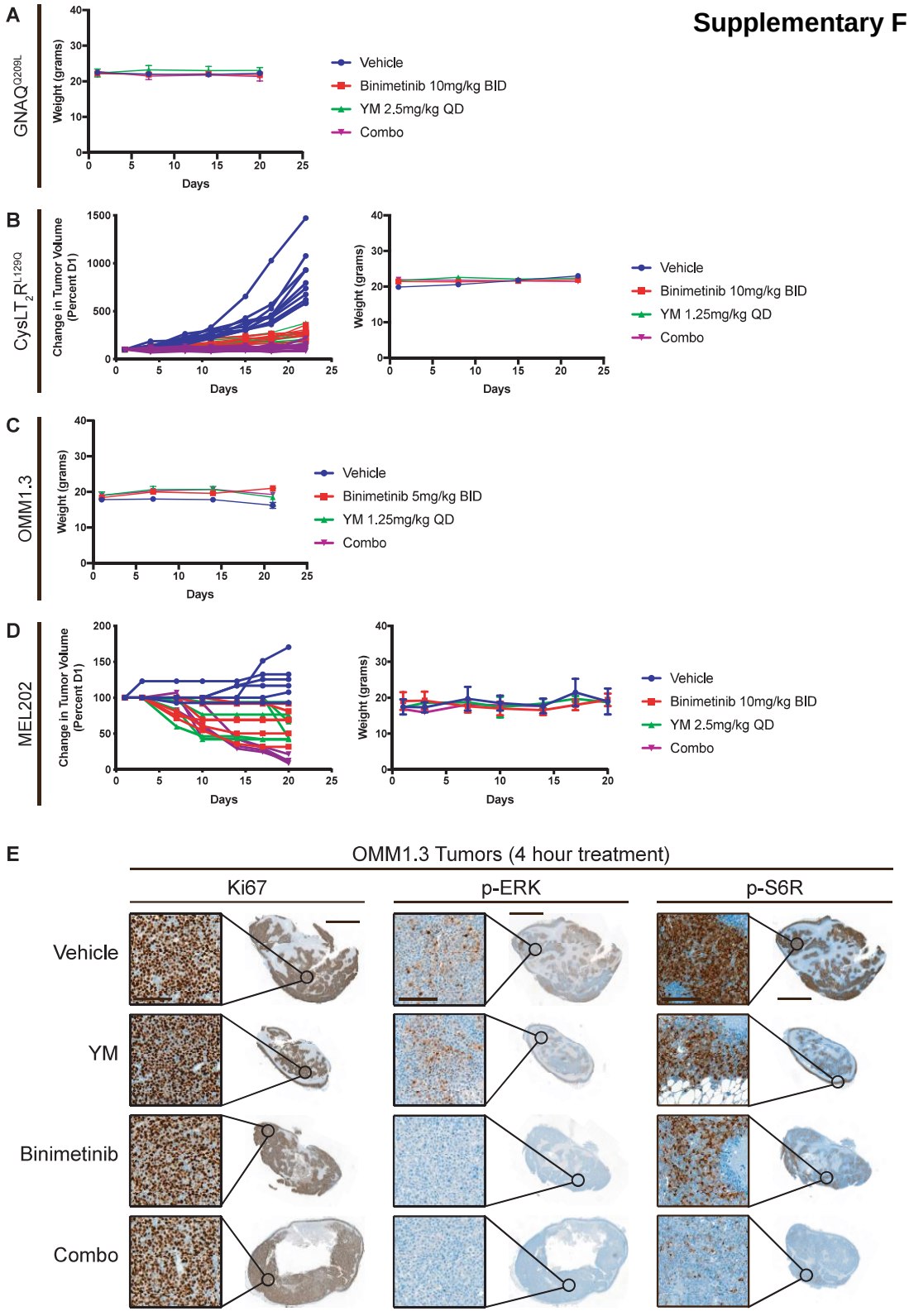

Supplementary Figure S6

(A) Weight of mice throughout experiment from Fig. 6A (mean ± SEM, n = 3-5). **(B)** Percent tumor volume of $CysLT_2R^{L129Q}$ melan-a allografts as individual flanks treated with vehicle, binimetinib, YM, or Combo for 22 days. Mouse weight throughout the course of experiment is plotted (right) (mean ± SEM, n = 5). **(C)** Weight for OMM1.3 xenografted mice from Fig. 6C (mean ± SEM, n = 2-5). **(D)** Percent tumor volume of Mel202 xenografts as individual flanks treated with vehicle, binimetinib, YM, or Combo for 20 days. Mouse weight throughout the course of experiment is plotted (right) (mean ± SEM, n = 2-3). **(E)** Immunohistochemistry of OMM1.3 tumors from Fig. 6D for Ki67, p-ERK, and p-S6R. Scale bar, 50μm for insert (left) and 2mm for whole tumor (right).

Supplementary Table S1: Site Directed Mutagenesis Primers

Gene	Site-Directed Mutation	Forward Primer	Reverse Primer
Synthetc CYSLTR2 L129Q Quickchange	c.386T>A	CAGCTCCATCTACTTCCAAACCGTGCTGAGCGTGG	CAGCTCCATCTACTTCCAAACCGTGCTGAGCGTGG
Synthetic GNAQ G48V Quickchange	c.143G>T	CTGCTGCTCGGGACAGTGGAGAGTGGCAAGAGT	ACTCTTGCCACTCTCCACTGTCCCGAGCAGCAG
Synthetic GNAQ R183Q Quickchange	c.548G>A	GATGTGCTTAGAGTTCAAGTCCCCACCACAGGG	CCCTGTGGTGGGGACTTGAACTCTAAGCACATC
Synthetic GNAQ Q209L Quickchange	c.626A>T	GTCGATGTAGGGGGCCTAAGGTCAGAGAGAAGA	TCTTCTCTCTGACCTTAGGCCCCCTACATCGAC
CYSLTR2 L129Q Quickchange	c.386T>A	AACACTCAGCACGGTCTGGAAATAAATACTGCTGTAC	GTACAGCAGTATTTATTTCCAGACCGTGCTGAGTGTT
GNAQ G48V Quickchange	c.143G>T	TCTTGCCACTCTCTACTGTCCCGAGCAGC	GCTGCTCGGGACAGTAGAGAGTGGCAAGA
GNAQ R183Q Quickchange	c.548G>A	CCCTGTGGTGGGGACTTGAACTCTAAG	GATGTGCTTAGAGTTCAAGTCCCCACCACAGGG
GNAQ Q209L Quickchange	c.626A>T	CTTCTCTCTGACCTTAGGCCCCCTACATCGA	TCGATGTAGGGGGCCTAAGGTCAGAGAGAAG

Supplementary Table S2: Western Blot Primary Antibodies

Target Protein	Catalog #	Company
GAPDH (1:5,000)	60004-I-Ig	Proteintech
MITF	12590S	CST
RASGRP3	3334S	CST
CRAF	53745S	CST
p-CRAF (S338)	9427S	CST
MEK1/2	4694S	CST
p-MEK1/2 (S217/221)	9154S	CST
ERK1/2	4696S	CST
p-ERK1/2 (T202/Y204)	4370S	CST
Cyclin D1	2922S	CST
c-KIT	3074S	CST
Vinculin-HRP	18799S	CST
p-P90RSK	9346S	CST
p-RASGRP3 (T133)	ab124823	Abcam
TRP2/DCT	ab74073	Abcam

Supplementary Table S3: IHC Primary Antibodies

p-ERK1/2 (T202/Y204) (1:400)	4370	CST
Ki67 (1:100)	Ab16667	Abcam
p-S6R (.36ug/ml)	4858	CST

Supplementary Table S4: qRT-PCR Primers

Primer Target	Forward Primer	Reverse Primer
hGNAQ	GAGCACAATAAGGCTCATGCAC	TTGTTGCGTAGGCAGGTAGG
hCYSLTR2	TATTTCCTGACCGTGCTGAGTGT	TGACATCAGAAGCCGAAAG
hKRAS	TAGGCAAGAGTGCCTTGACG	TGCTTCCTGTAGGAATCCTCT
hBRAF	ATTTGGGCAACGAGACCGAT	GTTGATCCTCCATCACCACGA
hRPL27	CATGGGCAAGAAGAAGATCG	TCCAAGGGGATATCCACAGA

Supplementary Table S5: Gene Sets used for transcriptomic analysis. * indicates custom gene sets. KEGG/GO/HALLMARK gene sets can be found on msigdb.

GO_CALCIUM_MEDIATED_SIGNALING
KEGG_MELANOGENESIS
TCGA_MEL_Gq_vs_RasRaf_UP*
TCGA_MEL_Gq_vs_RasRaf_DN*
Mouse_Gna11_vs_Braf_UP*
Mouse_Gna11_vs_Braf_DN*
HALLMARK_KRAS_SIGNALING_UP
HALLMARK_KRAS_SIGNALING_DN
HALLMARK_E2F_TARGETS
Pratilas_MAPK*
GO_CELL_CYCLE
Myc_Human*

Supplementary Table S6: HALLMARK gene set overlaps for all clusters

Gene Set Name	p-value	FDR q-value	-Log10 FDR
HALLMARK_E2F_TARGETS	2.89E-99	1.45E-97	96.838632
HALLMARK_G2M_CHECKPOINT	5.84E-81	1.46E-79	78.8356471
HALLMARK_MITOTIC_SPINDLE	5.38E-24	8.97E-23	22.0472076
HALLMARK_TNFA_SIGNALING_VIA_NFKB	5.63E-22	7.04E-21	20.1524273
HALLMARK_KRAS_SIGNALING_UP	4.96E-21	4.96E-20	19.3045183
HALLMARK_EPITHELIAL_MESENCHYMAL_TRANSITION	2.13E-17	1.52E-16	15.8181564
HALLMARK_ESTROGEN_RESPONSE_LATE	2.13E-17	1.52E-16	15.8181564
HALLMARK_MTORC1_SIGNALING	5.16E-14	3.22E-13	12.4921441
HALLMARK_HYPOXIA	2.02E-12	1.12E-11	10.950782
HALLMARK_IL2_STAT5_SIGNALING	1.05E-11	5.26E-11	10.2790143

Supplementary Table S7: HALLMARK gene set overlaps for cluster 1

Gene Set Name	p-value	FDR q-value	-Log10 FDR
HALLMARK_E2F_TARGETS	1.92E-128	9.60E-127	126.017729
HALLMARK_G2M_CHECKPOINT	4.75E-109	1.19E-107	106.924453
HALLMARK_MITOTIC_SPINDLE	2.74E-35	4.57E-34	33.3400838
HALLMARK_MTORC1_SIGNALING	1.46E-14	1.82E-13	12.7399286
HALLMARK_MYC_TARGETS_V1	1.58E-13	1.58E-12	11.8013429
HALLMARK_ESTROGEN_RESPONSE_LATE	1.41E-10	1.17E-09	8.93181414
HALLMARK_SPERMATOGENESIS	4.40E-10	3.14E-09	8.50307035
HALLMARK_DNA_REPAIR	1.77E-09	1.11E-08	7.95467702
HALLMARK_GLYCOLYSIS	3.07E-06	1.70E-05	4.76955108
HALLMARK_MYC_TARGETS_V2	3.86E-06	1.93E-05	4.71444269

Supplementary Table S8: HALLMARK gene set overlaps for cluster 2

Gene Set Name	p-value	FDR q-value	-Log10 FDR
HALLMARK_TNFA_SIGNALING_VIA_NFKB	7.04E-23	3.52E-21	20.4534573
HALLMARK_KRAS_SIGNALING_UP	8.10E-13	2.03E-11	10.692504
HALLMARK_INFLAMMATORY_RESPONSE	2.96E-10	4.94E-09	8.30627305
HALLMARK_IL2_STAT5_SIGNALING	4.67E-09	4.91E-08	7.30891851
HALLMARK_HYPOXIA	4.91E-09	4.91E-08	7.30891851
HALLMARK_MYC_TARGETS_V2	2.70E-06	2.25E-05	4.64781748
HALLMARK_COMPLEMENT	1.12E-05	6.25E-05	4.20411998
HALLMARK_EPITHELIAL_MESENCHYMAL_TRANSITION	1.12E-05	6.25E-05	4.20411998
HALLMARK_ESTROGEN_RESPONSE_EARLY	1.12E-05	6.25E-05	4.20411998

HALLMARK_UV_RESPONSE_DN	1.82E-05	9.12E-05	4.04000516

Supplementary Table S9: HALLMARK gene set overlaps for cluster 3

Gene Set Name	p-value	FDR q-value	-Log10 FDR
HALLMARK_TNFA_SIGNALING_VIA_NFKB	1.97E-07	9.87E-06	5.00568285
HALLMARK_HYPOXIA	6.01E-05	1.50E-03	2.82390874
HALLMARK_UV_RESPONSE_UP	3.26E-04	5.43E-03	2.26520017
HALLMARK_MYOGENESIS	7.90E-04	6.59E-03	2.18111459
HALLMARK_P53_PATHWAY	7.90E-04	6.59E-03	2.18111459
HALLMARK_XENOBIOTIC_METABOLISM	7.90E-04	6.59E-03	2.18111459
HALLMARK_UV_RESPONSE_DN	3.32E-03	2.37E-02	1.62525165
HALLMARK_APOPTOSIS	4.53E-03	2.83E-02	1.54821356
HALLMARK_MYC_TARGETS_V2	6.41E-03	3.43E-02	1.46470588
HALLMARK_INFLAMMATORY_RESPONSE	8.23E-03	3.43E-02	1.46470588

Supplementary Table S10: HALLMARK gene set overlaps for cluster 4

Gene Set Name	p-value	FDR q-value	-Log10 FDR
HALLMARK_EPITHELIAL_MESENCHYMAL_TRANSITION	6.31E-12	3.16E-10	9.50031292
HALLMARK_ESTROGEN_RESPONSE_LATE	5.28E-07	1.32E-05	4.87942607
HALLMARK_KRAS_SIGNALING_UP	6.68E-06	1.11E-04	3.95467702
HALLMARK_COAGULATION	1.24E-04	1.55E-03	2.8096683
HALLMARK_ANGIOGENESIS	2.67E-04	2.67E-03	2.57348874
HALLMARK_KRAS_SIGNALING_DN	6.83E-04	4.88E-03	2.31158018
HALLMARK_MYOGENESIS	6.83E-04	4.88E-03	2.31158018
HALLMARK_FATTY_ACID_METABOLISM	2.28E-03	1.42E-02	1.84771166
HALLMARK_APICAL_JUNCTION	5.27E-03	2.40E-02	1.61978876
HALLMARK_ESTROGEN_RESPONSE_EARLY	5.27E-03	2.40E-02	1.61978876

Supplementary Table S11: HALLMARK gene set overlaps for cluster 6

Gene Set Name	p-value	FDR q-value	-Log10 FDR
HALLMARK_INTERFERON_GAMMA_RESPONSE	3.57E-09	1.78E-07	6.74958
HALLMARK_INTERFERON_ALPHA_RESPONSE	2.20E-08	5.50E-07	6.25963731
HALLMARK_EPITHELIAL_MESENCHYMAL_TRANSITION	5.35E-07	8.91E-06	5.0501223
HALLMARK_UV_RESPONSE_DN	6.77E-05	8.46E-04	3.07262964
HALLMARK_P53_PATHWAY	4.02E-04	4.02E-03	2.39577395
HALLMARK_APOPTOSIS	1.06E-03	8.58E-03	2.06651271
HALLMARK_APICAL_SURFACE	1.20E-03	8.58E-03	2.06651271
HALLMARK_IL2_STAT5_SIGNALING	2.67E-03	1.51E-02	1.82102305
HALLMARK_KRAS_SIGNALING_DN	2.73E-03	1.51E-02	1.82102305
HALLMARK_COAGULATION	4.31E-03	2.16E-02	1.66554625

CHAPTER 3. ONGOING AND FUTURE DIRECTIONS

Chapter 1 reviewed key background information in the field of UVM whereas Chapter 2 discussed the recent contribution that our lab has made to the field. This closing chapter briefly discusses the ongoing work in our lab as well as highlighting new interesting developments in the field that have yet to be reported.

At the time of writing this I have been focusing on jumpstarting projects to hand off after my eventual departure. My main focus has been on performing a whole genome CRISPR screen in our mutation dependent melan-a cells. We hope to expand on AIM 3 in identifying essential proteins downstream of oncogenic Gαq that could be potential targets for treating the disease. In this screen, we are comparing vulnerabilities between parental, CYSLTR2^{L129Q} mutant, and NRAS^{Q61K} mutant melan-a cells in the hope of finding gene expression patterns unique to CYSLTR2^{L129Q} mutant cells. Another area we are interested in pursuing is the role of lineage specification in UVM tumorigenesis. Studies in CM have illustrated that differentiation state of melanomas can make the disease more aggressive or more resistant to treatment. We are interested in seeing if this dynamic is prevalent in UVM, especially given that UVM tends to be more pigmented and melanocytic than CM.

Beyond our work there have been many recent promising findings in the field. In the 2020 AACR digital conference two groups shared their work in targeting UVM. The first highlights upregulation of endothelin ET(B) receptor (*EDNRB*) as a potential resistance

mechanism to YM treatment (AACR 2020, Abstract 1812). They demonstrated that EDNRB ligand expression caused resistance in xenograft studies and that targeting EDNRB can break resistance. The second work highlighted co-targeting FAK and MEK, very similar to our work in Chapter 2, the key differences being that the FAK inhibitor is already in clinical trials as compared to YM/FR (AACR 2020, Abstract 6406) (Chua et al. 2020). However, one potential downfall when compared to YM/FR is that this combination treatment doesn't target PLCB-PKC signaling which could lead to compensatory signaling. Clinically, there still remains no FDA approved therapies for metastatic UVM, however, a recent drug from Immunocore, tebentafusp, has moved into phase three clinical trials. In brief, this drug is a bispecific fusion protein that targets gp100, a melanocyte lineage specific surface marker found in melanomas and melanocytes. This drug uses a CD3 T-cell engaging domain to direct T cells to target gp100-expressing cells, which is highly expressed in UVM (Damato et al. 2019; Middleton et al. 2020). Although tebentafusp showed an increase in overall survival when compared to investigator's choice it should be noted that this was done so on a small-scale patient population.

In the last several years there has been significant progression in understanding UVM as a disease, how it signals, how it develops, and vulnerabilities. As of now, there are no approved therapies for metastatic UVM, but given recent advances I am hopeful that there will be several therapeutic options in the near future.

BIBLIOGRAPHY

Akama-Garren, Elliot H, Nikhil S Joshi, Tuomas Tammela, Gregory P Chang, Bethany L Wagner, Da-Yae Lee, William M Rideout III, Thales Papagiannakopoulos, Wen Xue, and Tyler Jacks. 2016. “A Modular Assembly Platform for Rapid Generation of DNA Constructs.” *Scientific Reports* 6: 16836.

Akbani, Rehan, Kadir C. Akdemir, B. Arman Aksoy, Monique Albert, Adrian Ally, Samirkumar B. Amin, Harindra Arachchi, et al. 2015. “Genomic Classification of Cutaneous Melanoma.” *Cell* 161 (7): 1681–96. https://doi.org/10.1016/j.cell.2015.05.044.

Alexandrov, Ludmil B., Serena Nik-Zainal, David C. Wedge, Samuel A.J.R. Aparicio, Sam Behjati, Andrew V. Biankin, Graham R. Bignell, et al. 2013. “Signatures of Mutational Processes in Human Cancer.” *Nature* 500 (7463): 415–21. https://doi.org/10.1038/nature12477.

Ambrosini, Grazia, Christine A Pratilas, Li-Xuan Qin, Madhavi Tadi, Oliver Surriga, Richard D Carvajal, and Gary K Schwartz. 2012. “Identification of Unique MEK-Dependent Genes in GNAQ Mutant Uveal Melanoma Involved in Cell Growth, Tumor Cell Invasion, and MEK Resistance.” *Clinical Cancer Research* 18 (13): 3552–61.

Annala, Suvi, Xiaodong Feng, Naveen Shridhar, Funda Eryilmaz, Julian Patt, JuHee Yang, Eva M Pfeil, Rodolfo Daniel Cervantes-Villagrana, Asuka Inoue, and Felix Häberlein. 2019. “Direct Targeting of Gαq and Gα11 Oncoproteins in Cancer Cells.” *Sci. Signal.* 12 (573): eaau5948.

Arnold, J.J., K.J. Blinder, N.M. Bressler, S.B. Bressler, A. Burdan, L. Haynes, J.I. Lim, J.W. Miller, M.J. Potter, and A. Reaves. 2004. “Acute Severe Visual Acuity Decrease after Photodynamic Therapy with Verteporfin: Case Reports from Randomized Clinical Trials - TAP and VIP Report No. 3.” *American Journal of Ophthalmology* 137 (4): 683–96. https://doi.org/10.1016/j.ajo.2003.11.059.

Azab, M, M Benchaboune, K J Blinder, N M Bressler, S B Bressler, E S Gragoudas, G E Fish, Y Hao, L Haynes, and J I Lim. 2004. “Verteporfin Therapy of Subfoveal Choroidal Neovascularization in Age-Related Macular Degeneration: Meta-Analysis of 2-Year Safety Results in Three Randomized Clinical Trials: Treatment of Age-Related Macular Degeneration With Photodynamic Therapy and Vert.”

Bennett, Dorothy, Philip Cooper, and Ian Hart. 1987. “A Line of Non-Tumorigenic Mouse Melanocytes, Syngeneic with the B16 Melanoma and Requiring a Tumour Promoter for Growth.,” 414–18.

Boehm, Jesse S., Jean J. Zhao, Jun Yao, So Young Kim, Ron Firestein, Ian F. Dunn, Sarah K. Sjostrom, et al. 2007. “Integrative Genomic Approaches Identify IKBKE as a Breast Cancer Oncogene.” *Cell* 129 (6): 1065–79. https://doi.org/10.1016/j.cell.2007.03.052.

Campbell, Adrian P., and Alan V. Smrcka. 2018. “Targeting G Protein-Coupled Receptor Signalling by Blocking G Proteins.” *Nature Reviews Drug Discovery* 17 (11): 789–803. https://doi.org/10.1038/nrd.2018.135.

Carvajal, Richard D., Sophie Piperno-Neumann, Ellen Kapiteijn, Paul B. Chapman, Stephen Frank, Anthony M. Joshua, Josep M. Piulats, et al. 2018. “Selumetinib in Combination with Dacarbazine in Patients with Metastatic Uveal Melanoma: A

Phase III, Multicenter, Randomized Trial (SUMIT)." *Journal of Clinical Oncology* 36 (12): 1232–39. https://doi.org/10.1200/JCO.2017.74.1090.
Chattopadhyay, Chandrani, Dae Won Kim, Dan S. Gombos, Junna Oba, Yong Qin, Michelle D. Williams, Bita Esmaeli, et al. 2016. "Uveal Melanoma: From Diagnosis to Treatment and the Science in Between." *Cancer*, 2299–2312. https://doi.org/10.1002/cncr.29727.
Chen, X., Q. Wu, L. Tan, D. Porter, M. J. Jager, C. Emery, and B. C. Bastian. 2014. "Combined PKC and MEK Inhibition in Uveal Melanoma with GNAQ and GNA11 Mutations." *Oncogene* 33 (39): 4724–34. https://doi.org/10.1038/onc.2013.418.
Chen, Xu, Qiuxia Wu, Philippe Depeille, Peirong Chen, Sophie Thornton, Helen Kalirai, Sarah E. Coupland, Jeroen P. Roose, and Boris C. Bastian. 2017. "RasGRP3 Mediates MAPK Pathway Activation in GNAQ Mutant Uveal Melanoma." *Cancer Cell*. https://doi.org/10.1016/j.ccell.2017.04.002.
Chidiac, Peter, and Elliott M. Ross. 1999. "Phospholipase C-B1 Directly Accelerates GTP Hydrolysis by Gα(q) and Acceleration Is Inhibited by Gβγ Subunits." *Journal of Biological Chemistry* 274 (28): 19639–43. https://doi.org/10.1074/jbc.274.28.19639.
Chua, Vivian, Dominic Lapadula, Clinita Randolph, Jeffrey L. Benovic, Philip B. Wedegaertner, and Andrew E. Aplin. 2017. "Dysregulated GPCR Signaling and Therapeutic Options in Uveal Melanoma." *Molecular Cancer Research*. https://doi.org/10.1158/1541-7786.MCR-17-0007.
Chua, Vivian, Jane Mattei, Anna Han, Lauren Johnston, Kyleigh LiPira, Sara M. Selig, Richard D. Carvajal, Andrew E. Aplin, and Sapna P. Patel. 2020. "The Latest on Uveal Melanoma Research and Clinical Trials: Updates from the Cure Ocular Melanoma (CURE OM) Science Meeting (2019)." *Clinical Cancer Research*, no. 2019: 1–7. https://doi.org/10.1158/1078-0432.ccr-20-2536.
Crüsemann, Max, Raphael Reher, Isabella Schamari, Alexander O Brachmann, Tsubasa Ohbayashi, Markus Kuschak, Davide Malfacini, Alexander Seidinger, Marta Pinto-Carbó, and René Richarz. 2018. "Heterologous Expression, Biosynthetic Studies, and Ecological Function of the Selective Gq-signaling Inhibitor FR900359." *Angewandte Chemie International Edition* 57 (3): 836–40.
Damato, Bertil E., Joseph Dukes, Howard Goodall, and Richard D. Carvajal. 2019. "Tebentafusp: T Cell Redirection for the Treatment of Metastatic Uveal Melanoma." *Cancers* 11 (7). https://doi.org/10.3390/cancers11070971.
Dobin, Alexander, Carrie A Davis, Felix Schlesinger, Jorg Drenkow, Chris Zaleski, Sonali Jha, Philippe Batut, Mark Chaisson, and Thomas R Gingeras. 2013. "STAR: Ultrafast Universal RNA-Seq Aligner." *Bioinformatics* 29 (1): 15–21.
Feng, Xiaodong, Maria Sol Degese, Ramiro Iglesias-Bartolome, Jose P. Vaque, Alfredo A. Molinolo, Murilo Rodrigues, M. Raza Zaidi, et al. 2014. "Hippo-Independent Activation of YAP by the GNAQ Uveal Melanoma Oncogene through a Trio-Regulated Rho GTPase Signaling Circuitry." *Cancer Cell* 25 (6): 831–45. https://doi.org/10.1016/j.ccr.2014.04.016.
Field, Matthew G., Michael A. Durante, Hima Anbunathan, Louis Z. Cai, Christina L. Decatur, Anne M. Bowcock, Stefan Kurtenbach, and J. William Harbour. 2018. "Punctuated Evolution of Canonical Genomic Aberrations in Uveal Melanoma." *Nature Communications* 9 (1). https://doi.org/10.1038/s41467-017-02428-w.
Fujioka, Mamoru, Shigetaka Koda, Yukiyoshi Morimoto, and Klaus Biemann. 1988.

"Structure of FR900359, a Cyclic Depsipeptide from Ardisia Crenata Sims." *Journal of Organic Chemistry* 53 (12): 2820–25. https://doi.org/10.1021/jo00247a030.
Furney, Simon J., Malin Pedersen, David Gentien, Amaury G. Dumont, Audrey Rapinat, Laurence Desjardins, Samra Turajlic, et al. 2013. "SF3B1 Mutations Are Associated with Alternative Splicing in Uveal Melanoma." *Cancer Discovery* 3 (10): 1122–29. https://doi.org/10.1158/2159-8290.CD-13-0330.
Gill, Ryan M., Benjamin Buelow, Cheryl Mather, Nancy M. Joseph, Venancio Alves, Elizabeth M. Brunt, Ta Chiang Liu, et al. 2016. "Hepatic Small Vessel Neoplasm, a Rare Infiltrative Vascular Neoplasm of Uncertain Malignant Potential." *Human Pathology* 54: 143–51. https://doi.org/10.1016/j.humpath.2016.03.018.
Goldsmith, Z. G., and D. N. Dhanasekaran. 2007. "G Protein Regulation of MAPK Networks." *Oncogene*. https://doi.org/10.1038/sj.onc.1210407.
Graziano, M. P., and A. G. Gilman. 1989. "Synthesis in Escherichia Coli of GTPase-Deficient Mutants of G(Sα)." *Journal of Biological Chemistry* 264 (26): 15475–82.
Griewank, K. G., X. Yu, J. Khalili, M. M. Sozen, K. Stempke-Hale, C. Bernatchez, S. Wardell, B. C. Bastian, and S. E. Woodman. 2012. "Genetic and Molecular Characterization of Uveal Melanoma Cell Lines." *Pigment Cell & Melanoma Research*. https://doi.org/10.1111/j.1755-148X.2012.00971.x.
Griewank, Klaus G., Hansgeorg Müller, Louise A. Jackett, Michael Emberger, Inga Möller, Johannes A.P. Van De Nes, Lisa Zimmer, et al. 2017. "SF3B1 and BAP1 Mutations in Blue Nevus-like Melanoma." *Modern Pathology* 30 (7): 928–39. https://doi.org/10.1038/modpathol.2017.23.
Harbour, J. William, Michael D. Onken, Elisha D. O. Roberson, Shenghui Duan, Li Cao, Lori A. Worley, M. Laurin Council, Katie A. Matatall, Cynthia Helms, and Anne M. Bowcock. 2010. "Frequent Mutation of BAP1 in Metastasizing Uveal Melanomas." *Science*. https://doi.org/10.1126/science.1194472.
Huang, Jenny Li Ying, Oscar Urtatiz, and Catherine D. Van Raamsdonk. 2015. "Oncogenic G Protein GNAQ Induces Uveal Melanoma and Intravasation in Mice." *Cancer Research*. https://doi.org/10.1158/0008-5472.CAN-14-3229.
Inoue, Daichi, Guo Liang Chew, Bo Liu, Brittany C. Michel, Joseph Pangallo, Andrew R. D'Avino, Tyler Hitchman, et al. 2019. "Spliceosomal Disruption of the Non-Canonical BAF Complex in Cancer." *Nature* 574 (7778): 432–36. https://doi.org/10.1038/s41586-019-1646-9.
Janes, Matthew R., Jingchuan Zhang, Lian Sheng Li, Rasmus Hansen, Ulf Peters, Xin Guo, Yuching Chen, et al. 2018. "Targeting KRAS Mutant Cancers with a Covalent G12C-Specific Inhibitor." *Cell* 172 (3): 578-589.e17. https://doi.org/10.1016/j.cell.2018.01.006.
Jin, Chuan, Grammatiki Fotaki, Mohanraj Ramachandran, Berith Nilsson, Magnus Essand, and Di Yu. 2016. "Safe Engineering of CAR T Cells for Adoptive Cell Therapy of Cancer Using Long-term Episomal Gene Transfer." *EMBO Molecular Medicine* 8 (7): 702–11.
Johansson, Peter, Lauren G Aoude, Karin Wadt, William J Glasson, Sunil K Warrier, Alex W Hewitt, Jens Folke Kiilgaard, et al. 2016. "Deep Sequencing of Uveal Melanoma Identifies a Recurrent Mutation in PLCB4." *Oncotarget* 7 (4): 4624–31. https://doi.org/10.18632/oncotarget.6614.
Johnson, Chelsea Place, Ivana K. Kim, Bita Esmaeli, Ali Amin-Mansour, Daniel J.

Treacy, Scott L. Carter, Eran Hodis, et al. 2017. “Systematic Genomic and Translational Efficiency Studies of Uveal Melanoma.” *PLoS ONE* 12 (6): 1–17. https://doi.org/10.1371/journal.pone.0178189.

Joseph, Nancy M., Elizabeth M. Brunt, Celia Marginean, ILKe Nalbantoglu, Dale C. Snover, Swan N. Thung, Matthew M. Yeh, Sarah E. Umetsu, Linda D. Ferrell, and Ryan M. Gill. 2018. “Frequent GNAQ and GNA14 Mutations in Hepatic Small Vessel Neoplasm.” *American Journal of Surgical Pathology* 42 (9): 1201–7. https://doi.org/10.1097/PAS.0000000000001110.

Journée- De Korver, Hanneke J.G., Jendo A. Oosterhuis, and Jan E.E. Keunen. 1996. “Histologic Findings in Choroidal Melanomas after Transpupillary Thermotherapy.” *Investigative Ophthalmology and Visual Science* 37 (3): 234–39.

Jovanovic, Predrag, Marija Mihajlovic, Jasmina Djordjevic-Jocic, Slobodan Vlajkovic, Sonja Cekic, and Vladisav Stefanovic. 2013. “Ocular Melanoma: An Overview of the Current Status.” *International Journal of Clinical and Experimental Pathology* 6 (7): 1230–44.

Kamato, Danielle, Partha Mitra, Felicity Davis, Narin Osman, Rebecca Chaplin, Peter J. Cabot, Rizwana Afroz, et al. 2017. “Gaq Proteins: Molecular Pharmacology and Therapeutic Potential.” *Cellular and Molecular Life Sciences* 74 (8): 1379–90. https://doi.org/10.1007/s00018-016-2405-9.

Küsters-Vandevelde, Heidi V.N., David Creytens, Adriana C.H. van Engen-van Grunsven, Marcel Jeunink, Veronique Winnepenninckx, Patricia J.T.A. Groenen, Benno Küsters, Pieter Wesseling, Willeke A.M. Blokx, and Clemens F.M. Prinsen. 2016. “SF3B1 and EIF1AX Mutations Occur in Primary Leptomeningeal Melanocytic Neoplasms; yet Another Similarity to Uveal Melanomas.” *Acta Neuropathologica Communications* 4: 5. https://doi.org/10.1186/s40478-016-0272-0.

Küsters-Vandevelde, Heidi V.N., Ilse A.C.H. van Engen- van Grunsven, Sarah E. Coupland, Sarah L. Lake, Jos Rijntjes, Rolph Pfundt, Benno Küsters, Pieter Wesseling, Willeke A.M. Blokx, and Patricia J.T.A. Groenen. 2015. “Mutations in G Protein Encoding Genes and Chromosomal Alterations in Primary Leptomeningeal Melanocytic Neoplasms.” *Pathology and Oncology Research* 21 (2): 439–47. https://doi.org/10.1007/s12253-014-9841-3.

Küsters-Vandevelde, Heidi V.N., Menno R. Germans, Roy Rabbie, Mamunur Rashid, Roel Ten Broek, Willeke A.M. Blokx, Clemens F.M. Prinsen, David J. Adams, and Mark Ter Laan. 2018. “Whole-Exome Sequencing of a Meningeal Melanocytic Tumour Reveals Activating CYSLTR2 and EIF1AX Hotspot Mutations and Similarities to Uveal Melanoma.” *Brain Tumor Pathology* 35 (2): 127–30. https://doi.org/10.1007/s10014-018-0308-1.

Küsters-Vandevelde, Heidi V.N., Annelies Klaasen, Benno Küsters, Patricia J.T.A. Groenen, Ilse A.C.H. Van Engen-Van Grunsven, Marcory R.C.F. Van Dijk, Guido Reifenberger, Pieter Wesseling, and Willeke A.M. Blokx. 2010. “Activating Mutations of the GNAQ Gene: A Frequent Event in Primary Melanocytic Neoplasms of the Central Nervous System.” *Acta Neuropathologica* 119 (3): 317–23. https://doi.org/10.1007/s00401-009-0611-3.

Lapadula, Dominic, Eduardo Farias, Clinita E Randolph, Timothy J Purwin, Dougan McGrath, Thomas H Charpentier, Lihong Zhang, Shihua Wu, Mizue Terai, and

Takami Sato. 2019. “Effects of Oncogenic Gαq and Gα11 Inhibition by FR900359 in Uveal Melanoma.” *Molecular Cancer Research* 17 (4): 963–73.
Lito, Piro, Anna Saborowski, Jingyin Yue, Martha Solomon, Eric Joseph, Sunyana Gadal, Michael Saborowski, et al. 2014. “Disruption of CRAF-Mediated MEK Activation Is Required for Effective Mek Inhibition in KRAS Mutant Tumors.” *Cancer Cell* 25 (5): 697–710. https://doi.org/10.1016/j.ccr.2014.03.011.
Lito, Piro, Martha Solomon, Lian-Sheng Li, Rasmus Hansen, and Neal Rosen. 2016. “Allele-Specific Inhibitors Inactivate Mutant KRAS G12C by a Trapping Mechanism.” *Science* 351 (6273). https://doi.org/10.1126/science.aad6204.
Lomakin, Ivan B., and Thomas A. Steitz. 2013. “The Initiation of Mammalian Protein Synthesis and MRNA Scanning Mechanism.” *Nature* 500 (7462): 307–11. https://doi.org/10.1038/nature12355.
Love, Michael I., Wolfgang Huber, and Simon Anders. 2014. “Moderated Estimation of Fold Change and Dispersion for RNA-Seq Data with DESeq2.” *Genome Biology* 15 (12): 1–21. https://doi.org/10.1186/s13059-014-0550-8.
Luke, Jason J., Pierre L. Triozzi, Kyle C. McKenna, Erwin G. Van Meir, Jeffrey E. Gershenwald, Boris C. Bastian, J. Silvio Gutkind, et al. 2015. “Biology of Advanced Uveal Melanoma and next Steps for Clinical Therapeutics.” *Pigment Cell & Melanoma Research*. https://doi.org/10.1111/pcmr.12304.
Martin, Marcel, Lars Maßhöfer, Petra Temming, Sven Rahmann, Claudia Metz, Norbert Bornfeld, Johannes Van De Nes, et al. 2013. “Exome Sequencing Identifies Recurrent Somatic Mutations in EIF1AX and SF3B1 in Uveal Melanoma with Disomy 3.” *Nature Genetics* 45 (8): 933–36. https://doi.org/10.1038/ng.2674.
McCormick, Frank. 2018. “Targeting KRAS Directly.” *Annual Review of Cancer Biology* 2 (1): 81–90. https://doi.org/10.1146/annurev-cancerbio-050216-122010.
Middleton, Mark R., Cheryl McAlpine, Victoria K. Woodcock, Pippa Corrie, Jeffrey R. Infante, Neil M. Steven, Thomas R Jeffry Evans, et al. 2020. “Tebentafusp, A TCR/Anti-CD3 Bispecific Fusion Protein Targeting Gp100, Potently Activated Antitumor Immune Responses in Patients with Metastatic Melanoma.” *Clinical Cancer Research*, 5869–79. https://doi.org/10.1158/1078-0432.ccr-20-1247.
Möller, Inga, Rajmohan Murali, Hansgeorg Müller, Thomas Wiesner, Louise A. Jackett, Simone L. Scholz, Ioana Cosgarea, et al. 2017. “Activating Cysteinyl Leukotriene Receptor 2 (CYSLTR2) Mutations in Blue Nevi.” *Modern Pathology* 30 (3): 350–56. https://doi.org/10.1038/modpathol.2016.201.
Moore, Amanda R., Emilie Ceraudo, Jessica J. Sher, Youxin Guan, Alexander N. Shoushtari, Matthew T. Chang, Jenny Q. Zhang, et al. 2016. “Recurrent Activating Mutations of G-Protein-Coupled Receptor CYSLTR2 in Uveal Melanoma.” *Nature Genetics*. https://doi.org/10.1038/ng.3549.
Moore, Amanda R., Leili Ran, Youxin Guan, Jessica J Sher, Jenny Q Zhang, Catalina Hwang, Edward G Walzak, et al. 2018. “Novel GNA11 Q209L Mouse Model Reveals RasGRP3 as an Essential Signaling Node in Uveal Melanoma.” *Cell Reports* 22 (9): 2455–68. https://doi.org/10.1016/j.celrep.2018.01.081.
Moore, Amanda R., Scott C. Rosenberg, Frank McCormick, and Shiva Malek. 2020. “RAS-Targeted Therapies: Is the Undruggable Drugged?” *Nature Reviews Drug Discovery*, 1–20. https://doi.org/10.1038/s41573-020-0068-6.
Moroishi, Toshiro, Carsten Gram Hansen, and Kun-Liang Guan. 2015. “The Emerging

Roles of YAP and TAZ in Cancer." *Nature Reviews Cancer* 15 (2): 73–79.
Nes, Johannes A.P. van de, Christian Koelsche, Marco Gessi, Inga Möller, Antje Sucker, Richard A. Scolyer, Michael E. Buckland, et al. 2017. "Activating CYSLTR2 and PLCB4 Mutations in Primary Leptomeningeal Melanocytic Tumors." *Journal of Investigative Dermatology* 137 (9): 2033–35. https://doi.org/10.1016/j.jid.2017.04.022.
Nishikawa, Hiroyuki, Wenwen Wu, Ayaka Koike, Ryoko Kojima, Hiromichi Gomi, Mamoru Fukuda, and Tomohiko Ohta. 2009. "BRCA1-Associated Protein 1 Interferes with BRCA1/BARD1 RING Heterodimer Activity." *Cancer Research* 69 (1): 111–19. https://doi.org/10.1158/0008-5472.CAN-08-3355.
Nishimura, A., K. Kitano, J. Takasaki, M. Taniguchi, N. Mizuno, K. Tago, T. Hakoshima, and H. Itoh. 2010. "Structural Basis for the Specific Inhibition of Heterotrimeric Gq Protein by a Small Molecule." *Proceedings of the National Academy of Sciences*. https://doi.org/10.1073/pnas.1003553107.
O'Hayre, Morgan, José Vázquez-Prado, Irina Kufareva, Eric W Stawiski, Tracy M Handel, Somasekar Seshagiri, and J Silvio Gutkind. 2013. "The Emerging Mutational Landscape of G Proteins and G-Protein-Coupled Receptors in Cancer." *Nature Reviews Cancer* 13. https://doi.org/10.1038/nrc3521.
Onken, Michael D., Carol M. Makepeace, Kevin M. Kaltenbronn, Stanley M. Kanai, Tyson D. Todd, Shiqi Wang, Thomas J. Broekelmann, Prabakar Kumar Rao, John A. Cooper, and Kendall J. Blumer. 2018. "Targeting Nucleotide Exchange to Inhibit Constitutively Active G Protein a Subunits in Cancer Cells." *Science Signaling* 11 (546). https://doi.org/10.1126/scisignal.aao6852.
Patricelli, Matthew P., Matthew R. Janes, Lian Sheng Li, Rasmus Hansen, Ulf Peters, Linda V. Kessler, Yuching Chen, et al. 2016. "Selective Inhibition of Oncogenic KRAS Output with Small Molecules Targeting the Inactive State." *Cancer Discovery* 6 (3): 316–29. https://doi.org/10.1158/2159-8290.CD-15-1105.
Pratilas, Christine A., Barry S. Taylor, Qing Ye, Agnes Viale, Chris Sander, David B. Solit, and Neal Rosen. 2009. "V600EBRAF Is Associated with Disabled Feedback Inhibition of RAF-MEK Signaling and Elevated Transcriptional Output of the Pathway." *Proceedings of the National Academy of Sciences of the United States of America* 106 (11): 4519–24. https://doi.org/10.1073/pnas.0900780106.
Raamsdonk, Catherine D. Van, Vladimir Bezrookove, Gary Green, Jürgen Bauer, Lona Gaugler, Joan M. O'Brien, Elizabeth M. Simpson, Gregory S. Barsh, and Boris C. Bastian. 2009. "Frequent Somatic Mutations of GNAQ in Uveal Melanoma and Blue Naevi." *Nature*. https://doi.org/10.1038/nature07586.
Raamsdonk, Catherine D. Van, Klaus G. Griewank, Michelle B. Crosby, Maria C. Garrido, Swapna Vemula, Thomas Wiesner, Anna C. Obenauf, et al. 2010. "Mutations in GNA11 in Uveal Melanoma." *New England Journal of Medicine*. https://doi.org/10.1056/NEJMoa1000584.
Robertson, A. Gordon, Juliann Shih, Christina Yau, Ewan A. Gibb, Junna Oba, Karen L. Mungall, Julian M. Hess, et al. 2017. "Integrative Analysis Identifies Four Molecular and Clinical Subsets in Uveal Melanoma." *Cancer Cell* 32 (2): 204-220.e15. https://doi.org/10.1016/j.ccell.2017.07.003.
Rossi, Ernesto, Giovanni Schinzari, Ilaria Grazia Zizzari, Brigida Anna Maiorano, Monica Maria Pagliara, Maria Grazia Sammarco, Vincenzo Fiorentino, et al. 2019.

"Immunological Backbone of Uveal Melanoma: Is There a Rationale for Immunotherapy?" *Cancers* 11 (8): 1–12. https://doi.org/10.3390/cancers11081055.
Roszko, Kelly L, Ruiye Bi, Caroline M Gorvin, Hans Bräuner-osborne, Xiao-feng Xiong, Asuka Inoue, Rajesh V Thakker, Kristian Strømgaard, Thomas Gardella, and Michael Mannstadt. 2017. "Knockin Mouse with Mutant G α 11 Mimics Human Inherited Hypocalcemia and Is Rescued by Pharmacologic Inhibitors" 2 (9): 1–15.
Schrage, Ramona, Anna Lena Schmitz, Evelyn Gaffal, Suvi Annala, Stefan Kehraus, Daniela Wenzel, Katrin M. Büllesbach, et al. 2015. "The Experimental Power of FR900359 to Study Gq-Regulated Biological Processes." *Nature Communications*. https://doi.org/10.1038/ncomms10156.
Shen, Jie, Beibei Cao, Yatao Wang, Chenshen Ma, Zhuo Zeng, Liang Liu, Xiaolan Li, Deding Tao, Jianping Gong, and Daxing Xie. 2018. "Hippo Component YAP Promotes Focal Adhesion and Tumour Aggressiveness via Transcriptionally Activating THBS1/FAK Signalling in Breast Cancer." *Journal of Experimental and Clinical Cancer Research* 37 (1): 1–17. https://doi.org/10.1186/s13046-018-0850-z.
Sheng, Xinan, Yan Kong, Yiqian Li, Qiannan Zhang, Lu Si, Chuanliang Cui, Zhihong Chi, et al. 2016. "GNAQ and GNA11 Mutations Occur in 9.5% of Mucosal Melanoma and Are Associated with Poor Prognosis." *European Journal of Cancer* 65: 156–63. https://doi.org/10.1016/j.ejca.2016.06.019.
Shirley, Matthew D., Hao Tang, Carol J. Gallione, Joseph D. Baugher, Laurence P. Frelin, Bernard Cohen, Paula E. North, Douglas A. Marchuk, Anne M. Comi, and Jonathan Pevsner. 2013. "Sturge–Weber Syndrome and Port-Wine Stains Caused by Somatic Mutation in *GNAQ*." *New England Journal of Medicine* 368 (21): 1971–79. https://doi.org/10.1056/NEJMoa1213507.
Singh, Arun D., Mary E. Turell, and Allan K. Topham. 2011. "Uveal Melanoma: Trends in Incidence, Treatment, and Survival." *Ophthalmology* 118 (9): 1881–85. https://doi.org/10.1016/j.ophtha.2011.01.040.
Takasaki, Jun, Tetsu Saito, Masatoshi Taniguchi, Tomihisa Kawasaki, Yumiko Moritani, Kazumi Hayashi, and Masato Kobori. 2004. "A Novel Gaq/11-Selective Inhibitor." *Journal of Biological Chemistry* 279. https://doi.org/10.1074/jbc.M408846200.
Taniguchi, Masatoshi, Koji Nagai, Nakako Arao, Tomihisa Kawasaki, Tetsu Saito, Yumiko Moritani, Jun Takasaki, et al. 2003. "YM-254890, a Novel Platelet Aggregation Inhibitor Produced By." *THE JOURNAL OF ANTIBIOTICS* 56 (4): 358–63.
Taniguchi, Masatoshi, Ken Ichi Suzumura, Koji Nagai, Tomihisa Kawasaki, Tetsu Saito, Jun Takasaki, Ken Ichi Suzuki, Shigeo Fujita, and Shin Ichi Tsukamoto. 2003. "Structure of YM-254890, a Novel Gq/11inhibitor from Chromobacterium Sp. QS3666." *Tetrahedron* 59 (25): 4533–38. https://doi.org/10.1016/S0040-4020(03)00680-X.
Taniguchi, Masatoshi, Ken Ichi Suzumura, Koji Nagai, Tomihisa Kawasaki, Jun Takasaki, Mitsuhiro Sekiguchi, Yumiko Moritani, et al. 2004. "YM-254890 Analogues, Novel Cyclic Depsipeptides with Gαq/11inhibitory Activity from Chromobacterium Sp. QS3666." *Bioorganic and Medicinal Chemistry* 12 (12): 3125–33. https://doi.org/10.1016/j.bmc.2004.04.006.
Taylor, Veronica G., Paige A. Bommarito, and John J.G. Tesmer. 2016. "Structure of the Regulator of G Protein Signaling 8 (RGS8)-Gαq Complex: Molecular Basis for

Gα Selectivity.” *Journal of Biological Chemistry* 291 (10): 5138–45. https://doi.org/10.1074/jbc.M115.712075.
Uemura, Toshio, Tomihisa Kawasaki, Masatoshi Taniguchi, Yumiko Moritani, Kazumi Hayashi, Tetsu Saito, Jun Takasaki, Wataru Uchida, and Keiji Miyata. 2006. “Biological Properties of a Specific Gαq/11inhibitor, YM-254890, on Platelet Functions and Thrombus Formation under High-Shear Stress.” *British Journal of Pharmacology* 148 (1): 61–69. https://doi.org/10.1038/sj.bjp.0706711.
Uemura, Toshio, Hajime Takamatsu, Tomihisa Kawasaki, Masatoshi Taniguchi, Eisaku Yamamoto, Yuichi Tomura, Wataru Uchida, and Keiji Miyata. 2006. “Effect of YM-254890, a Specific Gαq/11 Inhibitor, on Experimental Peripheral Arterial Disease in Rats.” *European Journal of Pharmacology* 536 (1–2): 154–61. https://doi.org/10.1016/j.ejphar.2006.02.048.
Veroli, Giovanni Y Di, Chiara Fornari, Dennis Wang, Séverine Mollard, Jo L Bramhall, Frances M Richards, and Duncan I Jodrell. 2016. “Combenefit: An Interactive Platform for the Analysis and Visualization of Drug Combinations.” *Bioinformatics* 32 (18): 2866–68.
Wu, D., C. H. Lee, S. G. Rhee, and M. I. Simon. 1992. “Activation of Phospholipase C by the α Subunits of the G(q) and G11 Proteins in Transfected Cos-7 Cells.” *Journal of Biological Chemistry* 267 (3): 1811–17.
Xiong, Xiao-Feng, Hang Zhang, Christina R. Underwood, Kasper Harpsøe, Thomas J. Gardella, Mie F. Wöldike, Michael Mannstadt, David E. Gloriam, Hans Bräuner-Osborne, and Kristian Strømgaard. 2016. “Total Synthesis and Structure–Activity Relationship Studies of a Series of Selective G Protein Inhibitors.” *Nature Chemistry* 8 (11): 1035–41. https://doi.org/10.1038/nchem.2577.
Yoo, Jae Hyuk, Dallas S. Shi, Allie H. Grossmann, Lise K. Sorensen, Zong Zhong Tong, Tara M. Mleynek, Aaron Rogers, et al. 2016. “ARF6 Is an Actionable Node That Orchestrates Oncogenic GNAQ Signaling in Uveal Melanoma.” *Cancer Cell*. https://doi.org/10.1016/j.ccell.2016.04.015.
Yu, Fa Xing, Jing Luo, Jung Soon Mo, Guangbo Liu, Young Chul Kim, Zhipeng Meng, Ling Zhao, et al. 2014. “Mutant Gq/11 Promote Uveal Melanoma Tumorigenesis by Activating YAP.” *Cancer Cell*. https://doi.org/10.1016/j.ccr.2014.04.017.
Zehir, Ahmet, Ryma Benayed, Ronak H. Shah, Aijazuddin Syed, Sumit Middha, Hyunjae R. Kim, Preethi Srinivasan, et al. 2017. “Mutational Landscape of Metastatic Cancer Revealed from Prospective Clinical Sequencing of 10,000 Patients.” *Nature Medicine* 23 (6): 703–13. https://doi.org/10.1038/nm.4333.
Zhang, Hang, Xiao-Feng Xiong, Michael W. Boesgaard, Christina R. Underwood, Hans Bräuner-Osborne, and Kristian Strømgaard. 2017. “Structure-Activity Relationship Studies of the Cyclic Depsipeptide Natural Product YM-254890, Targeting the G_q Protein.” *ChemMedChem* 12 (11): 830–34. https://doi.org/10.1002/cmdc.201700155.
Zuidervaart, W., F. Van Nieuwpoort, M. Stark, R. Dijkman, L. Packer, A. M. Borgstein, S. Pavey, et al. 2005. “Activation of the MAPK Pathway Is a Common Event in Uveal Melanomas Although It Rarely Occurs through Mutation of BRAF or RAS.” *British Journal of Cancer*. https://doi.org/10.1038/sj.bjc.6602598.